Statistical Mechanics of End-Attached Polymer Interfaces

Thesis by

Jeremy Isaac Martin

In Partial Fulfillment of the Requirements

for the Degree of

Doctor of Philosophy

California Institute of Technology

Pasadena, California

1998

(Submitted September 18, 1997)

Acknowledgements

It is my pleasure to acknowledge the guidance of my advisor, Professor Zhen-Gang Wang, to whom I am deeply grateful. I am also pleased to acknowledge my group-mates Shuyan Qi, Wei Zheng and Celeste Chang for many fruitful discussions.

Abstract

This dissertation discusses several closely related problems involving end attached polymers at interfaces. The studies share a numerical self-consistent field approach which is described in detail in Chapter 1.

In Chapter 2, we consider irreversible polymer brushes (polymers densely end tethered to a surface). First, we discuss the adequacy of second virial treatments of interchain interactions. Next we examine the extent of interbrush penetration between compressed polymer brushes, and its effect on the interactions between them. Then we identify scaling variables which control the behavior of polymer brushes in polymeric solvents. Finally we investigate brush configurations and interactions in mixed solvents, where nonmonotonic interaction profiles are predicted with a longer range weak attraction, and strong repulsion at shorter separations.

In Chapter 3, we discuss the modification of spreading properties of a liquid on a solid surface by the addition of end-adsorbing polymers. An end-adsorption polymer additive can lead an otherwise non-spreading liquid to spread. A phase diagram for spreading of a liquid drop of fixed volume as a function of the concentration of end-adsorbing polymers and the energy of end-adsorption to the surface is obtained. The equilibrium thickness of a spread film is also calculated, and is shown to be closely related to the thickness of a self-assembled polymer brush in an unbounded fluid and relatively insensitive to the bare spreading power of the liquid or the Hamaker constant, which determine the equilibrium thickness of a film of a simple liquid.

Finally, in Chapter 4, we study the interaction forces between two plates in a semi-dilute solution of polymers each having one weakly adsorbing end-group. This system exhibits both repulsive and attractive interactions of comparable magnitude and well-separated length scales. The repulsion has a length scale of the end-to-end distance of the end-adsorbed polymer, and a magnitude which is proportional to the end-adsorption energy and the volume fraction of the polymer, and inversely proportional the chain molecular weight. At plate separations of order the correlation length of the solution, a depletion attraction sets in with a magnitude that scales with the bulk osmotic pressure.

Contents

List of Figures

List of Tables

Introduction

Polymer additives have been used to modify the surface properties of technologically important products since the earliest days of recorded history. For example, india ink, produced in India and China since before the Christian era, is made from carbon black and gum arabic, a naturally occurring plant gum containing complex biopolymers which contribute to the stability and adhesion of the ink. In modern times, polymers have become ubiquitous in industrial surface problems. Gum arabic, for example, finds application as a candy coating and in lithographic processes, in addition to its continued use in inks. In this century, and particularly since the development of modern polymer science in the 20s and 30s, new synthetic polymers have found applications to diverse surface problems including colloidal stabilization, thin film stabilization and tribology.

The development of a more mature understanding of the physics of polymers since the 30s brings with it the opportunity to systematically tailor the polymers to optimize their effect on surfaces. Ideally this optimization is based on a clear understanding of the mechanisms through which the polymers affect surface properties. These mechanisms are as diverse as the different polymers used, which include simple linear polymers, polyelectrolytes, polymer gels, copolymers and complex biological polymers like those in gum arabic. However, much of the physics underlying individual polymer systems is universal, and it is this universal physics we address in this dissertation. In particular, we examine several problems involving linear polymer chains attached by one end to an interface, and the effect these chains have on the properties of the interface.

In this dissertation, we focus on the two physical problems depicted in the cartoons below, the stabilization of colloidal suspensions and thin films. These two problems have in

Figure 0.1: Polymers stabilize colloids and thin films.

common some basic polymer physics, and it is the elucidation of these underlying principles

which is the central thread of the chapters which follow. For example, polymers end-tethered to colloids as shown can adopt a large number of configurations, but when two such colloids approach one another, the number of available configurations is restricted. The entropy cost associated with this loss of configurations leads to repulsive forces between the colloids which stabilize the suspension. Thin film stabilization provides a second example. A nonwetting liquid solid pair can be compatiblized by the addition of a polymer which is soluble in the liquid and end-functionalized to adsorb on the solid. The liquid with this additive will self-assemble at the liquid solid interface, as shown, into a layer of adsorbed polymers (called a polymer brush) swollen with the small molecule liquid so as to minimally restrict the polymer configurations. The stability and thickness of the resulting film, as well as the grafting density and configuration of the polymer additive, will be determined by the balance of the adsorption energy, the configurational entropy of the polymers, and the chemical potential of the adsorbing polymer additive. These brief examples illustrate the sort of problems upon which we hope to shed some light in the chapters which follow.

This dissertation is composed of three closely related studies which we have published in the last few years. All three studies involve end-attached polymers at interfaces, and they also share a common theoretical framework. On the other hand, the physical systems they describe are quite varied, and each requires its own introduction and literature survey. For this reason, and to avoid repetition, no extensive general introduction will be given here. Instead, after a short outline, we go directly to a general exposition of the theoretical framework underlying all of the work, given in Chapter 1, and then proceed to the individual studies. In order to highlight the common themes of the different studies, a short preface will precede each chapter explaining how it fits into the thesis as a whole.

The first study, in Chapter 2, examines irreversibly adsorbed polymer brushes in athermal solvent of various types. A polymer brush consists of end-grafted polymers at an interface grafted densely enough that they are stretched away from the interface. Three primary issues are addressed: the importance of higher order corrections in the virial expansion for the excluded volume interactions between chains (beyond the second order term), the importance of interbrush penetration, and the effect of solvent size and concentration on polymer brushes. Numerical results of the type described in Chapter 1 are presented in the context of scaling arguments, and in general the calculations are limited to very simple cases in order to highlight the importance of entropic effects on polymer brush configuration

and interactions.

The second study, in Chapter 3, is an expanded examination of end-attached polymers in polymer solutions, which are discussed briefly in Chapter 2. In particular we are interested in polymers with an adsorbing group at one end whose adsorption density is set by chemical equilibrium between a reservoir and the interface (see the right-hand cartoon below). These reversibly adsorbed (or self-assembled) polymer brushes differ from irreversibly

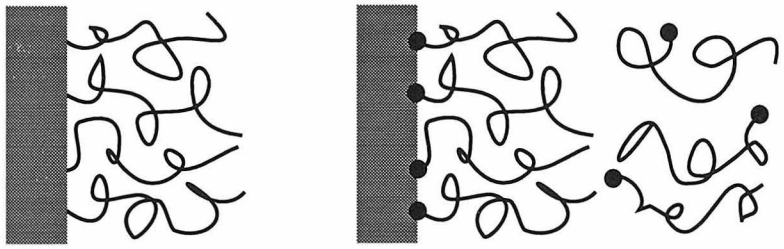

Figure 0.2: Chains may be either permanently end-grafted or reversibly end-adsorbed.

adsorbed polymer brush considered in Chapter 2 in a number of key areas, including their configurations under compression and the attendant force profiles. These brushes are examined in the context of stabilizing thin films, which share much of their basic physics with the colloidal interactions discussed in Chapter 2.

In the last chapter of the thesis, we consider the interaction forces between two plates in a semi-dilute solution of polymers each having one weakly adsorbing end-group. This problem is related to the previous study of reversibly adsorbed polymer brushes, focusing on lower grafting densities instead. This system is of special interest because it exhibits both repulsive and attractive interactions of comparable magnitude and well-separated length scales, and has important consequences for colloidal stabilization.

Chapter 1 General Theoretical Development

All of the studies described in this dissertation make use of a numerical self-consistent field approach to the calculation of configurational and thermodynamic properties of polymer solutions and blends. In this section we describe that approach, starting with a schematic explanation of the self-consistency condition.

The essential idea behind our self-consistent field treatment is to reduce the intractable many chain problem of interacting polymers into a more manageable single chain problem, by treating the interactions with other chains through a mean field. Consider, for example, a polymer brush composed of identical polymer chains end grafted to a solid surface, as shown in the cartoon below. In our model, the single tagged chain (the dark one) interacts with the other chains in the system through a mean field, π, which is dependent only on average properties of the system. For example, let us assume that π depends on the average density profile $\langle\phi\rangle$, so that $\pi = \pi(\langle\phi\rangle)$. The average density profile in turn depends upon the

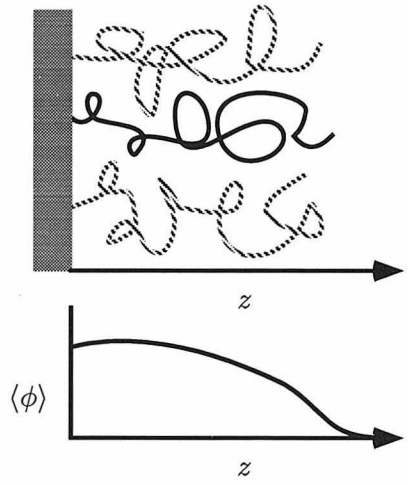

Figure 1.1: In the mean field a single tagged chain (darker) interacts with its neighbors through a mean field.

field π, which gives us a self-consistency condition, that is to find the field π^* which satisfies $\pi[\langle\phi(\pi^*)\rangle] = \pi^*$. Given $\phi(\pi)$ and $\pi(\phi)$, the self-consistent solution π^* is readily obtained by standard numerical methods. Therefore, the principal focus of the rest of the chapter is the derivation of convenient and computationally tractable self-consistent equations.

The three studies which constitute the bulk of this dissertation differ from one another in the details of the physical systems under examination, which has implications for the details of the theoretical treatment. Rather than to precisely describe the calculations for a particular study, we have chosen to derive the self-consistent equations in the simplest case for which all of the essential elements are present, namely an irreversibly grafted brush in a mixture of two monomeric solvents. The extension of this approach to the cases in the specific studies which follow is straightforward and not particularly illuminating. Therefore, these details will only be described in comments made in the individual studies. The formalism we use and variants of it are in wide use in this field; see for example Reference [1] and references therein.

Before diving into the derivation, a few comments on the general nature of our model are in order. The smallest size scale generally treated in polymer physics is the persistence length of the polymer, generally a few angstroms, which is the length scale above which a polymer appears to be a continuous flexible chain [2]. Polymers, as they are conceived within polymer physics, are a string of ideal "monomers," each separated by one persistence length and occupying one cubic persistence length. For simplicity we consider solvents of the same size as a single such monomer, and set the persistence length equal to one. Other simplifications arise from this coarse grained approach also; chemical interactions are treated with a simple nearest neighbor term since the decay length of more detailed interactions would be less than a persistence length, and the system can be treated as incompressible since these are liquid phases and will have no significant variation in their density on the scale of the persistence length. Finally, the coarse grained nature of this model makes it especially suitable for calculation on a lattice. Because no meaningful predictions can be made on length scales smaller than the ideal monomer size, using this as the lattice spacing does not result in the loss of any additional information.

Consider a system of n_P homopolymers, of degree of polymerization N and designated by the subscript P, grafted to a wall in a binary solvent mixture of two components designated by A and B. We assume that the monomers of the polymer and the solvent occupy a fixed volume of one unit, so that the total volume, V, is equal to $n_P N + n_A + n_B$ where n_A and n_B are determined by the equality of chemical potential with the reservoir which has a volume fraction of species A given by ϕ_A^r. Each polymer is parametrized with a variable s that increases discretely along its length such that the $s = 1$ end is grafted to the surface at

$z = 0$, where z is the coordinate of the direction normal to the surface and is given in units of the persistence length. The free end of the chain is at $s = N$. Using this parametrization we define functions, $\mathbf{r}_\gamma(s)$, that specify the space curve occupied by the γth polymer.

Figure 1.2: The space curve occupied by a particular chain configuration.

In order to arrive at our self-consistent field equations, we must begin with the full grand canonical partition function for the many chain system as described above,

$$\begin{aligned}\Xi(n_P, \mu_A, \mu_B) &= \frac{1}{n_P!} \prod_{\gamma=1}^{n_P} \prod_{s=1}^{N} \int d\mathbf{r}_\gamma(s) \delta[z_\gamma(1)] \sum_{n_A=0}^{\infty} \sum_{n_B=0}^{\infty} \frac{1}{n_A! n_B!} \prod_{\alpha=1}^{n_A} \prod_{\beta=1}^{n_B} \\ &\quad \times \int d\mathbf{r}_\alpha d\mathbf{r}_\beta \prod_{\mathbf{r}} \delta\left[\hat{\phi}_P(\mathbf{r}) + \hat{\phi}_A(\mathbf{r}) + \hat{\phi}_B(\mathbf{r}) - 1\right] \\ &\quad \times \exp\left\{-\beta\left[H_0(\{\mathbf{r}\}) + H_i(\hat{\phi}_P, \hat{\phi}_A, \hat{\phi}_B) - n_A\mu_A - n_B\mu_B\right]\right\}. \quad (1.1)\end{aligned}$$

For clarity I will go over this rather lengthy expression a piece at a time. First we have $\frac{1}{n_P!} \prod_{\gamma=1}^{n_P} \prod_{s=1}^{N} \int d\mathbf{r}_\gamma(s)$ which is the product of all possible configurations of each segment s of every chain γ. The delta function $\delta[z_\gamma(1)]$ constrains the first segment of each chain to lie in the $z = 0$ plane, where z is the component of $\mathbf{r}$ normal to the surface. Next, $\frac{1}{n_A! n_B!} \prod_{\alpha=1}^{n_A} \prod_{\beta=1}^{n_B} \int d\mathbf{r}_\alpha d\mathbf{r}_\beta$, allows all possible combinations and configurations of solvent molecules. This is followed by the incompressibility constraint, which is written in terms of the dimensionless monomer density operators for the polymer

$$\hat{\phi}_P(\mathbf{r}) = \sum_{\gamma=1}^{n_P} \sum_{s=1}^{N} \delta(\mathbf{r} - \mathbf{r}_\gamma(s)), \quad (1.2)$$

and the solvents

$$\hat{\phi}_A(\mathbf{r}) = \sum_{\alpha=1}^{n_A} \delta(\mathbf{r} - \mathbf{r}_\alpha). \quad (1.3)$$

The incompressibility constraint, $\prod_{\mathbf{r}} \delta\left[\hat{\phi}_P(\mathbf{r}) + \hat{\phi}_A(\mathbf{r}) + \hat{\phi}_B(\mathbf{r}) - 1\right]$, assures that no two species occupy the same point in space (which has been temporarily discretized). This constraint implicity accomplishes the difficult task of choosing non-overlapping configura-

tions for all of the polymers and solvent molecules. Next is the Hamiltonian, which has two terms, accounting for chain connectivity and local interactions respectively. $H_0(\{\mathbf{r}\})$ accounts for the chain connectivity; for a ball and spring model of the polymer, H_0 is a harmonic term which reflects the stretching of the monomers, and in a lattice model it constrains the sequential segments to be on adjacent sites. The second part of the Hamiltonian is an interaction term,

$$\begin{aligned} H_i(\hat{\phi}_P, \hat{\phi}_A, \hat{\phi}_B) &= \frac{1}{2}\sum_{\alpha,\beta}\int d\mathbf{r}\epsilon_{\alpha\beta}\hat{\phi}_\alpha(\mathbf{r})\langle\langle\hat{\phi}_\beta(\mathbf{r})\rangle\rangle \\ &= \int d\mathbf{r}\chi_{PA}\hat{\phi}_P(\mathbf{r})\langle\langle\hat{\phi}_A(\mathbf{r})\rangle\rangle + \chi_{PB}\hat{\phi}_P(\mathbf{r})\langle\langle\hat{\phi}_B(\mathbf{r})\rangle\rangle + \chi_{AB}\hat{\phi}_A(\mathbf{r})\langle\langle\hat{\phi}_B(\mathbf{r})\rangle\rangle \\ &\quad + \frac{1}{2}\epsilon_{AA}\hat{\phi}_A(\mathbf{r}) + \frac{1}{2}\epsilon_{BB}\hat{\phi}_B(\mathbf{r}) + \frac{1}{2}\epsilon_{PP}\hat{\phi}_P(\mathbf{r}), \end{aligned} \tag{1.4}$$

where $\epsilon_{\alpha\beta}$ is the interaction energy between species α and β, the sum over α and β accounts for all interaction pairs, the notation $\langle\langle\hat{\phi}_i(\mathbf{r})\rangle\rangle$ is the monomer density of species i averaged over the nearest neighbors of site $\mathbf{r}$, and χ_{AB} is the Flory interaction parameter which is commonly used in the polymer literature,

$$\chi_{AB} \equiv \epsilon_{AB} - \frac{1}{2}\epsilon_{AA} - \frac{1}{2}\epsilon_{BB}. \tag{1.5}$$

The chemical potential is obtained for an incompressible homogeneous solution in the reservoir,

$$\mu_A = \mu_A^r = \left.\frac{\partial F^r(n_A, n_B)}{\partial n_A}\right|_{n_B} = \log\phi_A^r - 1 + \chi_{AB}{\phi_B^r}^2 + \frac{1}{2}\epsilon_{AA}, \tag{1.6}$$

where $F^r(n_A, n_B)$ is the free energy of the reservoir in the mean field approximation

$$F^r(n_A, n_B) = n_A\log\phi_A^r - n_A + n_B\log\phi_B^r - n_B + n_A\chi_{AB}\phi_B + \frac{1}{2}n_A\epsilon_{AA} + \frac{1}{2}n_B\epsilon_{BB}. \tag{1.7}$$

The partition function as written in Equation 1.1 is intractable because of the coupling between segments through the microscopic density operators; $\hat{\phi}_P(\mathbf{r})$, which depends upon the configuration of all chains, and $\hat{\phi}_A(\mathbf{r})$ and $\hat{\phi}_B(\mathbf{r})$, which depend upon the positions of all A and B molecules respectively. This difficulty is overcome by replacing the microscopic density operators with macroscopic field variables (one at each point in space) which do not depend upon the microscopic configuration. This transformation uncouples the equations

inside the integral, but it transfers the difficulty to the functional integration, which will contain all of the complexity of the original problem. We avoid this difficulty by evaluating the functional integration using a saddle point approximation, where the saddle point lies on the imaginary axis.

The transformation to the macroscopic field variables is accomplished by insertion of the following identity

$$1 = \int \mathcal{D}\Phi_P(\mathbf{r})\delta[\hat{\phi}_P(\mathbf{r}) - \Phi_P(\mathbf{r})] \tag{1.8}$$

and the standard integral representation for the delta functions,

$$\delta[\Phi_P(\mathbf{r}) - \hat{\phi}_P(\mathbf{r})] = \mathcal{N} \int \mathcal{D}W_P(\mathbf{r}) \exp[iW_P(\mathbf{r})(\Phi_P(\mathbf{r}) - \hat{\phi}_P(\mathbf{r}))] \tag{1.9}$$

where $\mathcal{N}$ is a constant. Anticipating that the saddle point lies on the imaginary axis, we replace W_P, W_A, W_B and Π with their negative imaginary components. We also shift the variable W_P by $\frac{1}{2}\beta\epsilon_{PP}$ and shift the chemical potentials of A and B by $\frac{1}{2}\beta\epsilon_{AA}$ and $\frac{1}{2}\beta\epsilon_{BB}$ respectively so that the constant self-interaction terms do not appear in the self-consistent equations (they cancel out of the partition function in any case).

The partition function becomes

$$\begin{aligned}\Xi(n_P, \mu_A, \mu_B) &= \mathcal{N}^4 \int \prod_{\mathbf{r}} \mathcal{D}\Phi_P(\mathbf{r})\mathcal{D}W_P(\mathbf{r})\mathcal{D}\Phi_A(\mathbf{r})\mathcal{D}W_A(\mathbf{r})\mathcal{D}\Phi_B(\mathbf{r})\mathcal{D}W_B(\mathbf{r})\mathcal{D}\Pi(\mathbf{r}) \\ &\quad \times \exp[-\mathcal{W}(\Phi_P, W_P, \Phi_A, W_A, \Phi_B, W_B, \Pi)]\end{aligned} \tag{1.10}$$

where

$$\begin{aligned}\mathcal{W} &= -\log Q_P(n_P, W_P) - q_A(W_A)\mathcal{Z}_A - q_B(W_B)\mathcal{Z}_B - \int d\mathbf{r} \{-\beta\chi_{PA}\Phi_P(\mathbf{r})\langle\langle\Phi_A(\mathbf{r})\rangle\rangle \\ &\quad -\beta\chi_{PB}\Phi_P(\mathbf{r})\langle\langle\Phi_B(\mathbf{r})\rangle\rangle + \chi_{AB}\Phi_A(\mathbf{r})\langle\langle\Phi_B(\mathbf{r})\rangle\rangle + \Pi\left[\Phi_P(\mathbf{r}) + \Phi_A(\mathbf{r}) + \Phi_B(\mathbf{r}) - 1\right] \\ &\quad -W_P(\mathbf{r})\Phi_P(\mathbf{r}) - W_A(\mathbf{r})\Phi_A(\mathbf{r}) - W_B(\mathbf{r})\Phi_B(\mathbf{r})\}\end{aligned} \tag{1.11}$$

Q_P is the canonical partition function for the chains

$$Q_P(n_P, W_p) \equiv \frac{1}{n_P!} \prod_{\gamma=1}^{n_P} \prod_{s=1}^{N} \int d\mathbf{r}_\gamma(s)\delta[z_\gamma(1)] \exp\left[-\beta H_0(\{\mathbf{r}_\gamma\}) - \int d\mathbf{r} W_P(\mathbf{r})\hat{\phi}_P(\mathbf{r})\right] \tag{1.12}$$

$q_A(W_A)$ is the single particle partion function for the solvent,

$$q_A(W_A) \equiv \int d\mathbf{r} \exp[-W_A(\mathbf{r})] \tag{1.13}$$

and $\mathcal{Z}_A$ is the fugacity of species A

$$\mathcal{Z}_A \equiv \exp(\beta\mu_A). \tag{1.14}$$

Now we make our self-consistent mean field approximation using a saddle point method by approximating the functional integral by the maximum of its integrand on the imaginary axis. Thus the grand potential, $W = \mathcal{W}[\phi_P, w_P, \phi_A, w_A, \phi_B, w_B, \pi]$ where ϕ_P, w_P, ϕ_A, w_A, ϕ_B, w_B and π are the values of the functions for which $\mathcal{W}$ attains its minimum. Minimizing $\mathcal{W}$ with respect to the seven fields, we obtain the following seven self-consistent equations:

$$w_P(\mathbf{r}) = -\beta\chi_{PA}\langle\langle\phi_A(\mathbf{r})\rangle\rangle - \beta\chi_{PB}\langle\langle\phi_B(\mathbf{r})\rangle\rangle + \pi(\mathbf{r}) \tag{1.15}$$

$$w_A(\mathbf{r}) = -\beta\chi_{PA}\langle\langle\phi_P(\mathbf{r})\rangle\rangle - \beta\chi_{AB}\langle\langle\phi_B(\mathbf{r})\rangle\rangle + \pi(\mathbf{r}) \tag{1.16}$$

$$w_B(\mathbf{r}) = -\beta\chi_{PB}\langle\langle\phi_P(\mathbf{r})\rangle\rangle - \beta\chi_{AB}\langle\langle\phi_A(\mathbf{r})\rangle\rangle + \pi(\mathbf{r}) \tag{1.17}$$

$$\phi_P(\mathbf{r}) + \phi_A(\mathbf{r}) + \phi_B(\mathbf{r}) = 1 \tag{1.18}$$

$$\phi_A(\mathbf{r}) = \frac{\mathcal{D}q_A\mathcal{Z}_A}{\mathcal{D}w_A(\mathbf{r})} = \exp\left[w_A + \beta\mu_A\right] \tag{1.19}$$

$$\phi_B(\mathbf{r}) = \frac{\mathcal{D}q_B\mathcal{Z}_B}{\mathcal{D}w_B(\mathbf{r})} = \exp\left[w_B + \beta\mu_B\right] \tag{1.20}$$

$$\begin{aligned}
\phi_P(\mathbf{r}) &= \frac{1}{\mathcal{Q}_P}\frac{\mathcal{D}\mathcal{Q}_P}{\mathcal{D}w_P(\mathbf{r})} \\
&= \frac{1}{\mathcal{Q}_P}\frac{1}{n_P!}\prod_{\gamma=1}^{n_P}\prod_{s=1}^{N}\int d\mathbf{r}_\gamma(s)\delta[z_\gamma(1)]\hat{\phi}_P(\mathbf{r})\exp\left[-\beta H_0(\{\mathbf{r}_\gamma\}) + \int d\mathbf{r}w_P(\mathbf{r})\hat{\phi}_P(\mathbf{r})\right] \\
&= \frac{1}{\mathcal{Q}_P}\frac{1}{n_P!}\sum_{\gamma=1}^{n_P}\sum_{s=1}^{N}\delta(\mathbf{r}-\mathbf{r}_\gamma(s)) \\
&\qquad \times\prod_{\gamma=1}^{n_P}\prod_{s=1}^{N}\int d\mathbf{r}_\gamma(s)\delta[z_\gamma(1)]\exp\left[-\beta H_0(\{\mathbf{r}_\gamma\}) + \int d\mathbf{r}w_P(\mathbf{r})\hat{\phi}_P(\mathbf{r})\right] \\
&= \frac{\sum_{s=1}^{N} G(\mathbf{0},\mathbf{r};s)\int d\mathbf{r}' G(\mathbf{r},\mathbf{r}';s)}{\int d\mathbf{r}' G(\mathbf{0},\mathbf{r}';1)}
\end{aligned} \tag{1.21}$$

where

$$G(\mathbf{r}', \mathbf{r}''; s) = \prod_{s=1}^{N} \int d\mathbf{r}_\gamma(s)\delta[z_\gamma(1)] \exp\left[-\beta H_0(\{\mathbf{r}_\gamma\}) + \int d\mathbf{r} w_P(\mathbf{r})\hat{\phi}_P(\mathbf{r})\right] \tag{1.22}$$

is the Green's function or two point correlation function, which is the contribution to the overall partition function from chain segments s units long which begin at $\mathbf{r}'$, and end at $\mathbf{r}''$. The calculaton of the Green's function is accomplished following the lattice method first proposed by DiMarzio and Rubin [3]. In this approach, the polymer configurations can be exactly enumerated on a lattice and the Green's functions are obtained using a recursion relation

$$G(\mathbf{r}, \mathbf{r}'; s) = \langle\langle G(\mathbf{r}, \mathbf{r}'; s-1)\rangle\rangle \exp\left[w_P(\mathbf{r}')\right] \tag{1.23}$$

and the initial condition

$$G(\mathbf{r}, \mathbf{r}'; 0) = \delta(\mathbf{r} - \mathbf{r}') \exp\left[w_P(\mathbf{r})\right], \tag{1.24}$$

where the notation $\langle\langle G(\mathbf{r}, \mathbf{r}'; s)\rangle\rangle$ indicates the average of the Green's functions for chain segments s units long which start at $\mathbf{r}$ and end at the nearest neighbor sites of $\mathbf{r}'$. Alternately, the Green's functions can be obtained in continuous space using a bead and spring model for the polymers. In that case, $H_0(\{\mathbf{r}_\gamma\})$ would give the contribution from intersegmental stretching, but in a lattice treatment it is simply a constraint.

Some of the seven self-consistent equations can be easily solved before resorting to numerical methods. Specifically, substituting the values of w_A and w_B from Equations 1.16 and 1.17 into the expression for $\phi_A(\mathbf{r})$ and $\phi_B(\mathbf{r})$ (Equations 1.19 and 1.20) and substituting these in turn into Equation 1.18 allows π to be expressed solely in terms of the different volume fractions. Likewise, substituting this expression for π into Equation 1.15 and using this result to obtain the Green's functions in Equation 1.21, we obtain three self-consistent equations in the variables ϕ_A, ϕ_B and ϕ_P. Because of incompressibility (Equation 1.18) only two of these need to be solved numerically. The numerical procedure essentially consists of taking an initial guess at the $\phi(\mathbf{r})$ profiles, and iteratively refining these profiles to minimize the difference between them and the calculated profiles.

Once the self-consistent solution to these equations has been found, all of the thermodynamic and configurational averages are readily obtained. For example, the density profiles

of the different species are given directly from the solutions of the self consistent equations. The average location of chain ends or other configurational properties are easily obtained from the Green's functions. The grand potential of the system is obtained from Equation 1.11, and other thermodynamic properties like the lateral pressure or the forces between brushes is also readily obtained and will be discussed in later chapters.

The solution of the self-consistent equations is accomplished by standard mathematical methods, and is relatively efficient. For example, complete configurational and thermodynamic information for grafted chains of molecular weight up to several thousand monomers can be obtained using a standard computer workstation in a matter of minutes. This efficiency is obtained without sacrificing details of the configurational information, or making any assumptions about the average chain density. Indeed, the lattice treatment of the chain statistics means that *all* configurations are enumerated, and that no approximations beyond the mean-field approximation are necessary. These strengths will be highlighted in the next chapter.

Bibliography

[1] Freed, K. F. *Renormalization Group Theory of Macromolecules* Wiley: New York, 1987.

[2] de Gennes, P. G. *Scaling Concepts in Polymer Physics* Cornell University Press: Ithaca, NY, 1979.

[3] DiMarzio, E. A.; Rubin, R.J. *J. Chem. Phys.* **1971**, *55*, 4318.

Chapter 2 Polymer Brushes: Scaling, Compression Forces, Interbrush Penetration, and Solvent Size Effects

This work, published in slightly modified form under the title Polymer Brushes: Scaling, Compression Forces, Interbrush Penetration, and Solvent Size Effects, *with Z.-G. Wang, is the first study I carried out at Caltech, and provides much of the groundwork for the studies which follow. I have removed most of the theoretical development, which is described in the previous chapter, and made some other corrections and revisions to make the presentation of key results in Section 2.2.3 more consistent with results in later chapters.*

Abstract

This work discusses results of a self-consistent field calculation of conformational and thermodynamic properties of polymers end-grafted to a surface in athermal solvents. Three primary issues are addressed. First, we address the question raised recently by Carignano and Szleifer as to whether the second virial treatment of previous numerical and analytical self-consistent field theories provides an adequate description of polymer brushes. We show that, for grafted chains that are sufficiently long, there exists a broad range of grafting densities where the lateral pressure *and* the brush thickness both scale as predicted by the second virial treatment. For shorter chains (of 100 monomers or less) no distinct scaling regime is observed. A related effect due to finite chain lengths is the interpenetration of brushes upon compression and its importance to compression forces. We find that even for quite large chains (of up to 1000 monomers) there is significant interbrush penetration at high compression. However, the force profiles are relatively insensitive to penetration at such high compressions. Instead, finite chain lengths affect the interaction forces most prominently at the onset of the interactions. Next we address the crossover from wet brushes to dry brushes as the molecular weight of the solvent increases. This crossover is driven purely by entropic effects and is interpreted on the basis of the conformation of the polymeric solvent molecules in the vicinity of the brush. It is found that the state of the brush is determined by two crossover scaling variables, the ratio of the degree of polymerization of the free and grafted chains N_f/N_g, and $N_f\sigma^2$, where σ is the grafting density. Finally we investigate brush configurations and interactions in mixed solvents. It is observed that for polymer brushes in a solution of mixed free polymers and monomers, there are three distinct regimes in the interactions between two brushes. Upon the onset of the interaction, the brushes attract one another as the solvent is transferred from an unfavorable proximity to the brush to the infinite reservoir. Then there is a very rapidly increasing repulsive force as the brushes begin to overlap and the remainder of the free polymer is removed from the system. Once all of the polymeric component has been squeezed out of the brushes, the compression becomes indistinguishable from the compression of brushes in a monomeric solvent.

2.1 Introduction

Linear polymers end grafted to a surface or interface densely enough to substantially interact with each other are called polymer brushes, and have been the subject of considerable theoretical and experimental investigation in the last two decades. The crowding of the grafted polymer chains causes them to stretch anisotropically away from the surface into configurations not seen in the bulk. The anisotropy of the brush environment also strongly affects other molecules which find themselves in or near the brush, especially species with substantial configurational freedom such as free (ungrafted) polymers. This leads to modification of the properties of the surface to which the brush is attached.

Polymer brush problems are important in such diverse fields as colloidal stabilization and biomedicine. Colloids coated with a grafted polymer layer will repel one other due to unfavorable entropic interactions between their brush coated surfaces, thereby discouraging flocculation and stabilizing the suspension. These inter-particle interactions are sensitive to grafted polymer size and grafting density, and also to the solvent quality and composition. Thus, a thorough understanding of the factors influencing the brush interactions will enable a greater control of the stabilization process [1, 2]. Similarly, a careful choice of biopolymers grafted to a drug particle surface will control its interaction with other species in blood, and can effect a medically beneficial specificity in the drug's absorption [3, 4, 5].

Polymer brushes are also of theoretical importance as a model of the behavior of tethered polymers [6], arising, for example, when diblock copolymers adsorb at the interface between two incompatible fluids, or self assemble in their pure state in order to minimize contact between their incompatible blocks. In the strong segregation limit, the incompatible blocks of the copolymers will form what are essentially back to back polymer brushes. Thus the prediction of the complex copolymer morphologies is built upon the polymer brush theory and is sensitively dependent upon it [7, 8].

Experimentally, polymer brush configurations have been studied using various techniques including synchrotron x-ray fluorescence, neutron scattering and nuclear-reaction analysis while force balance techniques have provided information about polymer brush interactions (for a short review of earlier theoretical and experimental work on polymer brushes, see Milner's review article [9]).

The many aspects of the polymer brush problem have been examined by numerous

groups using a variety of approaches. In fact, the great variety of the systems under study (end-adsorbing, block copolymer or grafted chains in solvents of varying quality, composition, etc.) has perhaps obscured some fundamental entropic effects governing brush behavior. There remain a few outstanding issues regarding these basic entropic effects which we will address in this paper. The first problem we address is the adequacy of second virial treatments of the excluded volume interaction. These treatments have recently been questioned in spite of their apparent success in describing brush profiles and heights. This raises the issue of finite chain length effects, which we examine as manifested by the interpenetration of two brushes under compression. Next we address the crossover from wet brushes in small monomeric solvents to dry brushes in large polymeric solvents. The two limiting cases are very well understood; however, it is not clear whether there exist any universal features in the intermediate solvent case. Finally we examine the effect of mixed solvents on polymer brushes, emphasizing again the universal features of the problem.

Because so much work has been done on the polymer brush problem, our paper will unavoidably duplicate in some instances results which have been previously presented. This is necessary in order to present the varied brush phenomena in a unified context in which they are best understood. In the remainder of this introduction we will review some of the previous work on polymer brushes in order to frame and motivate our own work.

The first theoretical investigations of the polymer brush problem were by Alexander [10] and de Gennes [11, 12, 13] in the late seventies. These authors made the simplifying assumption that the segment density profile is a step function of thickness h and that the free ends of the chains are distributed exclusively at the end of the brush. For a weakly interacting, moderately dense brush, with grafting density σ (the number of chains per unit area) and polymerization index N_g, minimization of the free energy per chain $f \sim h^2/N_g a^2 + w\sigma N_g^2/h$ leads to $h \sim (\sigma a^2 w)^{\frac{1}{3}} N_g$. For a polymer brush in a melt of free polymer of polymerization index $N_f \geq N_g$, the brush collapses completely and the application of an incompressibility condition yields $h = N_g \sigma v$, where v is the monomer volume.

The simple scaling theory of Alexander and de Gennes was improved by Milner, Witten and Cates (hereafter MWC) [14] using an analytic local self consistent field (SCF) theory. They relax the assumption that the free ends of the chain are distributed exclusively at the extremity of the brush and instead determine their distribution self-consistently. The

chains are taken to be in the strongly-stretched long-chain limit, such that the deviation of a chain from its most probable configuration is neglected and it follows a deterministic path. Following this approach, expressions are derived for the free energy (including the prefactors) and the distributions for individual segments as well as the overall segment density profile. The resulting density profile resembles a parabola, rather than the step function assumed by Alexander and de Gennes. A similar theory has been developed independently by Semenov [15] and Zhulina and coworkers [16].

The MWC parabolic profile is consistent with experimental density measurements [17] and agrees fairly well with numerical mean field [18, 19] and computer simulation results [20, 21] with a few significant exceptions. First of all, the MWC approach accounts for excluded volume interactions using only the second virial coefficient. Thus the theory is only strictly valid for brushes of very low density, i.e., $\sigma N_g/h \ll 1$. When higher grafting densities are examined, the excluded volume interactions are underestimated compared to fully incompressible systems. Second, because the MWC theory incorporates the stretching energy through a Gaussian stretching term, the chains are infinitely extensible. This is expected to be a good approximation for moderate chain distortions, but in a moderately dense strongly-stretched brush, the chain height may be closer to the contour length than the radius of gyration. In this limit the finite extensibility of the chain is certainly important. Shim and Cates have addressed this problem in the context of the MWC model, using a non-Gaussian stretching term [22]. Finally, the segment density profile of the Milner theory terminates rather abruptly — dying off roughly linearly with $(h - z)$ — at a well defined brush height h beyond which there is no segment density. This is of course a great improvement over the discontinuity in the step function profile of the scaling theory. However, numerical calculations and simulations of finite length grafted chains show an asymptotically decaying profile which is only identically zero beyond the fully extended length of the chain (i.e., $\Phi_g(z > N_g) = 0$).

Although the MWC parabolic brush theory differs substantially from the step function scaling argument, their common use of a Gaussian stretching term and a second virial coefficient excluded volume term in the free energy balance results in equivalent scaling of overall quantities such as the brush height h. Experimental results consistent with the predicted scaling of brush height have been obtained [23]. Also numerical calculations [18, 19, 24] and simulations [20, 21] for finite length chains *appear* to obey the predicted

$h \sim N_g \sigma^{\frac{1}{3}}$ scaling. The latter has been taken as a confirmation of the adequacy of the second virial treatment of the problem. However, recent work by Carignano and Szleifer [25] has called into question this conclusion. Carignano and Szleifer use a mean field approach to calculate a probability distribution function for a set of 2.85×10^6 self avoiding chain configurations of $N_g = 50$ by minimizing the free energy subject to an overall (i.e., polymer plus solvent) incompressibility constraint. The direct application of an incompressibility constraint is equivalent to using the full virial expansion. They find good agreement with recent molecular dynamics simulations by Grest [26] for both the shape and scaling of the density profile, and for the lateral pressure Π_g of the brush. While their results for the *shape* and *scaling* of the density profile appear to agree with the $h \sim N_g \sigma^{\frac{1}{3}}$ predictions of the analytical self consistent field theory, they do not observe the scaling of Π_g with σ predicted by the second virial treatments. They conclude that, at least for chains of the size they examined, the second virial treatment of the analytical SCF theories is inadequate.

Another important question which polymer brush theories must address is the compression of two polymer brushes. This is obviously crucial to applying the polymer brush model to problems such as colloidal stabilization. The analytical MWC theory makes a good starting point. As a consequence of considering only each chain's most probable path, the MWC theory does not allow two brushes under compression to penetrate one another at all. The resulting force, like the profiles, is expected to be asymptotically correct as $N_g \to \infty$. However, for finite chains there are some corrections which must be considered.

We have already mentioned that finite chains exhibit an asymptotically decaying "tail" in their uncompressed segment density profiles. These tails will obviously result in a weak long range onset of the repulsion between two brushes not captured in the parabolic model. Secondly, for finite chains we do not expect interpenetration to be negligible. In fact, computer simulations [27, 28] and numerical results for finite chains [29] show substantial inter-brush penetration. It seems intuitively likely that the extent of such interpenetration will increase with the extent of compression, and it is not yet clear what effect it will have on the calculated interactions between two brushes.

In addition to grafted chain size and grafting density, the configuration and interactions of polymer brushes will also be determined by the properties of the solvent. Up to now we have described only polymer brushes in an athermal (good) small molecule solvent. In these conditions the polymers swell by absorbing solvent in order to maximize their entropy,

resulting in a "wet" brush state. This is in contrast to the situation of a "dry" brush, which occurs in an energetically unfavorable (bad) small molecule solvent or a large molecule solvent ($N_f \geq N_g$). In the dry brush, the grafted chains do not mix appreciably with the solvent. In the crossover region between these two cases, the extent of brush swelling is sensitive to the solvent quality, size and composition (in mixed solvent cases). The effect of small molecule solvent quality has been addressed extensively by analytical SCF techniques by Zhulina and coworkers [30], and by numerical SCF techniques by Scheutjens and coworkers [31]. Calculations have also been performed on dry brushes in large molecule solvents $N_f \geq N_g$ [32]. However, the crossover regime $1 < N_f \leq N_g$ is less well understood. In his 1980 paper on polymer brushes, de Gennes works out a scaling argument from which it is possible to derive some asymptotic scalings for some regions of parameter space [13]. Zhulina and Borisov have extended their analytical local SCF approach to the problem [33]. Also, van Zanten has recently extended the mean field approach, originally developed by Lai and Halperin [34] for grafted chains of finite extensibility, to address the polymeric solvent case in both pure and mixed solvents of varying size and quality [35]. *However, the polymer brush in a polymeric solvent is much less well understood than the small solvent case.*

The driving force behind brush collapse as the free polymer size increases is the configurational distortion of the free polymer in the anisotropic environment of the brush. This free chain stretching is also responsible for more complicated effects in mixed solvents. It was observed experimentally in 1975 that sterically stabilized colloidal suspensions (i.e., colloidal particles with grafted polymer chains on them) were destabilized upon addition of free polymer to the solvent and then restabilized at higher polymer content [1]. These effects have been studied using numerical polymer brush calculations by Scheutjens and coworkers and by analytical techniques by Wijmans and coworkers [2, 36].

A polymer brush in a mixed solvent will be selectively permeable to free species of different sizes. Thus in a solution of free polymers in a monomeric solvent, the brush will swell by absorbing monomeric solvent but will exclude the free polymers. These local changes in relative solvent concentration have important consequences for brushes under compression. As the plates are compressed and solvent is transferred to the reservoir, the overall composition of the solvent between the brushes changes. This introduces an attractive regime of the interaction which is the essential cause of the destabilization of sterically stabilized colloidal suspensions upon the addition of free polymer to the solvent.

At higher compressions the larger solvent will be completely excluded from the brushes, leading to a repulsive interaction. The details of the mixed solvent brush interactions and the application of results from this problem to the more complex colloidal stabilization problem are dependent on many factors including the relative size of the polymeric components and the grafted chains, any energetic interactions, any curvature of the grafting surfaces, etc. In order to isolate and understand the basic entropic origins of these effects, we will examine only the simplest case, $N_{f_1} = N_g$, $N_{f_2} = 1$ for athermal systems between flat walls, and relate our results back to simpler pure solvent effects.

The detailed derivation of our self-consistent field method has already been presented in the general theoretical development in the last chapter. It is worth mentioning, however, that using the method described there, it is possible to calculate the configurations and interactions of polymer brushes of up to $N_g = 1000$ in a solvent of an arbitrary number of species of arbitrary molecular weight. Although it is possible to include enthalpic interactions between the various species, as demonstrated in that development, we choose to suppress any energetic interactions in order to highlight the unique entropic effects associated with polymer brushes.

We perform our calculations on a lattice for several reasons. First, lattice calculations allow the explicit consideration of finite chain size effects. Second, the method we present retains the finite extensibility of the grafted chains. Third, the incompressibility condition built into our model implicitly includes all terms of the virial expansion. Finally, the lattice method we use need not include any vacancies, which allows us to make contact with the bulk free energy expressions for polymer mixing. Self consistent theories which treat more accurately the single chain's configuration have been developed by Carignano and Szleifer [25], but for our purposes the simpler lattice model suffices and has the additional benefit of allowing chain lengths up to $N_g = 1000$, which bring us clearly into the long chain limit described by the analytical theories.

2.2 Results/Discussion

In this section we present numerical results for polymer brushes in pure solvent and binary solvent mixtures. The principal points of interest are each presented below in subsections. First we test the adequacy of analytical predictions based solely on second virial interactions

for polymer brushes in a good monomeric solvent by an examination of the scaling of brush height h and lateral pressure Π_g with grafting density σ. Then we examine the importance of finite chain effects, and especially interbrush penetration, on the interaction profiles for two brushes under compression in an athermal solvent. Next we examine the scaling of polymer brushes in pure solvents of arbitrary molecular weight $1 \leq N_f \leq N_g$; in particular the collapse of the brush as N_f increases is elucidated by examining the unfavorable stretching of a free chain inside the brush. And finally we examine the effect of a mixed solvent on the configuration and interaction profiles of polymer brushes.

2.2.1 Monomeric Solvent

Scaling Relations

As mentioned previously, the scaling relations for a polymer brush in a (good) monomeric solvent were first derived by Alexander [10] and de Gennes [11]. These authors made the simplifying assumptions that the segment density profile was a step function, and that the free ends of the chains were distributed exclusively at the outer extremity of the brush. These assumptions lead to the prediction that $h \sim N_g \sigma^{\frac{1}{3}}$.

The more detailed theory of Milner, Witten and Cates (MWC) [14] relaxes the assumption in the Alexander and de Gennes theory that the free ends of the grafted chains are distributed exclusively at the extremity of the brush. Rather the free end distribution is determined using an analytic self-consistent theory which is asymptotically correct in the $N_g \to \infty$ limit. This leads to a more physically reasonable parabolic density profile for the brush which compares well with a lattice self consistent field calculation by Hirz [19] using the second virial interaction. Both the scaling argument of Alexander and de Gennes and the MWC parabolic brush model account for excluded volume interactions solely by a second virial interaction. This leads to their common scaling for $h(\sim N_g \sigma^{\frac{1}{3}})$ and other average quantities.

Clearly, the $h \sim N_g \sigma^{\frac{1}{3}}$ is valid only within a certain range of grafting density. In particular, the brush height h should scale as a linear power of σ as $\sigma \to 1$. On the other hand, when σ is so small that the chains hardly touch each other, h should be of the order of the radius of gyration and should be independent of σ. The average lateral distance between grafted chains is roughly $\sigma^{-\frac{1}{2}}$. In order to have substantial stretching of

the chain, the natural radius of gyration of the chains must be larger than this distance, i.e., $\sigma \gg N_g^{-2\nu} a^{-2}$. To be consistent with our mean field calculation, we take $\nu = \frac{1}{2}$.

In the high density region, in order that the effects of third and higher virial coefficients are insignificant, we must have

$$\frac{N_g \sigma}{h} \gg \left(\frac{N_g \sigma}{h}\right)^2, \qquad \text{or} \qquad \frac{N_g \sigma}{h} \ll 1.$$

A self consistent criterion is obtained by substituting $h \approx N\sigma^{\frac{1}{3}}$ into the above inequalities, yielding, $\sigma^{\frac{2}{3}} \ll 1$ or $\sigma \ll 1$. Thus we expect the $\sigma^{\frac{1}{3}}$ scaling to hold for $N_g^{-1} \ll \sigma \ll 1$. *Note, however, that a virial expansion to any number of terms will still result in* $h \sim N_g$. Thus we expect only a lower bound $N_g^{-1} \ll \sigma$ to apply to this scaling. More importantly, this implies that only the $h \sim \sigma^{\frac{1}{3}}$ can be taken as evidence of the adequacy of the second virial treatment [13].

From the preceding argument we conclude that in order to have a distinctive range of σ where h scales as $\sigma^{\frac{1}{3}}$, the grafted chain must be quite long. Moreover, the scaling of h with σ is neither the only test of the second virial treatment, nor a sufficient proof that this treatment has captured the most important physical effects. Indeed, the question of the conditions (grafted chain length, grafting density, and in some cases solvent quality) under which the scaling arguments apply, and even the existence of any such range of conditions, has been a subject of some controversy recently.

The original MWC paper reports some results of Hirz for chains of $N_g = 200, \sigma = 0.1$ which obey the $\sigma^{\frac{1}{3}}$ scaling for σ varying over a factor of six [14, 19]. However, because of the weak dependence on σ, this corresponds to a variation of brush height of less than a factor of two. For this reason it is desirable to examine the scaling of other quantities than the brush height to test the predictions of scaling theories based on the retention of only the second virial coefficient. There are several possible quantities for which scaling predictions exist, including the free energy of the grafted chains and the lateral pressure of the brush, which is defined as

$$\Pi_g \equiv -\left(\frac{\partial G}{\partial A}\right)_{n_g}. \tag{2.1}$$

Shaffer has recently published Monte Carlo simulation results which suggest that the scaling of the free energy per chain is well described by second virial theories, even at fairly short chain lengths ($N_g \leq 80$) [42]. In molecular dynamics simulations by Grest, however,

chains of 50 units did not obey the predicted scaling of brush height with grafting density at constant surface pressure. Of course the conditions under which the predicted scaling is observed is not necessarily the same for every quantity. Indeed, even the presentation of the data (for instance which combinations of variables are plotted) can affect whether the predicted scaling appears to hold. However, if the second virial picture is adequate, there should be some threshold conditions for chain length and grafting density above which the scaling of all properties is as predicted.

Carignano and Szleifer [25] have examined the scaling of Π_g with σ for chains of $N_g = 50$ in Θ solvents in an attempt to account for inconsistencies between the second virial treatment predictions and the simulation results of Grest [26] for lateral pressure. Both the scaling argument and the MWC parabolic brush theory predict the scaling $\Pi_g \sim N\sigma^x$, where $x = 5/3$ in order to be consistent with our mean field approach or $x = 11/6$ from the scaling theories [10]. In a Θ solvent both approaches predict $x = 2$. Using the fully incompressible method mentioned in the introduction, they are able to reproduce the simulation results of Grest [26]. However, they find no distinct regime exhibiting the anticipated $\Pi \sim \sigma^2$ scaling. Rather they find a continuously changing σ dependence, which they attribute to the importance of later terms in the virial expansion. As further evidence of this assertion, they show that they can obtain good agreement with pressures calculated for a *parabolic* profile using the full virial expansion. It should be noted, however, that the parameter used to obtain this fit is not that obtained in the MWC theory, and gives poor agreement for brush height. They conclude that while the MWC and other analytical theories correctly predict the *shape* and *scaling* of the profile, they are inadequate for the prediction of more sensitive quantities, including the lateral pressure, at least for the chain lengths they considered ($N_g \leq 50$).

In order to test this conclusion, and to determine if and when the second virial treatment is adequate, we have calculated the scaling of both the brush height and the lateral pressure for brushes of $N_g = 200$ and 1000 (we have also calculated the pressure in the $N_g = 50$ case for comparison). In Figure 2.1 is plotted the brush height h versus the grafting density σ on a log-log scale. The height h is defined as twice the moment of the segment density profile, i.e., $h \equiv 2 \times \sum_z z\Phi_g(z)$. This definition ensures that for a step function profile h is simply the width of the step function. In the $N_g = 200$ case, we observe, as described by MWC, a range of σ of almost one order of magnitude which scales nearly as $\sigma^{\frac{1}{3}}$. However, the

scaling must pass through this value, and for $N_g = 200$ a distinct regime of the predicted scaling is not clearly identifiable. For the $N_g = 1000$ case, on the other hand, the regime in which the $\sigma^{\frac{1}{3}}$ scaling applies has broadened considerably, and supports the validity of the second virial approach in this regime.

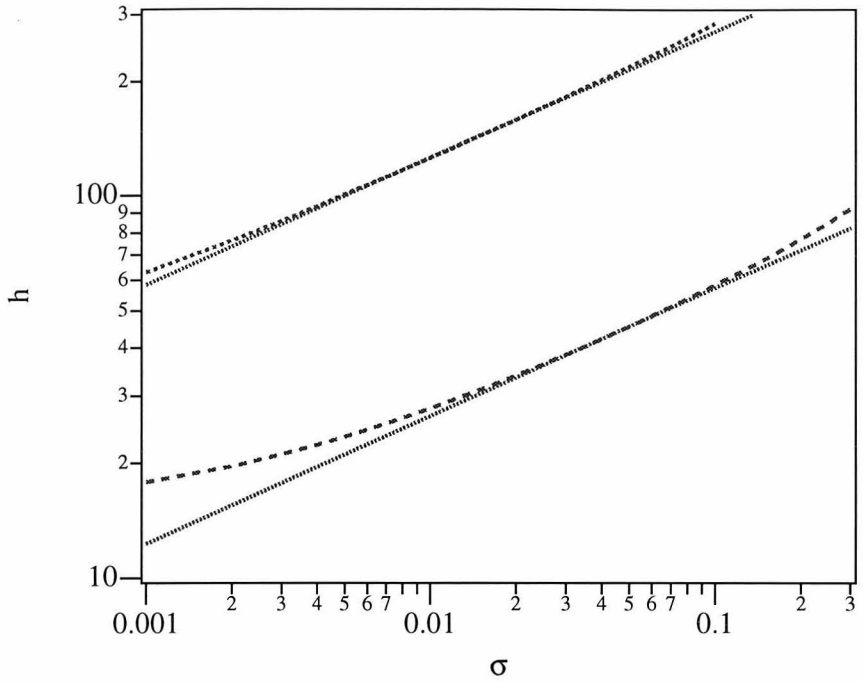

Figure 2.1: The brush height h versus grafting density σ for $N_g = 200$ (dashed line) and $N_g = 1000$ (dotted line) plotted on a log-log scale with the predicted $N_g\sigma^{\frac{1}{3}}$ scaling (small dotted lines).

Next we look for an equivalent regime exhibiting $\Pi_g \sim \sigma^{\frac{5}{3}}$ scaling as predicted by the second virial coefficient. In Figure 2.2 is plotted Π_g versus σ on a log-log scale. For $N_g = 50$ the scaling passes through $\sigma^{\frac{5}{3}}$ very quickly, confirming the finding of Carignano and Szleifer that no scaling existed in that case. However, for $N_g = 200$ the scaling passes through this value much more slowly, and for $N_g = 1000$ there is almost two orders of magnitude which exhibit nearly the predicted scaling.

We conclude that because of the weak dependence on σ and the very general linear scaling with N_g, the $h \sim N_g\sigma^{\frac{1}{3}}$ scaling *appears* more general than the validity of the second virial treatment. In fact, the assumption that only the second virial coefficient interaction is significant appears to be justified over a non-vanishing range of σ only for rather large N_g (of at least several hundred units). This means that for many experimental and practical

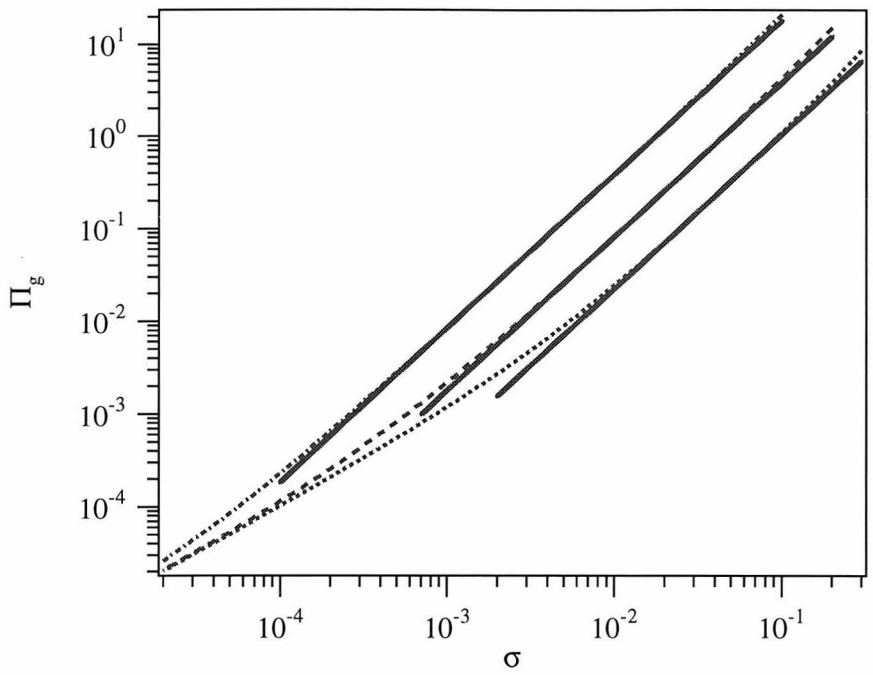

Figure 2.2: The lateral pressure Π_g versus grafting density σ for $N_g = 1000$ (dot dashed line), $N_g = 200$ (dashed line) and $N_g = 50$ (dotted line) plotted on a log-log scale. The solid lines show the predicted $\sigma^{\frac{5}{3}}$ scaling.

circumstances, a more detailed treatment than the second virial must be considered in order to correctly predict brush free energies and pressures. However, for larger chains ($N_g \geq 1000$) the second virial approach does appear appropriate.

Brushes Under Compression

The most important direct application of polymer brushes is the steric stabilization of colloidal suspensions. Two surfaces coated with grafted polymer layers in a good monomeric solvent will repel one another due to unfavorable steric interactions between the two brushes as they begin to overlap. An understanding of the dependence of these interbrush interactions on the brush parameters (i.e., brush size N_g and density σ in the athermal monomeric solvent case, and more generally the solvent quality, size and concentration as well) is clearly of great importance, and has been investigated theoretically [9, 14, 24], experimentally [5, 43], and by computer simulation [27, 44, 45] by many groups including those mentioned earlier.

An important and unresolved question in the consideration of interbrush interactions is the extent to which the two brushes interpenetrate. The analytical theory of MWC,

which treats brushes in the long chain limit, allows no interbrush penetration at all. This assumption arises from the neglect of all but the most probable path for each chain. On the other hand, numerical treatments [2] and simulations [27, 28] of finite length chains show considerable interbrush penetration. It is intuitively clear that interbrush penetration will be unavoidable for relatively short chains. However, it is not so clear at what chain lengths or grafting densities it will become negligible.

In order to determine the extent and importance of interbrush penetration, we have calculated the segment density profiles and force curves for two brushes under compression. In each case the calculation is performed twice, allowing and disallowing interpenetration. The force is defined $F = -\frac{\partial G^{ex}}{\partial L}$ where the brush compression L is equal to $\frac{1}{2}$ the distance between the two plates. In order to disallow interpenetration, we calculate the interaction profile of a single brush with a hard wall a distance L from the brush, since in the absence of interpenetration this is identical to one half of a two brush compression. We performed this calculation for brushes of $N_g = 200$ and $N_g = 1000$ units in monomeric solvent with a grafting density of $\sigma = 0.1$ which falls in the strongly stretched regime for both brush lengths. In Figure 2.3 are presented the scaled segment density profiles for the two brush lengths as they are compressed. In each case curves are presented for brushes which were allowed (solid lines) and not allowed (dotted lines) to interpenetrate. In the upper frames the brushes are uncompressed and therefore there is no difference between the penetrating and nonpenetrating profiles. However, as the compression is increased, the extent of penetration becomes larger and larger. As expected these effects are more pronounced in the smaller brush ($N_g = 200$). In fact, the rather extreme lack of interpenetration in the $N_g = 1000$ and the sharp profile for the most compressed brush confirm the assumption that interpenetration is negligible for $N_g \to \infty$.

The profiles in Figure 2.3 gives us some insight into the extent of interbrush penetration for substantially compressed brushes. On the other hand, we expect the effect of interbrush penetration to have important effects on brush interactions at very slight compressions as well. In Figure 2.4 are plotted the force curves for the compression of the two brushes described above. In both cases the force is calculated both allowing and disallowing interpenetration. We observe first that for the compression values at which the most significant interpenetration was observed ($L/N_g\sigma^{\frac{1}{3}} = 0.54$), the force curves for all four cases are nearly identical. However, at the onset of the interbrush interactions, both chain size and interpen-

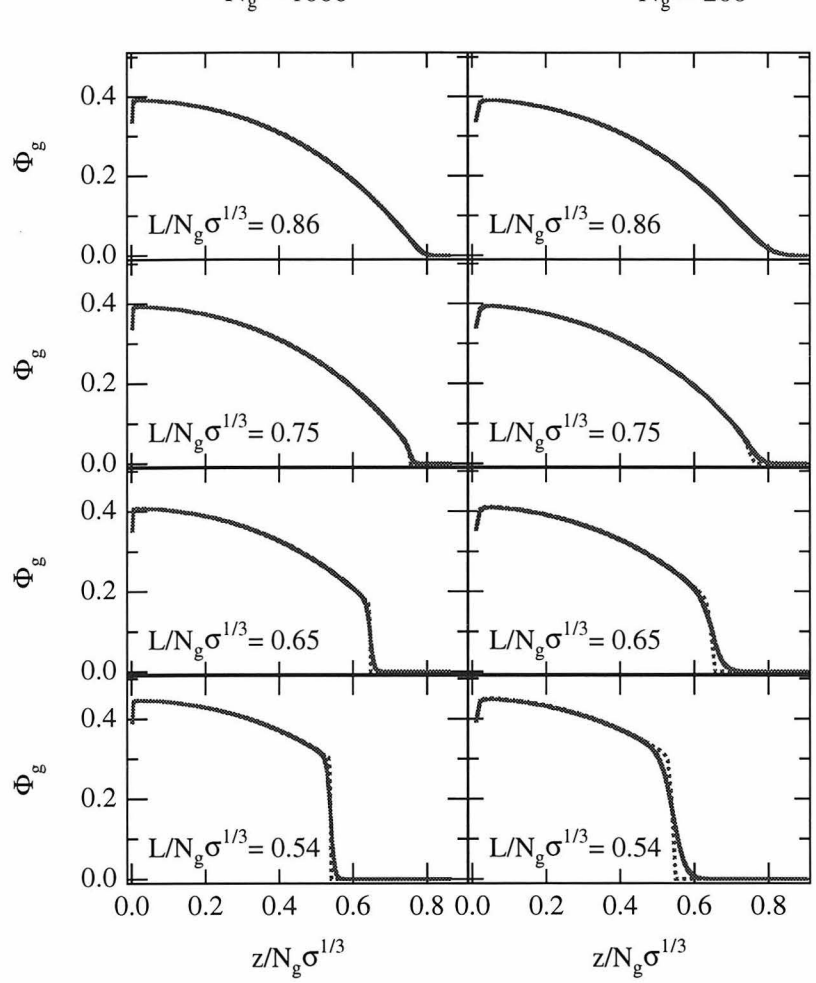

Figure 2.3: The segment density profiles for brushes of $N_g = 1000, 200$ at various compressions in monomeric solvent with $\sigma = 0.1$ both allowing (solid line) and disallowing (dashed line) interbrush penetration.

etration affect the interaction. The shorter chain has a longer range repulsive interaction with a more gradual onset regardless of interpenetration. This occurs because the shorter chains deviate more from the parabolic profile observed in the long chain limit. In this limit a well defined brush height is predicted, beyond which there will be no segment density. However, simulations and calculations for *finite* length chains predict a smoothly decaying asymptotic "tail" as seen in the upper right frame of Figure 2.3. This tail becomes more prominent for shorter chains (e.g., see the upper right frame of Figure 2.3), leading to an earlier onset of repulsion. These tails will interact with each other, creating a weak long range repulsive interaction, even before the parabolic portion of the profiles interact. These conclusions are consistent with experimental findings [5].

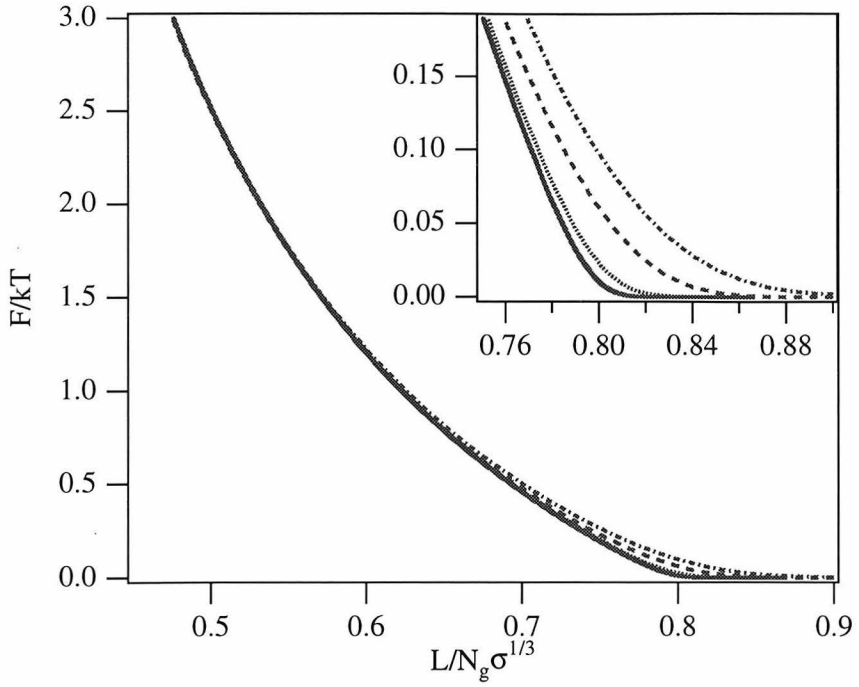

Figure 2.4: The force per unit area is plotted versus the compression L scaled by N_g. The inset shows the onset region in an expanded scale. Brushes of $N_g = 200$ (dashed and dot-dashed lines) and 1000 (solid and dotted lines) are shown allowing (solid and dashed lines) and disallowing (dotted and dot-dashed lines) interpenetration.

The onset of the repulsive interaction is especially sensitive to the question of interpenetration (see inset of Figure 2.4). This occurs because the asymptotically decaying tails of the brushes interact very weakly with one another. However, when interpenetration is disallowed, they are being compressed, in effect, by a hard wall. Thus at separations where only the asymptotic tails of the brushes are compressed, the effect of interpenetration will be substantial. From Figure 2.3 we see that the asymptotic tail of these profiles begins at $L/N_g\sigma^{\frac{1}{3}} = 0.8$, and it is observed in the inset of Figure 2.4 that the effect of interpenetration is quite strong beyond this point. The length and density of this tail are much greater for the smaller brush, and consequently the effect of interpenetration is greater as well. At greater compressions the forces associated with the compression of the parabolic portion of the brush dominate the end effects, and interpenetration becomes insignificant.

The extent of equilibrium interbrush penetration has implications for the dynamics of polymer brush compression as well as for the equilibrium properties. Interpenetration will presumably occur by a slow mechanism involving chain rearrangement, while overall compression of the individual brushes can occur rapidly along the existing contour of the grafted

chains. Thus we expect rapid compression to occur initially without substantial interpenetration, with interpenetration occurring on longer time scales leading to a relaxation of the repulsive interbrush forces.

Before continuing it is worth mentioning the importance of short chain results. Although the use of relatively short chains ($N_g \leq 200$) in some studies has been motivated by the inaccessibility (experimental or computational) of longer chains, many of these studies have chosen such chain lengths because of the intrinsic importance of the system they address. An important case is the application of polymer brush theory to biomedical problems [5] where medical factors limit the choice of polymers. In such a case the analytical theories derived in the long chain limit are not appropriate, and numerical calculations such as those described here will be required to accurately understand the details of brush configurations and interactions.

2.2.2 Polymeric Solvent

The behavior of a polymer brush is complicated by the consideration of variable solvent conditions. A great deal of work has been done on brushes in monomeric solvents of varying quality (i.e., with varying enthalpic interactions with the brush), both analytically [30], numerically [22, 25], experimentally [46] and by computer simulation [47]. The case of athermal polymeric solvents is, by contrast, relatively unexplored. De Gennes [13] has made some preliminary scaling arguments regarding the intermediate size polymeric solvent conditions $1 < N_f < N_g$, and Zhulina and Borisov [33] have developed an analytic self consistent field theory for approaching the problem. Brush behavior in a polymeric solvent has also been studied experimentally using nuclear reaction analysis [48].

In contrast to a polymer brush in a (good) monomeric solvent—which will absorb solvent and stretch to minimize excluded volume interactions—a polymer brush in a polymer melt of chains length ($N_f \geq N_g$) will collapse and expel nearly all of the solvent, leading to trivial scaling determined by incompressibility $\Phi_g \approx 1$ and $L \approx N_g\sigma$. This occurs primarily because the anisotropic environment of the brush stretches the polymeric solvent into unfavorable configurations. The solvents respond by leaving the brush, leading to its gradual collapse as the solvent distortions become more severe and the configurational entropy of the solvents becomes more important. In Figure 2.5 are displayed the segment density profiles for a brush of $N_g = 400$ monomers at grafting density $\sigma = 0.1$ for variable solvent size as indicated. At

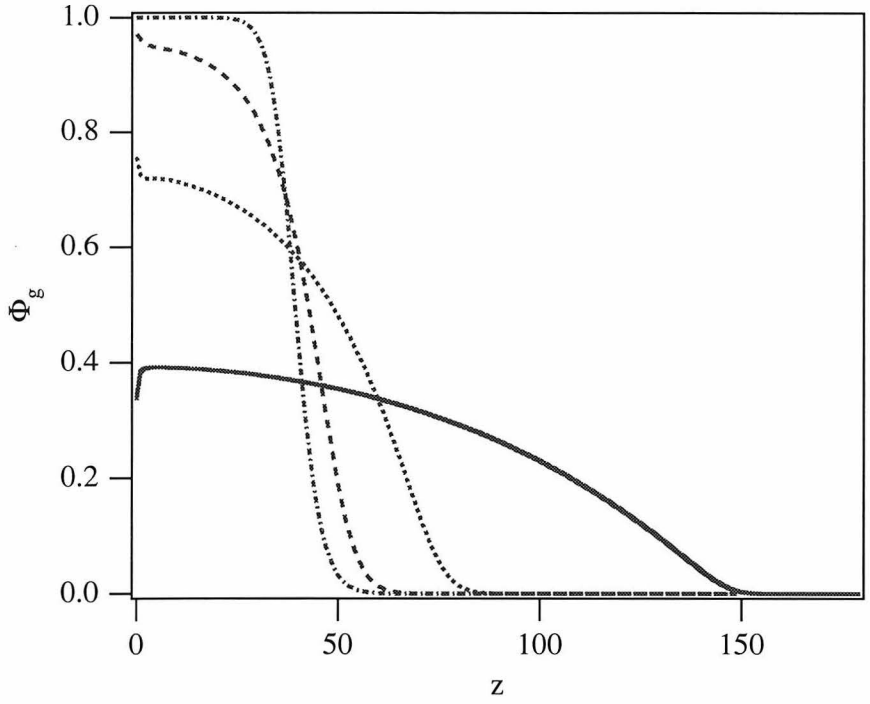

Figure 2.5: Segment density profiles for a brush ($N_g = 400, \sigma = 0.1$) are shown in solvents of $N_f = 1$ (solid line), $N_f = 10$ (dotted line), $N_f = 50$ (dashed line), $N_f = N_g = 400$ (dot-dashed line).

intermediate solvent molecular weights, the brush still absorbs solvent and stretches, but as N_f goes to N_g, the solvent leaves the brush, which is collapsed to a step function like profile with no absorbed solvent.

In the case of a polymer brush in a polymeric solvent, it is not possible to make the simple scaling predictions which have been made in the monomeric case. We can, however, determine the relevant scaling variables and make some predictions for certain limits. Following the treatment of de Gennes, we construct an expression for the brush and solvent free energy by adding the stretching and compression terms for the brush to the free energy of mixing for the brush and the solvent. As in the monomeric solvent case, we begin with the step function profile approximation so that $\Phi_g = N_g\sigma/h$ and $\Phi_f = 1 - \Phi_g$. We write the free energy

$$f/kT = \frac{h}{\sigma N_f}\Phi_f \log \Phi_f + \frac{h^2}{N_g} + \frac{N_g}{h^2} \tag{2.2}$$

where the first term is the free energy of mixing for the free polymer (the grafted chain has no translational freedom and therefore no such term), the second is the elastic energy of stretching, the last is the elastic energy of compression, and numerical constants of order

unity have been omitted. After minimization of the free energy with respect to h and some algebra, we obtain

$$\Phi_g \ln(1-\Phi_g) + \Phi_g^2 - N_f\sigma^2 + \frac{N_f\Phi_g^4}{N_g^2\sigma^2} = 0.$$

From this expression it follows that Φ_g and h can be written in terms of an unknown function g of two scaling variables,

$$\Phi_g = g(N_f\sigma^2, \frac{N_f}{N_g}) \qquad \text{and} \qquad h = N_g\sigma g^{-1}(N_f\sigma^2, \frac{N_f}{N_g}). \tag{2.3}$$

The validity of the approximations inherent in this approach are confirmed by the data presented in Table 1. The individual input parameters, N_g, N_f and σ are varied while holding the scaling variables $X \equiv N_f/N_g$ and $Y \equiv N_f\sigma^2$ constant, and the reduced brush height $h/N_g\sigma$ is essentially unchanged.

Table 2.1: The reduced brush height scales with N_f/N_g and $N_f\sigma^2$

N_f/N_g	$N_f\sigma^2$	N_g	N_f	σ	$h/N_g\sigma$
0.02	0.0036	800	16	0.015	4.12
0.02	0.0036	450	9	0.020	4.16
0.02	0.0036	200	4	0.030	4.26
0.02	0.0036	50	1	0.060	4.52
0.1	0.2304	1000	100	0.048	1.300
0.1	0.2275	810	81	0.053	1.306
0.1	0.2304	640	64	0.060	1.306
0.1	0.2333	490	49	0.069	1.306
0.1	0.2304	360	36	0.080	1.314
0.1	0.2304	250	25	0.096	1.322
0.1	0.2304	160	16	0.120	1.332
0.1	0.2304	90	9	0.160	1.352

We have examined the dependence of the brush height h with these variables and have made the following scaling observations. For $\sigma^2 N_f \gg 1$ the solvent will not penetrate the brush at all regardless of the other scaling variable N_f/N_g, resulting in the dry brush scaling $h \sim N_g\sigma$. For large free polymers $N_f/N_g \geq 1$ grafted sparsely enough that the grafted chains interact with the solvent, the free chains screen the excluded volume interaction of the grafted chains, leading to the ideal scaling $h \sim N_g^{\frac{1}{2}}$. And finally, in the small solvent swollen brush regime, we have the scaling $N_f \sim N_g\sigma^{\frac{1}{3}}N_f^{-\frac{1}{3}}$ scaling. This last result was

predicted by de Gennes [13] and has been observed experimentally by Budkowski et al. [48].

The apparent success of the scaling argument in predicting the average description of the brush, i.e., brush height h, leads us to wonder whether the scaling behavior may not be more universal. Recall that the scaling of the Flory argument is preserved in the more detailed MWC theory. Thus we plot in Figure 2.6 the reduced segment density profiles from several of the brushes described in the lower group of data in table 1. It is observed that despite

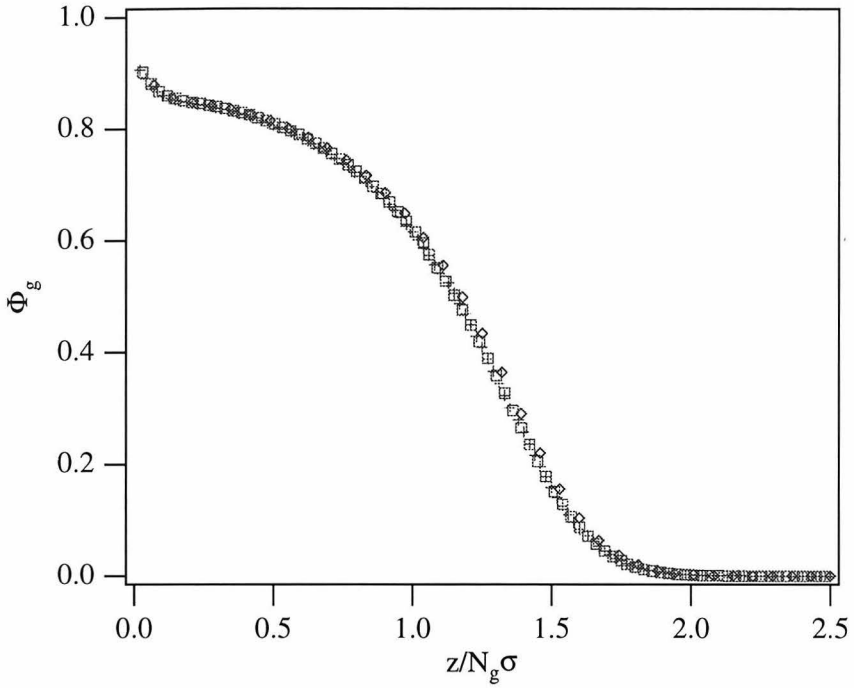

Figure 2.6: The segment density profiles for the brushes described in table 1 are plotted against $z/N_g\sigma$; + ($N_g = 1000, N_f = 100, \sigma = 0.048$), □ ($N_g = 640, N_f = 64, \sigma = 0.060$), ◇ ($N_g = 250, N_f = 25, \sigma = 0.096$).

the fact that the scaling argument treated the brush in an average way—equivalent to assuming a step function density profile—the *shape* of the profiles are superimposable when the quantities plotted are appropriately scaled. Thus it seems that not only the aggregate properties, such as brush height, but also the density profiles themselves are determined by the scaling combinations N_g/N_f and $N_f\sigma^2$ (with the exception of some extreme cases such as $\sigma \approx 1$).

This is an especially interesting observation since the scaling of the extreme cases, $N_f = 1$ or $N_f \geq N_g$, is relatively trivial. In the good monomeric solvent case, in the regime where second virial interactions dominate, the scaling follows quite directly from the free

energy expression given in the introduction. The dry brush scaling follows trivially from incompressibility, and is therefore certain to be universal. However, the existence of a universal scaling regime for grafted chains in intermediate solvent conditions, where a free polymer term enters the free energy expression, is far less obvious.

Solvent Stretching

As has already been mentioned, the unfavorable stretching of the polymeric solvent coils in the anisotropic environment of the brush drives the solvent out leading to the collapse of the brush. It is of interest then to know the extent of this stretching and how it compares to a grafted chain. First, recall from the theory section that, in our calculation, the only difference between a grafted and a free chain is that one end of the grafted chain is fixed at the wall. Thus a solvent chain of $N_f = N_g$ which finds itself with one end in layer $z = 1$ will be stretched to precisely the same extent as a grafted chain. Chains not so close to the wall will be less distorted, and solvent chains in the isotropic environment sufficiently far outside the brush are completely unstretched. The relative solvent stretching (in the z coordinate) $r(z)$ is given by the ratio of the square root of the mean squared end to end distance of the solvent chains as a function of the location of one end, and the bulk value of this same quantity,

$$r(z) = \frac{\sqrt{\mathcal{Z}_f \sum_{z'} (z - z')^2 G(z, z'; N_f)}}{\sqrt{(N_f - 1)/3}}, \tag{2.4}$$

where $\sqrt{(N_f - 1)/3}$ is the end to end distance in the bulk.

In Figure 2.7a and b are plotted the relative solvent stretching $r(z)$ versus end location for a free polymer $N_f = 500$ in a polymer brush ($N_g = 500, \sigma = 0.05$). In Figure 2.7a the solvent is purely polymeric, and in 2.7b is a very dilute polymer solution in monomeric solvent ($\Phi_f^{res} = 10^{-5}$) with $\sigma = 0.05$. For both solvent conditions the relative stretching goes up sharply inside the brush, reaching maximum values of 1.7 and 10 times their value in the bulk respectively. The free polymer is substantially more stretched in the wet brush than in the dry brush. This result is required by the equivalence of the free chain with an end at the wall with a grafted chain. Thus, even when a brush is highly swollen and has a relatively low segment concentration, its extreme anisotropy makes it a highly unfavorable environment for a free polymer. There are two other features of interest on Figures 2.7a

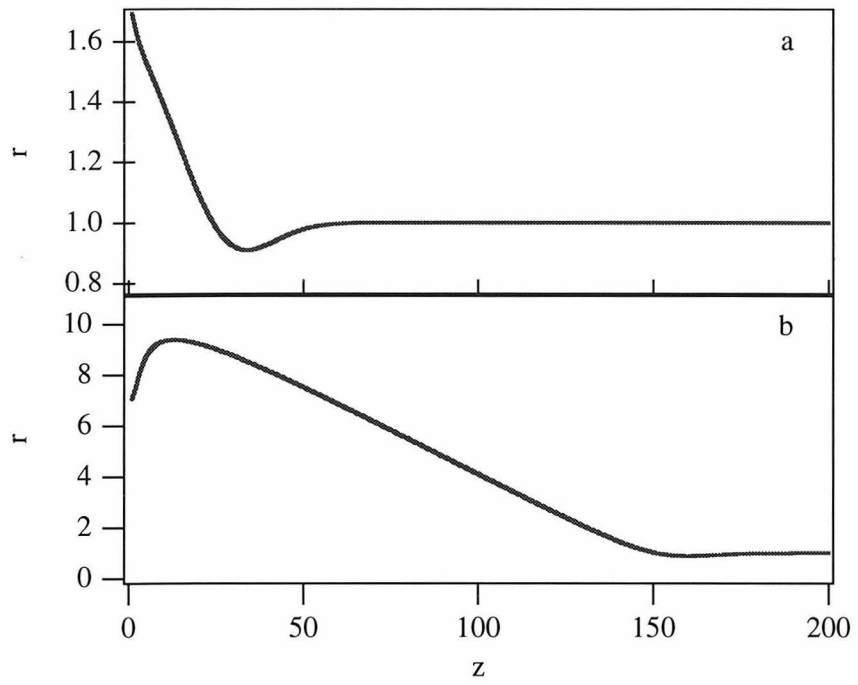

Figure 2.7: The solvent stretching in the z direction, r, is shown as a function of solvent end position for a free chain of $N_f = 500$ in a polymer brush in: **a**, a polymer melt solvent ($N_g = N_f = 500, \sigma = 0.05$); **b**, a very dilute monomer polymer/monomer blend solvent ($N_g = N_f = 500, \sigma = 0.05, \Phi_f^{res} = 10^{-5}$).

and 2.7b, the minimum at the brush end in 2.7a and the dip in the extent of stretching right at the wall in 2.7b. These features have the same origin, which is best understood by analogy to the case of a free polymer near a hard wall. Because polymer configurations which intersect the wall are disallowed, configurations lateral to the wall become relatively favored. This results in a swelling of the polymer in the lateral directions and a slight shrinkage in the direction perpendicular to the wall. The configurations of a polymer melt near a wall and other related problems have been studied recently by Theodorou [49]. This is also what is happening at the end of the brush, which functions as a sort of "soft wall," in Figure 2.7a. This "wall" in the case of the wet brush in Figure 2.7b is so soft that the stretching resulting from the anisotropy of the environment cancels the "soft wall" effect. However, lateral expansion occurs at the real wall ($z = 0$) in this case. This occurs because the dip in the brush segment density near the wall favors polymer configurations which swell in this region rather than moving into the denser brush region farther from the wall. In the polymer melt case there is no such dip in brush segment density at the wall, and consequently no such lateral stretching.

In addition to driving the collapse of the brush, the solvent stretching has several other implications which merit discussion. First of all, the anisotropic environment of the brush and the distorted configurations of species within it will affect the chemical reactions which take place there. This is of special interest in biological systems, since biopolymer reactivity is highly configuration dependent. Second, the solvent stretching in a brush will selectively affect the diffusion of polymeric species across membranes coated with a grafted polymer layer, favoring the diffusion of smaller species since these are better able to penetrate the brush.

Finally, solvent stretching within a brush has implications for the compression forces of polymer brushes. The first and most obvious effect of increasing the solvent size is to collapse the brush, leading to more dense brushes and a compressed and therefore steeper repulsive interaction profile. A second, more subtle effect must also be considered. As the brushes are compressed, the solvent is transported from the vicinity of the brush to an isotropic reservoir of bulk solvent. This eliminates the stretching of those solvent molecules and lowers the overall free energy accordingly. As long as the free polymer is pure, incompressible and not larger than the grafted chains, $N_f \leq N_g$, this will always be a smaller effect than the brush compression, leading to an overall repulsive interaction between the brushes. However, when $N_f > N_g$ the configurational entropy of the solvent can dominate that of the grafted chains, resulting in an attractive interaction between the two brushes. These dry brush effects (where $N_f \geq N_g$) have been studied by Shull using a numerical SCF theory for chains of up to 800 units long [32].

2.2.3 Mixed Solvents

The interaction between two polymer brushes (where $N_g \geq N_f$) in a pure solvent is always repulsive because the favorable free energy change of the polymeric solvent, upon being transferred to the isotropic reservoir, is more than offset by the increase in the unfavorable steric interactions between the two brushes. In a mixed solvent, however, local variation in the relative concentration of the solvent species in and near the brush complicate the situation, and can lead to an attractive region in the compression force profile. In order to isolate the entropic effect of mixed solvents, without introducing too many additional parameters, we will focus on a mixed solvent of two chemically identical species, a majority monomeric component, and a minority polymer solvent of the same molecular weight as

the grafted chains, both in chemical equilibrium with a reservoir of volume fraction of free chains Φ_f^{res}.

The interactions between polymer brushes in a dilute polymer solvent have been examined before by a number of groups including van Lent, Israels, Scheutjens and Fleer [2], who use a numerical SCF theory similar to our own and also summarize the previous work on the problem. However, they calculate interaction potentials for grafted chains in a mixed solvent with polymeric solvent molecules larger than the grafted chains. As mentioned in the previous section, it was subsequently shown by Shull [32] that even in an unmixed polymeric solvent of the sizes they examine ($N_f \gg N_g$), there will be an attractive portion of the interaction profile. To emphasize the effect of mixed solvents and eliminate the possibility of a molecular weight induced attraction, we consider $N_g \geq N_f$ in a monomeric solvent and vary only Φ_f^{res}.

We have already examined the stretching of a pure polymeric solvent in a polymer brush environment and the resulting collapse of the brush. In a mixed solvent system, however, the polymeric component can leave the vicinity of the brush while the brush remains swollen with the monomeric component. For solvents with a large size disparity, the brush will act as a semi-permeable membrane, completely excluding the polymeric component, while swelling with the monomeric component. The brush is then compressed by the osmotic pressure of the excluded polymer solvent, leading to a compressed density profile. In Figure 2.8 are shown the segment density profiles for a polymer brush (solid line), and the polymeric component of the solvent (dotted line). The first feature to notice in the uncompressed profile in the upper left is that while the brush is swollen considerably from its collapsed dry brush configuration in a pure polymer melt ($h = 146$ versus $h = 53$), it is compressed significantly relative to its size in a pure monomer solvent ($h = 219$) due to osmotic pressure of the polymeric solvent excluded from the brush. In fact, its profile resembles a parabolic profile clipped off at roughly $z = 150$. Next we notice that the polymeric solvent volume fraction inside the brush is essentially zero (at $z \leq 140$), and it only reaches its bulk value beyond the end of the brush (at $z = 165$). As the brush is compressed in the later frames of Figure 2.8, the polymeric component of the solvent gradually leaves the gap. In fact, there is no appreciable increase in the grafted chain segment density until all of the free chains have left the gap. For this reason the onset of repulsive interactions between the two brushes is delayed by the presence of free chains, as is shown in the force profiles in Figure

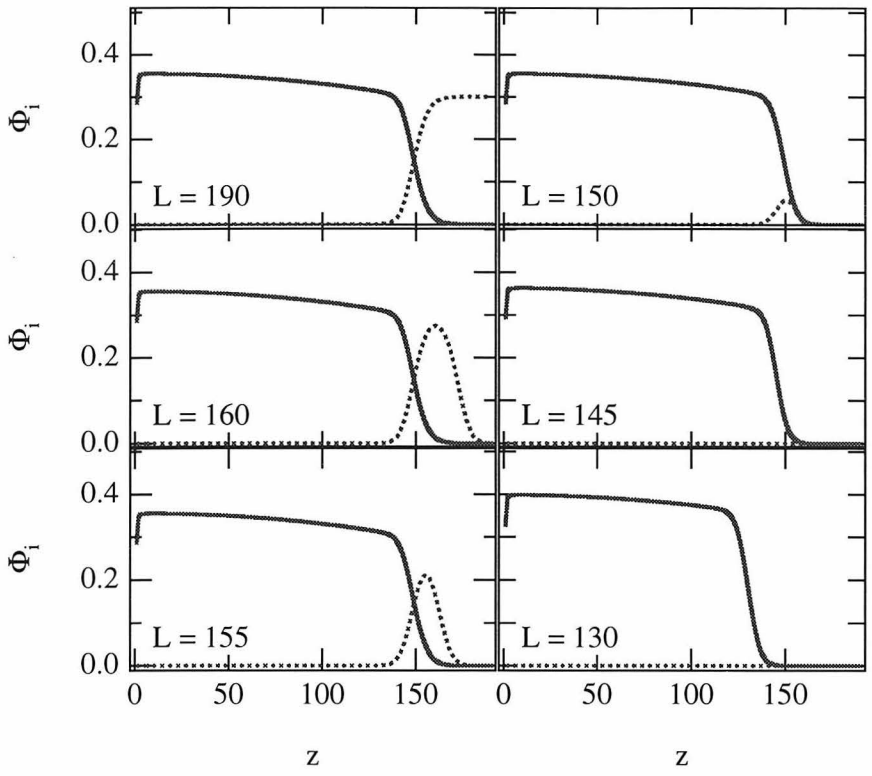

Figure 2.8: The segment density profiles for both the grafted (solid lines) and free chains (dotted lines) are shown for a polymer brush ($N_g = N_f = 1000, \sigma = 0.05$) in a mixed solvent ($\Phi_f = 0.3$) at various compressions as indicated.

2.9. In Figure 2.9 are presented the interaction profiles for the aforementioned brushes with variable polymer volume fraction as indicated. Comparing the force curve for the $\Phi_f^{res} = 0.3$ (the dashed line) shown also in Figure 2.8, the onset of the repulsive interaction between opposed brushes is at approximately $z = 150$, which is consistent with the density profiles. Moreover, the force required to compress the brush at this point is exactly equal to the additional force required to further compress a brush in a monomeric solvent which has already been mechanically compressed to the same extent. This equivalence of osmotic and mechanical compression is shown in the inset in the upper right corner of Figure 2.9, where the sum of the force curves and the osmotic pressures are plotted. Plotted this way, the compression profiles nearly superimpose once the delayed onset of interaction has been taken into consideration. This is not surprising, since at these compressions the solvent between the brush in mixed solvent is almost purely monomeric, thus the polymeric component in the reservoir has no impact on the additional force required to compress the brush.

In addition to the repulsive steric interactions between the brushes, the mixed solvent

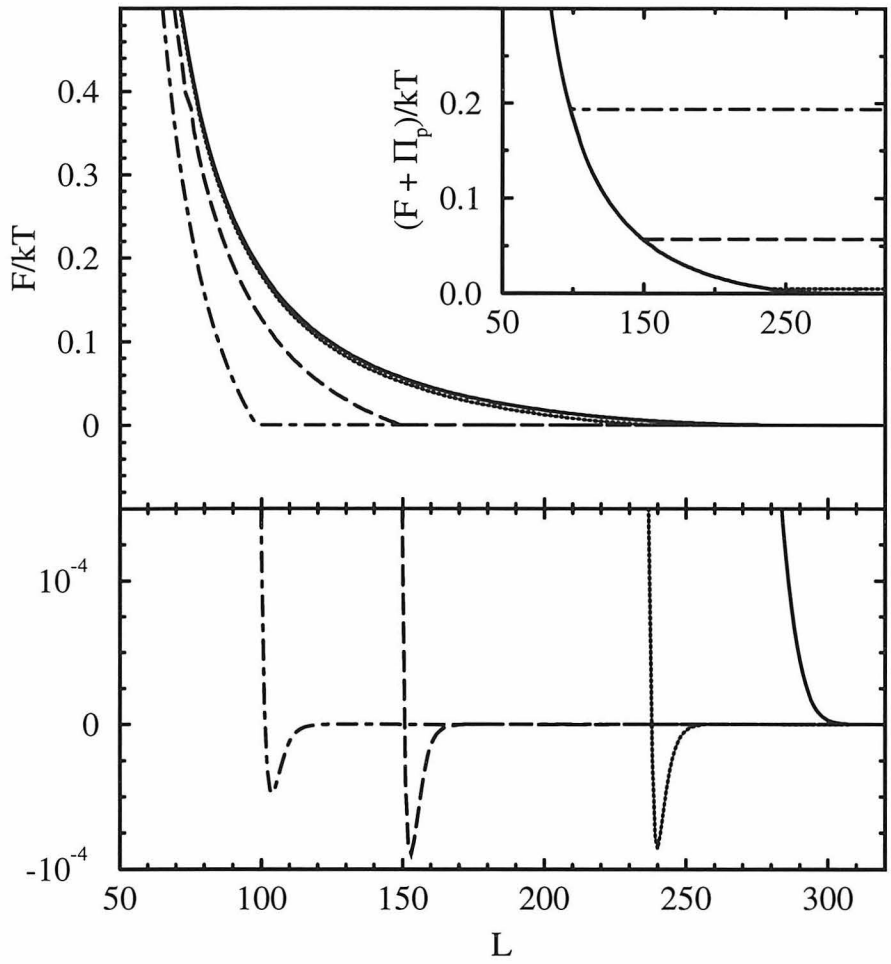

Figure 2.9: The force per unit area is shown versus compression for a polymer brush ($N_g = N_f = 1000, \sigma = 0.05$) in a mixed solvent of bulk concentration of $\Phi_f^{res} = 0.0$ (solid line), $\Phi_f^{res} = 0.1$ (dotted line), $\Phi_f^{res} = 0.3$ (dashed line), and $\Phi_f^{res} = 0.5$ (dot-dashed line).

case introduces weak attractive interactions between the brushes at the onset of interaction, as shown in the expanded scale at the bottom of Figure 2.9. The existence of an attractive region in the interaction profile will have negative consequences for the stabilizing effect of surface grafted polymers on colloidal suspensions when free polymers are present in solution. It was observed experimentally 20 years ago that the presence of free polymer had a destabilizing effect on sterically stabilized colloidal suspensions [1]. It was also observed that more concentrated polymer solutions restabilized the suspension.

The mechanism of attractive interaction between polymer brushes in a mixed solvent is not specific to polymer brushes, and is more easily understood by a brief description of a simpler problem of the same origin: the attraction of hard walls in the presence of a mixed polymer/monomer solvent. The polymeric component of an athermal polymer/monomer

mixture is repelled by a hard wall because it has fewer configurations available to it than it does in the bulk. This repulsion is balanced by the free energy of mixing, resulting in the depletion of the polymer species near the wall. This depletion region extends a distance δ away from the wall roughly equal to the radius of gyration of the polymer in the bulk for a dilute solution, and the correlation length for a semi-dilute solution. When two such plates are compressed to a distance of less than 2δ, some of the fluid which remains in the unfavorable depletion region is transported to a bulk reservoir with the resulting free energy of mixing. This results in a reduction of the free energy of the system and an attraction between the plates (of magnitude set by the osmotic pressure of the polymer solution) which continues until all of the solution has been transported from the vicinity of the plates to the reservoir.

Likewise, the local concentration of polymers will be depleted both inside the brush and at the interface between a polymer brush and a polymer solution. This depletion leads to attraction between polymer brushes as seen in Figure 2.9. However, as the regions depleted of polymeric solvent begin to overlap, leading to attraction, the polymer brushes overlap also, leading to repulsion. Because the depletion of the polymeric solvent component extends slightly beyond the edge of the brush, attraction dominates at the onset of interaction. However, the repulsive interactions between the brushes soon take over. The magnitude of the depletion attraction is set by the osmotic pressure of the polymeric component of the solvent, and this leads the osmotic pressure adjusted force curves to superimpose in the upper right-hand inset of the figure. However, the magnitude of the attractive minimum in the force curves depends on the extent to which the depletion attraction overpowers the steric repulsion, which requires that the depleted region extend beyond the edge of the polymer brush. However, the extent to which the depleted region extends beyond the edge of the brush goes down with higher osmotic pressures, so that less and less of the osmotic attraction is felt before the repulsive interactions overwhelm the attractive interactions. Thus, for the data shown in Figure 2.9, the strength of the attraction is only 1.5%, 0.16% and 0.03% of the osmotic pressure for $\Phi_f^{res} = 0.1$, 0.3, and 0.5 respectively. The net effect of increasing osmotic pressure is therefore a nonmonotonic dependence on Φ_f^{res}, with a maximum attractive force at roughly $\Phi_f^{res} = 0.3$. Thus, a relatively small volume fraction of free polymer impurity is sufficient to establish an attractive interaction, which will become less important at higher polymer volume fractions. This is qualitatively consistent with

experimental observations, but it should be remembered that the case described here—with athermal polymers, solvents and surface interactions—is highly idealized. On the other hand, this idealized system has the advantage of isolating the origin and magnitude of specific effects like the osmotic pressure attraction, without any confusion about the role of competing effects originating in interaction energies, or molecular weight dependence, or other factors.

2.3 Summary

In this paper we have attempted to resolve a few of the lingering questions about polymer brushes. First it was shown that because the linear dependence of brush height h on N_g is independent of the number of terms kept in the virial expansion, and because of the relatively weak $\frac{1}{3}$ dependence on grafting density σ, the segment density profiles are well predicted by the MWC theory [14] even when higher terms in the virial expansion are not negligible. At moderate chain lengths of $N_g \leq 50$, more than one term of the virial expansion is required to accurately describe the brush and to predict other quantities such as the lateral pressure Π_g [25]. However, for N_g of several hundred or more, a distinct regime does emerge in which the scaling predicted by second virial treatments is observed for the lateral pressure Π_g in addition to the brush height h and segment density profile $\Phi_g(z)$.

Next we examined the importance of finite length effects, and especially inter-chain penetration, on the interactions of polymer brushes under compression. It was observed that, despite appreciable interbrush penetration even for long highly stretched chains ($N_g = 1000, \sigma = 0.1$), under high compression, the effect on the force profile at these compressions is minimal. By contrast, finite length effects are fairly dramatic at the onset of brush interactions. Weak long range interactions resulting from the overlap of the tail of the segment density profiles are much more pronounced for smaller chains, and are very sensitive to interbrush penetration.

The more general problem of a polymer brush in a polymeric solvent was considered next. Following the scaling argument of de Gennes [13], we arrived at and verified two relevant scaling variables, N_f/N_g and $N_f\sigma^2$, which determine not only the height but also the profile of brushes in the crossover from small to large solvents. The collapse of the brush during this

crossover was related to the stretching of the free polymer in the anisotropic environment of the brush. This in turn led to an examination of brushes in a mixed polymeric/monomeric solvent. It was observed that only the monomeric solvent would substantially penetrate the brush, and that the effect of the polymeric solvent is to compress the brush by osmotic pressure. The extent of this compression is determined by the volume fraction of the polymeric species in the reservoir Φ_f^{res}. Finally, the interactions between such brushes in mixed solvents are examined. First a weak attractive interaction is observed, caused by the osmotic pressure of the solvent compressing the region depleted of free polymer near the brush. Then, as the two brushes begin to overlap, repulsive interactions begin to dominate. And once all of the polymeric solvent has left the brush, the force profiles are identical to those for the compression of a brush in a monomeric solvent with the exception of a shift of exactly the osmotic pressure of the solvent. The attractive interaction is not monotonic in Φ_f^{res}, and beyond some volume fraction the repulsive terms overpower the osmotic attraction leading to a purely repulsive interaction at high volume fractions.

2.4 Acknowledgments

This research is supported in part by The Petroleum Research Fund, administered by The American Chemical Society.

Bibliography

[1] Li-In-On, F. K. R.; Vincent, B.; Waite, F. A. ACS Symp. Ser. **1975**, *9*, 165.

[2] van Lent, B.; Israels, R.; Scheutjens, J. M. H. M.; Fleer, G. J. *J. Colloid Interface Sci.* **1990**, *137*, 380.

[3] Lasic, D.; Martin, F. J.; Gabizon, A.; Huang S. K. *Biochim. Biophys. Acta* **1991**, *1070*, 187.

[4] Papahadjopoulos, D.; Allen, T. M.; Gabizon, A.; Mayhew, E.; Matthey, K.; Huang, S. K.; Lee, K. D.; Woodle, M. C.; Lasic, D. D.; Redman, C.; Martin, F. J. *J. Proc. Natl. Acad. Sci. USA* **1991**, *88*, 11460.

[5] Kuhl, T. L.; Leckband, D. E.; Lasic, D. D.; Israelachvili, J. N. *Biophysical Journal* **1994**, *66*, 1479.

[6] Halperin, A.; Tirrell, M.; Lodge, T. P. *Adv. Polymer Sci.* **1992**, *100*, 31.

[7] Wang, Z. -G.; Safran, S. A. *J. Phys.* (Paris) **1990**, *51*, 1990.

[8] Leibler, L. *Makromol. Chem. Makromol. Symp.* **1988**, *15*, 1.

[9] Milner, S. T. *Science* **1991**, *251*, 905.

[10] Alexander, S. *J. Phys.* (Paris) **1977**, *38*, 977.

[11] de Gennes, P. G. *J. Phys* (Paris) **1976**, *37*, 1443.

[12] de Gennes, P. G. *Scaling Concepts in Polymer Physics* Cornell University Press: Ithaca, NY, 1979.

[13] de Gennes, P. G. *Macromolecules* **1980**, *13*, 1069.

[14] Milner, S. T.; Witten, T. A.; Cates, M. E. *Europhys. Lett.* **1988**, *5*, 413. Milner, S. T.; Witten, T. A.; Cates, M. E. *Macromolecules* **1988**, *21*, 2610.

[15] Semenov, A. N. *Sov. Phys. JETP* **1975**, *61*, 733.

[16] Skvortsov, A. M.; Gorbunov, A. A.; Pavlushkov, V. A.; Zhulina, E. B.; Borisov, O. V.; Priamitsyn, V. A. *Polym. Sci. USSR* **1988**, *30*, 1706; Zhulina, E. B.; Borisov, O. V.; Priamitsyn, V. A. *Polym. Sci. USSR* **1989**, *31*, 205.

[17] Field, J. B.; Toprakcioglu, C.; Ball, R. C.; Stanley, H. B.; Dai, L.; Barford, W.; Penfold, J.; Smith, G.; Hamilton, W. *Macromolecules* **1992**, *25*, 434.

[18] Milner, S. T. *J. Chem. Soc. Faraday Trans.* **1990**, *86*, 1349.

[19] Hirz, S. unpublished thesis, University of Minnesota, cited by Milner [14].

[20] Grest, G. S.; Murat, M. *Macromolecules* **1989**, *22*, 4054; *Phys. Rev. Lett* **1989**, *63* 1074.

[21] Chakrabarti, A.; Toral, R. *Macromolecules* **1990**, *23*, 2016.

[22] Shim, D. F. K.; Cates, M. E. *J. Phys. France* **1989**, *50*, 3535.

[23] Auroy, P.; Auvray, L.; Leger, L. *Macromolecules* **1991**, *24*, 2523.

[24] Cosgrove, T.; Heath, T.; van Lent, B.; Leermakers, F.; Scheutjens, J. M. H. M. *Macromolecules* **1987**, *20*, 1692.

[25] Carignano, M. A.; Szleifer, I. *J. Chem Phys* **1993**, *98*, 5006; *J. Chem Phys* **1994**, *100*, 3210.

[26] Grest, G. S. *Macromolecules* **1994**, *27*, 418.

[27] Dickman, R.; Anderson, P. E. *J. Chem. Phys.* **1993**, *99*, 3112.

[28] Chakrabarti, A.; Nelson, P.; Toral, R. *J. Chem. Phys.* **1994**, *100*, 748.

[29] Evers, O. A.; Schuetjens, J. M. H. M.; Fleer, G. J. *Macromolecules* **1990**, *23*, 5221; Evers, O. A.; Schuetjens, J. M. H. M.; Fleer, G. J. *J. Chem. Soc., Faraday Trans* **1990**, *86*, 1333; Evers, O. A.; Schuetjens, J. M. H. M.; Fleer, G. J. *Macromolecules* **1991**, *24*, 5558.

[30] Zhulina, E. B.; Borizov, O. B.; Priamitsyn, V. A.; Birshtein, T. M. *Macromolecules* **1991**, *24*, 140.

[31] Wijmans, C. M.; Scheutjens, J. M. H. M.; Zhulina, E. B. *Macromolecules* **1992**, *25*, 2657.

[32] Shull, K. R. *J. Chem. Phys.* **1991**, *94*, 5723.

[33] Zhulina, E. B.; Borizov, O. V.; Brombacher, L. *Macromolecules* **1991**, *24*, 4679.

[34] Lai, P.-Y.; Halperin, A. *Macromolecules* **1991**, *24*, 4981; *Macromolecules* **1992**, *25*, 6693.

[35] van Zanten, J. H. *Macromolecules* **1994**, *27*, 5052.

[36] Wijmans, C. M.; Zhulina, E. B.; Fleer, G. J. *Macromolecules* **1994** *27*, 3238.

[37] Edwards, S. F. *Proc. Phys. Soc.* (London) **1965**, *85*, 613.

[38] Schuetjens, J. M. H. M.; Fleer, G. J. *J. Phys. Chem.* **1979**, *83*, 1619. Schuetjens, J. M. H. M.; Fleer, G. J. *J. Phys. Chem.* **1980**, *84*, 178.

[39] Ben-Shaul, A.; Szleifer, I.; Gelbart, W. M. *J. Chem. Phys.* **1985**, *83*, 3597; *83*, 3612; *Proc. Net. Acad. Sci. USA* **1984**, *81*, 4601.

[40] McQuarrie, D. A. *Statistical Mechanics*, Harper Collins: New York, 1976.

[41] DiMarzio, E. A.; Rubin, R.J. *J. Chem. Phys.* **1971**, *55*, 4318.

[42] Shaffer, J. S. *Phys. Rev. E* **1994**, *50*, R683.

[43] Taunton, H. J.; Toprakcioglu, C.; Fetters, L. J.; Klein, J. *Macromolecules* **1990**, *23*, 571.

[44] Lai, P.-Y.; Binder, K. *J. Chem. Phys.* **1991**, *95*, 9288; Lai, P.-Y.; Binder, K. *J. Chem. Phys.* **1992**, *97*, 586.

[45] Lai, P.-Y.; Zhulina, E. B. *Macromolecules* **1992**, *25*, 5201.

[46] Auroy, P.; Auvray, L. *Macromolecules* **1992**, *25*, 4134.

[47] Grest, G. S.; Murat, M. *Macromolecules* **1993**, *26*, 3108.

[48] Budkowski, A.; Steiner, U.; Klein, J.; Fetters, L. J. *Europhys. Lett.* **1992**, *20*, 499.

[49] Theodorou, D. N. *Macromolecules* **1988**, *21*, 1391; 1400; *Macromolecules* **1989**, *22*, 4578; 4589.

Chapter 3 Effects of Polymer Brush Self-Assembly on Spreading and Thin Film Stability

This work, published with Z.-G. Wang and M. Schick, extends the numerical and scaling results of the previous chapter by considering reversibly end-adsorbed polymers. Besides the addition of reversible adsorption, the focus of this paper is also shifted to an entirely different physical problem, and therefore requires a different background of experimental results, and modifications to the formulation of the model and the presentation of results.

Abstract

This paper discusses the modification of several spreading properties of a liquid on a solid surface by the addition of end-adsorbing polymers. End-adsorption of the polymers at the liquid-solid interface decreases the interfacial free energy. If this decrease is sufficient to overcome the negative spreading power of an otherwise non-spreading liquid, the liquid will spread on the surface. Using a self-consistent field method, we construct a phase diagram for spreading of a liquid drop of fixed volume as a function of the concentration of end-adsorbing polymers and the energy of end-adsorption to the surface. The equilibrium thickness of a spread film is also calculated and is shown to be closely related to the thickness of a self-assembled polymer brush in an unbounded fluid, but relatively insensitive to the bare spreading power of the liquid or the Hamaker constant which determine the equilibrium thickness of a film of a simple liquid. When a solid surface of a given area is covered by a film thicker than the predicted equilibrium thickness of a spread film, an instability due to the depletion attraction causes the excess liquid to form drops on top of the spread film of the equilibrium thickness.

3.1 Introduction

The addition of end adsorbing polymers (EAP) to a compatible liquid can alter spreading and stabilize mechanically cast films. The polymer additive lowers the interfacial energy by adsorbing at the solid-liquid interface to form a self-assembled polymer brush (SAPB). The decrease in the interfacial free energy due to adsorption can become sufficiently large as to overcome the negative spreading power of an otherwise non-spreading liquid and cause it to spread. In this paper we discuss several key issues concerning spreading induced by the addition of EAPs: the quantity of EAP additive required to cause a nonspreading liquid-solid pair to spread, the thickness of the resulting film, and the role and configuration of the SAPB within it. We also discuss the related problem of stabilizing mechanically cast films containing EAP additives.

The need for stable thin films in industrial processes is widespread, ranging from the paint industry to semiconductor lithography [1]. The behavior of polymers in thin films, and the factors affecting film breakup and dewetting are also of considerable fundamental scientific interest.

We study the change in spreading of an otherwise nonspreading liquid on a solid surface when an EAP species is added. In order to highlight the most fundamental processes, we consider the minimal set of parameters necessary to reproduce the observed phenomena. Specifically we study the spreading of a liquid film composed of an EAP additive—a linear polymer with a head group that is attracted to the solid-liquid interface—in a liquid which is a good solvent for the EAP.

Special emphasis is given to the *self-assembly* of EAP brushes as it relates to spreading and film stabilization. We use a lattice self-consistent field method which provides complete configurational and thermodynamic information for chains of up to 1000 segments. To understand the origin of these phenomena, the numerical data is presented in the context of simpler scaling arguments.

After a brief consideration of the background and theoretical preliminaries in Section 3.2, we examine the self-assembly of an EAP brush in bulk liquid in Section 3.3, obtaining the surface excess free energy of brush formation, and the scaling behavior of an EAP brush in an unbounded liquid. The magnitude of the excess free energy due to end-adsorption relative to the (negative) spreading power sufficiently determines the thermodynamic ten-

dency for spreading. Next, we consider the configurational and thermodynamic properties of a spreading film of finite thickness: in Section 3.4, we discuss the spreading of a liquid in equilibrium with a reservoir on a *fixed area* (an open system), and in Section 3.5, we discuss the spreading of a *finite drop* on a surface of *unlimited area*, where we further distinguish between a drop of fixed volume and composition (a closed system) and a drop of fixed volume but variable composition determined by equilibrium with a reservoir (a semi-open system). The open and closed systems are directly related to experimental situations, while the semi-open system is a convenient conceptual construct for studying the thermodynamics of the closed system. The analyses in these two sections provide the equilibrium film thickness (of both the open and closed systems) and the phase diagram for spreading of a drop of fixed volume as a function of the amount of EAP additive and the adsorption energy of the head group. A key finding in Section 3.4 is the existence of a free energy minimum at film thickness roughly equal to the self-assembled brush height in the unbounded liquid. This minimum is due to the depletion attraction between end-adsorbed brush and the air-liquid interface. In Section 3.6, the preceding results are used to discuss the stabilization of mechanically cast films. In particular we examine the protection an EAP additive provides against film rupture and dewetting of the solid and its effect on the uniformity of the film thickness in the context of experimental results of Yerushalmi-Rosen and Klein et al. [2, 3]. Finally, some concluding remarks are made in Section 3.7 about the strengths and weaknesses of EAP additives used to promote spreading or stabilize films.

3.2 Background and theoretical considerations

The spreading of a nonvolatile liquid on an ideal smooth surface has been understood in terms of the surface tensions of the relevant surfaces since it was formulated by Young more than 150 years ago [4]. The tendency for a liquid to spread on a solid surface is described by the spreading power, S, defined as $S \equiv \gamma_{SA}^{\circ} - \gamma_{SL} - \gamma_{LA}$, where γ_{SL} and γ_{LA} are the interfacial free energies of the solid-liquid and liquid-air interfaces and γ_{SA}° is the interfacial free energy between the bare solid and air. As the bare surface is not necessarily the equilibrium configuration, γ_{SA}° is not necessarily the experimentally measured interfacial free energy between solid and air. If $S > 0$, the bare surface is definitely not the minimum free energy configuration, and the film will spread and thin. If $S < 0$ and the bare surface

is furthermore the configuration with the lowest free energy, spreading is unfavorable and the film will break up into droplets [5]. More detailed analyses of the microscopic shapes of droplets performed by de Gennes [6] and Brochard-Wyart et al. [7] predict that in addition to complete and partial wetting, certain combinations of the spreading power and van der Waals interactions will lead to "pseudo-partial" wetting, in which a droplet is surrounded by a microscopically thin wetting film.

The spreading of a liquid-solid pair can be altered by addition of a solute species, especially a surfactant or polymer. Macromolecular additives will drastically increase the thickness of the interfacial region. End-adsorbing polymers (EAPs) aggregated at an interface, for example, may be as thick as tens or hundreds of nanometers. Thus, for thin films the interfacial region may contain a nonvanishing part of the overall system volume and a majority of the surface active species, making it difficult to separate the interfacial and bulk energies. For this reason the behavior and interfacial free energy of polymers at an interface must be considered explicitly, and may depend on all of the variables of the system including film thickness and bulk composition. The spreading of a dilute or semi-dilute non-adsorbing polymer solution in a non-volatile solvent has been studied by Halperin, Pincus and Alexander [8] and by Boudoussier [9]. In the former, a dilute polymer solution spread into a film thinner than the polymer's radius of gyration is studied. The configurational entropy cost of confining the polymer leads to a deformation of the film surface and an attractive interaction between polymer chains which may lead to a two-dimensional phase separation. Boudoussier studies a broader range of polymer concentrations, and predicts a phase diagram with four phases: a spread polymer solution film, a non-spread droplet of polymer solution, and two other phases in which these two states are in equilibrium with pure solvent films [9]. This is analogous to the "pseudo-partial" wetting of the pure liquid with the additional complication that the solution separates to form the surrounding, essentially polymer-free, wetting film. These effects are purely entropic and can act only to disfavor the formation of uniform thin films.

Adsorbing polymeric additives may favor spreading, and are therefore useful in the many applications where this is desirable. Polymers may adsorb at an interface either through an end group attracted to the interface, or through a uniform attractive interaction of the monomers with the interface, or a combination of the two. In this paper we consider end adsorbing polymers (EAPs), in particular a flexible EAP additive of N segments and volume

fraction Φ in a liquid which is a good (athermal) solvent for the polymer. The EAPs are assumed to be nonadsorbing at either the solid-liquid or liquid-air interface except for a functional group at one end of the chains which has an attachment energy of ϵ (in units of kT) at the solid-liquid interface and is otherwise indistinguishable from the other chain segments. Thus we ignore aggregation of the head groups (micellization) and adsorption at the liquid-air interface. (These features will enrich the behavior of the system, but will not alter the essential conclusions of this study.) Further simplicity is achieved by considering an incompressible system with polymer segments chemically identical to the solvent molecules both with volume of one unit (equal to one cubic Kuhn length). Thus the system volume $V = nN + n_s$ where n and n_s are the number of EAPs and solvent molecules respectively. This constitutes the minimal set of parameters with which the wetting effects of EAP additives can be described. It reduces to Boudoussier's problem of nonadsorbing polymers when $\epsilon = 0$ and to Brochard-Wyart's problem of simple fluids characterized by H and S when no polymers are present.

The chemical potentials of the EAP and solvent, μ and μ_s respectively, are partial derivatives of the Helmholtz free energy F

$$\mu = \left(\frac{\partial F(n, n_s)}{\partial n}\right)_{n_s} \qquad \mu_s = \left(\frac{\partial F(n, n_s)}{\partial n_s}\right)_{n} \tag{3.1}$$

and $F = n\mu + n_s\mu_s$ in the bulk, by virtue of the Euler theorem. Here we have made use of the incompressibility assumption and have ingored the inconsequential constant pV term. For an incompressible system n and n_s, and therefore μ and μ_s, are not independent. Therefore, we use the notation μ to denote what in reality is an exchange chemical potential (i.e., the free energy change upon exchanging polymer and solvent with the reservoir). For open systems in equilibrium with a reservoir, either μ, or equivalently the reservoir composition Φ^{res}, can be specified. Configurational information is obtained from the segment density profile $\Phi(z)$, which is the local volume fraction of EAP segments a distance z from the surface, averaged over the plane parallel to the surface. The adsorbed segment density profile $\Phi_a(z)$ is the analogous profile for the adsorbed segments only, and of course the unadsorbed EAP chain density is given by the difference. The actual system composition is obtained by averaging over the thickness l of the film, $\Phi = l^{-1}\int_0^l \Phi(z)dz$, and the end attachment density, defined as the number of end-adsorbed chains per unit area, is given

by $\sigma = N^{-1} \int_0^l \Phi_a(z) dz$.

All of the necessary thermodynamic and configurational quantities are efficiently obtained using a lattice self-consistent field method described in Reference 10. The details of the calculation are spelled out in that reference, but in essence all of the configurations of the polymeric species are enumerated on a lattice, with the inter-chain and intra-chain interactions accounted for by a mean field which enforces incompressibility self-consistently. An extensive discussion of the virtues and limitations of various approaches to similar problems has been given in the literature [10, 11], and we will not approach the question here beyond noting that because this method explicitly considers incompressibility, rather than using a second virial approach, it can cover chain densities from the semi-dilute all the way up to the melt (at the mean field level).

The use of EAPs described in the work is closely related to studies of the modification of wetting properties by irreversibly grafted polymer brush formation. The wetting of a polymer brush covered surface by a simple fluid or a mixture of two fluids has been studied by Johner and Marques [12]. They show that different interactions between the two liquids, the brush chains and the substrate can result in several novel layer configurations, as the brush "traps" one species selectively, and may alter the wetting properties of the underlying substrate. Leibler et al. [13] have studied the wetting of a grafted polymer surface by a melt of compatible chains using analytical methods and find that chains which are much smaller than the grafted chains will wet the surface, while chains which are much larger will not. These results are in agreement with more detailed self-consistent field calculations we have performed [14], and with the experimental results of Liu et al. [15]. They examined polystyrene (PS) films spread on the surface of polyvinylpyridine-polystyrene block copolymer films oriented into lamellae with the PS block present at the vacuum interface and found that the homopolymer dewets the surface of the brush when its molecular weight is roughly five times that of the PS block of the copolymer.

Recently Yerushalmi-Rosen and Klein et al. [2, 3] have studied the effect of polymer additives on the stability of spin cast oligostyrene films on silicon surfaces. They find that addition of high molecular weight polystyrene does not protect the film from the rapid rupture and subsequent dewetting of the silicon which is observed also for the pure oligostyrene film. However, if some of the polystyrene is replaced with end-functionalized polystyrene—which end-adsorbs on the silicon surface forming a polymer brush—the film

is stabilized against rupture and dewetting. Below some threshold for the total volume fraction of high molecular weight polystyrene, the film forms small "holes," which do not penetrate to the silicon surface, and do not appear to lead to dewetting of the silicon surface. We will comment on these experiments in some detail in Section 3.6.

Finally, self-consistent and analytical mean field methods have been applied to the wetting of a surface covered with an irreversibly grafted polymer brush. Schlanger, Leermakers and Koopal have applied self-consistent field methods to the wetting of bare and grafted surfaces by binary polymer solvent mixtures [16]. Dan has used analytic methods to study the effect of free polymer additive on the spreading of a partially wetting droplet on a surface covered with grafted polymers [17]. Because the problem she studies is closely related to ours, we comment on her work in some detail.

In Dan's calculation, it is assumed that the brush density can be approximated by a step-function profile of a thickness and density independent of the added free polymer chains. Using a mean-field square-gradient density functional for the free chains, she finds that spreading is favored when the concentration of the free chains exceeds a critical value (determined among other things by the polymer-surface interaction). However, this critical concentration is found to be lower for a repulsive polymer-surface interaction than for an attractive polymer-surface interaction — this is a rather counter intuitive result. We have independently performed a self-consistent field calculation for exactly the system Dan studies with a hard-wall polymer-surface interaction (where, by Dan's result, one expects to find maximum enhancement of spreading) and find that adding free polymers disfavors spreading at all concentrations. We thus believe her result is erroneous and is probably a consequence of assuming a constant, step-function-like brush profile unperturbed by the addition of free polymers.

3.3 Self-assembled brush formation in an unbounded fluid

3.3.1 Scaling behavior of self-assembled brushes

In this section the configuration and free energy of a self-assembled brush of end adsorbing polymers (EAPs) in an unbounded fluid (Figure 3.1) of composition (volume fraction) Φ is examined. Theoretical treatment of end-attached polymers was pioneered by de Gennes [18] and Alexander [19] who approximated the profile of the brush as a step function of height h.

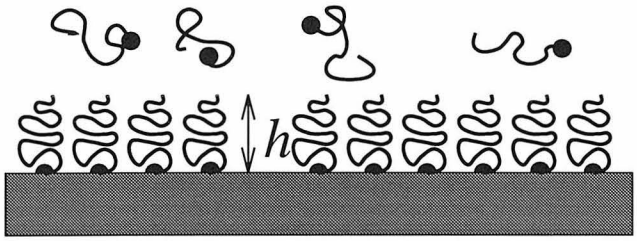

Figure 3.1: Schematic illustration of a self-assembled end-adsorbing polymer brush in an unbounded liquid. Notice the increased density and stretched configuration of the adsorbed chains.

They used scaling arguments to predict successfully much of the behavior of brush systems for both irreversibly anchored and self-assembled brushes. Much subsequent study has been directed towards irreversibly grafted polymer brushes (fixed grafting density σ) [11, 20, 21]. However, special features of self-assembled brushes—in particular the dependence of the grafting density on the other parameters of the system—lead to unique behavior relevant to our study. These scaling arguments clarify the interpretation of the numerical results of our more detailed self-consistent field calculation, and so we review them here.

Scaling in low density limit

Scaling predictions for reversibly adsorbed or self-assembled brushes compare quite well to the results of our self-consistent field calculation. In the low Φ limit, the grafted chains are laterally dilute and do not interact with one another. This condition is met when the distance between grafted chains is much larger than the unperturbed radius of gyration of the polymer[1]; $\sigma \ll \frac{1}{N}$. The chemical potential per adsorbed chain includes the lateral translational entropy on the surface, the end-adsorption energy, and the configurational entropy cost of a polymer attached to a hard wall[2] and is of the order of the translational entropy of the isolated polymer chain in the bulk,

$$\log \sigma - \epsilon + \frac{1}{2} \log N \sim \log \frac{\Phi}{N}. \tag{3.2}$$

[1] In accord with our mean field approximation, we use exponents appropriate to gaussian rather than self-avoiding chains.

[2] The entropy cost of a polymer near a hard wall is $(\gamma_1 - 1) \log N$ where $\gamma_1 = \frac{1}{2}$ for a mean field or gaussian chain. See Reference [22].

This leads to the scaling prediction $\sigma \sim N^{-\frac{3}{2}}\Phi e^{\epsilon}$ which is observed on the left in Figure 3.2. From this scaling we get a threshold for the dilute regime in terms of N and ϵ, $\Phi \ll N^{\frac{1}{2}}e^{-\epsilon}$. Because the adsorbed chains do not interact, their configuration, called the mushroom configuration, is independent of Φ and ϵ. The mean field treatment is not an appropriate approach to the mushroom regime, and these results are shown primarily in order to present a complete and coherent description. More precise treatments of this regime require separate treatment of inter-chain and intra-chain interactions, as used, for example, by Carignano and Szleifer [23]

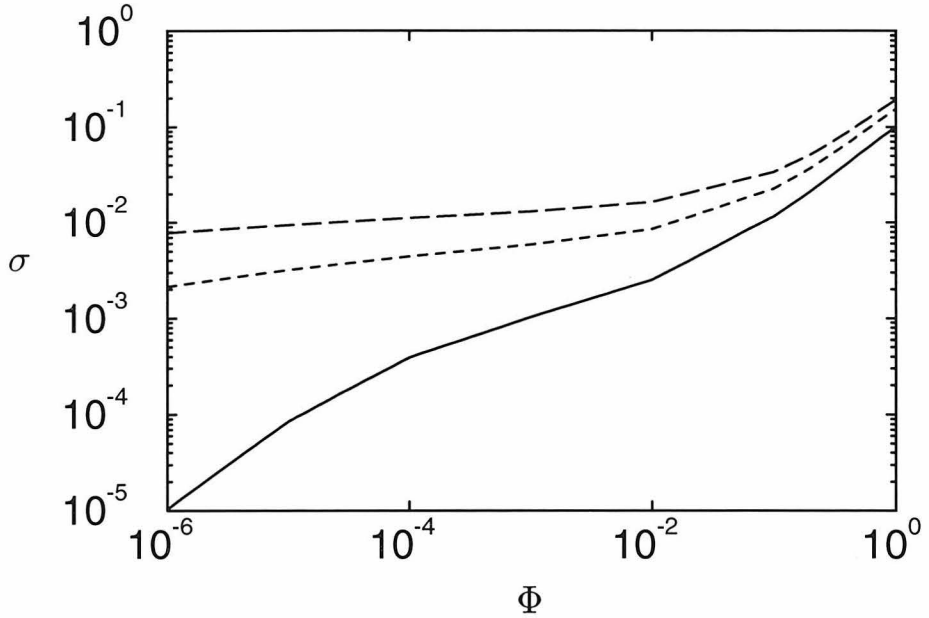

Figure 3.2: End adsorption density σ versus the composition (volume fraction) Φ in log-log scale for three end adsorption energies, $\epsilon = 10$ (solid line), 20 (dashed line), 30 (long-dashed line). The curves show three distinct scaling regimes; at low σ, $\sigma \sim \Phi$ (σ is not low enough to see this for all three curves), at intermediate σ an intermediate scaling which gets broader and less steep as ϵ increases, and at high σ the linear scaling reappears.

Scaling for brush in dilute solution

An increase of the concentration of EAPs leads to a further increase in the adsorption density. Adsorption beyond the overlap density given by $\sigma \sim \frac{1}{N}$ leads to stretching in the direction normal to the surface. This is the so-called polymer brush regime. If the EAP chains in solution are still dilute, then the only change in the free energy comes from the configurational entropy of the adsorbed chains. Following de Gennes we treat the brush as uniform in density with a height h. The free energy of a grafted chain includes a stretching

term and an excluded volume term,

$$f \sim \frac{h^2}{N} + N\frac{N\sigma}{h}. \tag{3.3}$$

Minimizing with respect to h, one obtains the brush height $h \sim N\sigma^{\frac{1}{3}}$, and therefore $f \sim N\sigma^{\frac{2}{3}}$. The free energy balance for a self-assembled brush is

$$\log\sigma - \epsilon + N\sigma^{\frac{2}{3}} \sim \log\frac{\Phi}{N} \tag{3.4}$$

which leads to a scaling of

$$\sigma^{\frac{2}{3}} \sim \left(\frac{\epsilon}{N}\right)\left[1 + \frac{\log\Phi/N}{\epsilon}\right]. \tag{3.5}$$

Thus σ is weakly dependent on Φ as observed in the plateau region of Figure 3.2. In the limit of large ϵ, the plateau becomes flat, and the scaling of σ becomes $\sigma \sim (\epsilon/N)^{\frac{3}{2}}$ which leads to $h \sim N\sigma^{\frac{1}{3}} \sim N^{\frac{1}{2}}\epsilon^{\frac{1}{2}}$, independent of Φ.

Scaling for brush in concentrated solution

When Φ in the solution becomes comparable to the value in the brush, a new scaling regime is established. The density of the brush is approximately the same as the solution density, and since the solution does not penetrate the brush significantly, $\Phi \sim N\sigma/h$. Substituting the scalings for σ and h from the previous section, one finds that the lower limit of this regime is $\Phi \sim \frac{\epsilon}{N}$. The excluded volume interactions are screened at these higher densities so the stretching term balances ϵ directly (the lateral translational entropy also becomes unimportant at high densities)

$$\frac{h^2}{N} \sim \epsilon. \tag{3.6}$$

which leads to the scalings $h \sim N^{\frac{1}{2}}\epsilon^{\frac{1}{2}}$ and

$$\sigma \sim \frac{\Phi h}{N} \sim \Phi\sqrt{\frac{\epsilon}{N}}. \tag{3.7}$$

This predicted linear scaling is seen in the right-hand side of Figure 3.2 and in Figure 3.3. The threshold for the high density limit, $\Phi \sim \frac{\epsilon}{N}$, is consistent with what is shown in these figures.

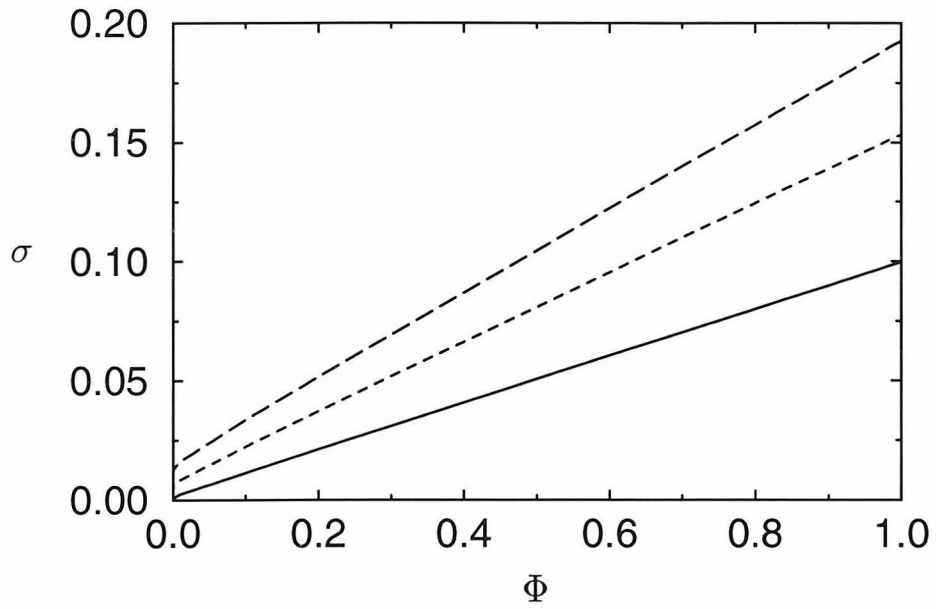

Figure 3.3: End adsorption density σ versus the composition (volume fraction) Φ in linear-linear scale for three end adsorption energies, $\epsilon = 10$ (solid line), 20 (dashed line), 30 (long-dashed line). The high Φ linear scaling is clearly visible in this figure.

Self-regulation of chain configuration

In the scalings described above, the adsorbed chain height h is weakly dependent on Φ or completely independent of it. Obviously, the chain height and configuration change in the transition between the scaling regimes since the mushroom configuration expected in the dilute limit is not the same as the brush configuration at higher EAP content. However, the scaling of the brush height in a concentrated solution is the same as the large ϵ limit for a brush in dilute solution, $h \sim N^{\frac{1}{2}}\epsilon^{\frac{1}{2}}$, and more importantly this configuration is independent of Φ. This can be understood phenomenologically as arising from the finite attachement energy ϵ. As chain crowding and stretching increase, the free energy of an adsorbed chain increases until the configurational entropy cost of stretching equals ϵ. The chains will stretch no further than this threshold because any additional configurational entropy cost would overpower the energetic attachment energy, resulting in desorption. *The self-regulating brush height of self-assembled polymer brushes contrasts sharply with the behavior of irreversibly grafted polymer brushes* [10, 24]. In Figure 3.4 the per chain segment density profiles $\Phi_a(z)/\sigma$ are shown for chains in the different scaling regimes. In the low Φ limit, the adsorbed chains are in a mushroom configuration, which changes to a brush profile relatively insensitive to Φ in the brush regime.

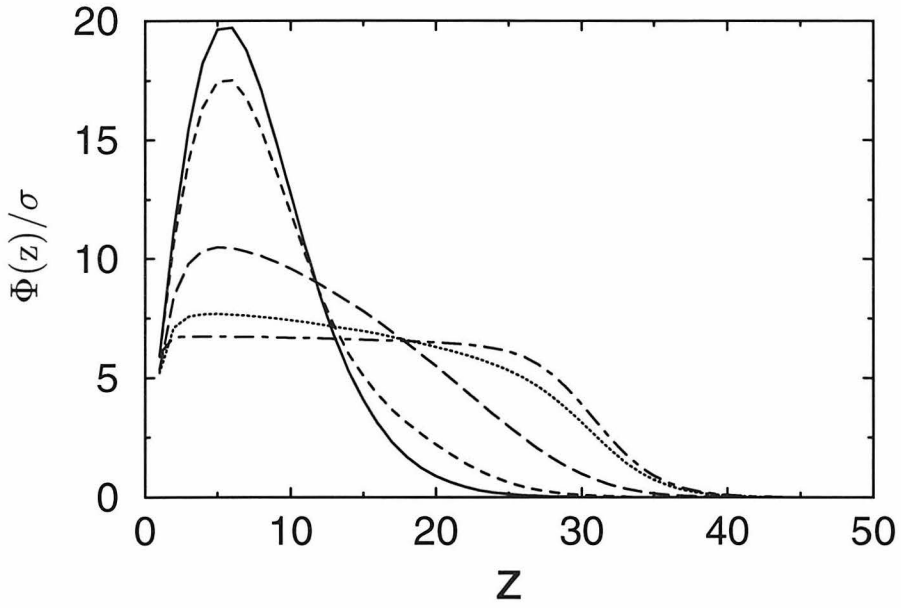

Figure 3.4: The segment density profiles normalized by end attachment density for an EAP additive of $N = 200$, $\epsilon = 20$ with composition $\Phi \to 0$ (solid line), 10^{-6} (dashed line), 10^{-3} (long-dashed line), 0.1 (dotted line), 0.5 (dot-dashed line). The normal distance z is in units of the lattice spacing, which we take to be the Kuhn length. In the dilute limit the chains adopt a mushroom configuration, while for $\Phi > 0.1$ the adsorbed chains are in the brush regime and their configuration is independent of concentration.

3.3.2 Thermodynamics of end-adsorbed polymers in an unbounded liquid

The appropriate thermodynamic potential for an interface in an unbounded liquid (an open system) is the grand potential $W(\mu)$, which is defined

$$W(\mu) \equiv F[\Phi(\mu)] - (n\mu + n_s\mu_s), \tag{3.8}$$

where $\Phi(\mu)$ is the composition which minimizes W subject to μ. The relevant quantity is the change in the grand potential when liquid from an infinite reservoir spreads on a surface to form a film covering an area A. Consideration of finite film effects is left to the next section. In this section we assume the film is thick enough so that the liquid-air interface does not interact with the polymer brush. Since $F^{\text{res}}(\Phi) = n\mu + n_s\mu_s$, there is no polymer contribution to W by the reservoir, and

$$W^{\text{initial}}(\Phi) = A\gamma^{\circ}_{SA}, \tag{3.9}$$

$$W^{\text{final}}(\mu) = F[\Phi(\mu)] - (n\mu + n_s\mu_s) + A(\gamma_{LA} + \gamma_{SL}). \tag{3.10}$$

For a fixed area A the grand potential per unit area is appropriate:

$$\begin{aligned}
\Delta\tilde{w}(\mu) &= \frac{1}{A}\Delta W(\mu) && (3.11)\\
&= \frac{1}{A}\left[W^{\text{final}}(\mu) - W^{\text{initial}}(\mu)\right] && (3.12)\\
&= \frac{1}{A}\{F[\Phi(\mu)] - (n\mu + n_s\mu_s)\} \\
&\quad +(\gamma_{LA} + \gamma_{SL} - \gamma^{\circ}_{SA}) && (3.13)\\
&= \tilde{f}^{\text{ex}}[\Phi(\mu)] - S && (3.14)
\end{aligned}$$

where $\tilde{f}^{\text{ex}}(\Phi) = \frac{1}{A}\{F[\Phi(\mu)] - (n\mu + n_s\mu_s)\}$ is the excess free energy per unit area due to adsorption at the solid-liquid interface.

The quantity $\tilde{f}^{\text{ex}}(\Phi)$ shown in Figure 3.5 has a rather simple form—linear over most Φ on the scale shown in the figure—which is strikingly similar to the behavior of the density of end-adsorbed chains σ in Figure 3.3. This is a consequence of the self-regulating configuration of the self-assembled polymer brush discussed above. Free energy contributions from stretching, excluded volume and attachment energy are, on a per adsorbed chain basis, independent of Φ, but σ increases linearly with Φ. And this leads to a simple proportionality between $\tilde{f}^{\text{ex}}(\Phi)$ and Φ as observed.

When $\tilde{f}^{\text{ex}}[\Phi] \leq S$ the excess free energy of the EAP brush is enough to overcome the unfavorable (since $S < 0$) interfacial free energy cost of spreading, and the liquid will spread on the surface. It is not known at this point what the thickness of the resulting film will be; it is only known that covering the bare surface is preferable to leaving it exposed to air. A representative value of S is shown on Figure 3.5 for an organic polymer $0.25kT/a^2$ (indicated with a dashed horizontal line) where a is a Kuhn length or lattice spacing in the calculation. The intercept of $\tilde{f}^{\text{ex}}[\Phi]$ with this line indicates the minimum EAP content Φ necessary to cause spreading. Thus for $N = 200$, $\epsilon = 10$ no spreading is expected at any EAP content up to pure EAP melt, while for $\epsilon = 20$ spreading will first occur at 13%, and at $\epsilon = 30$ only 3% EAP content is necessary.

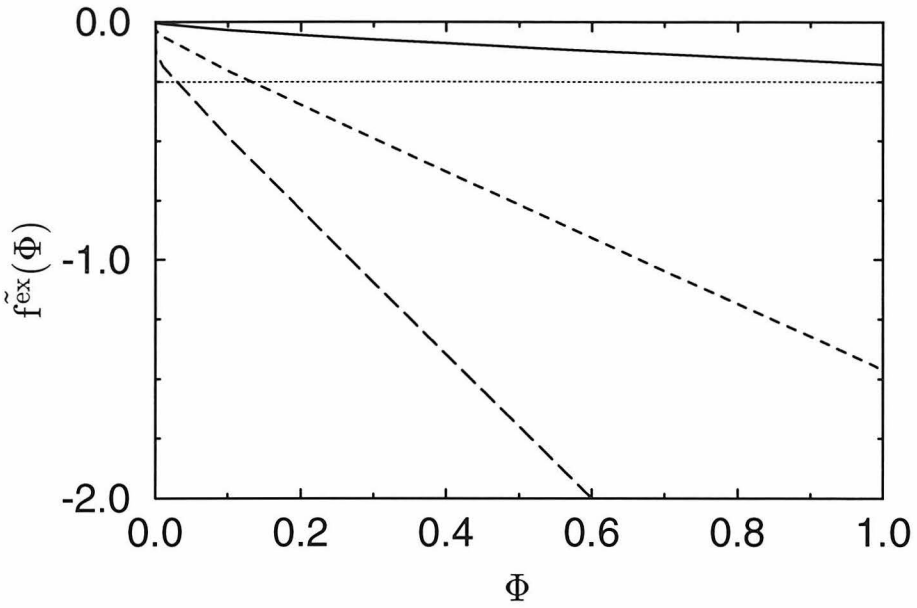

Figure 3.5: The excess free energy per unit area, $\tilde{f^{ex}}(\Phi)$ for an unbounded liquid is shown as a function of composition (Φ) for $N = 200$, $\epsilon = 10$ (solid line), 20 (dashed line), 30 (long-dashed line). The simple linear behavior is a consequence of the Φ independence of chain configuration and the simple linear dependence of σ.

3.4 Spreading from an infinite reservoir

In the previous section it was determined under what conditions the driving force for self-assembly of an EAP brush is sufficient to overcome the unfavorable surface tension cost to form a thick film. In this section the thickness and EAP configuration in such a film is addressed. Physically two types of films can be distinguished: a film covering a surface of fixed area and in equilibrium with a reservoir (an open system), and a film spread from a drop of liquid of fixed volume and composition on a surface of unlimited area (a closed system). In the first case, the amount of liquid on top of the surface is not fixed a priori, but rather is determined by the excess free energy per unit area. An excess free energy which decays monotonically with increasing thickness of the film implies the formation of a macroscopically thick film, whereas a free energy minimum at some finite thickness implies the formation of a microscopic layer of corresponding thickness [5, 25]. This section discusses the thermodynamics of the open system. This discussion is important for two reasons: first, the open system is conceptually simpler than the closed system and allows us to focus on the physics of polymer brush self-assembly in a film without having to consider constraints introduced by the fixed volume and composition. All of the thermodynamic information

for the open system can be used by appropriate thermodynamic transformation to study the behavior of a closed system; this will be discussed in the next section. Second, the behavior of an open system is directly related to the stability of the mechanically cast films discussed in Section 3.6. Indeed it will be shown that when the film thickness is larger than the equilibrium thickness predicted for the open system, the excess liquid will form droplets on top of the stable film, effectively *creating* a reservoir for the stable film.

3.4.1 Self-assembled polymer brushes are cropped rather than squeezed

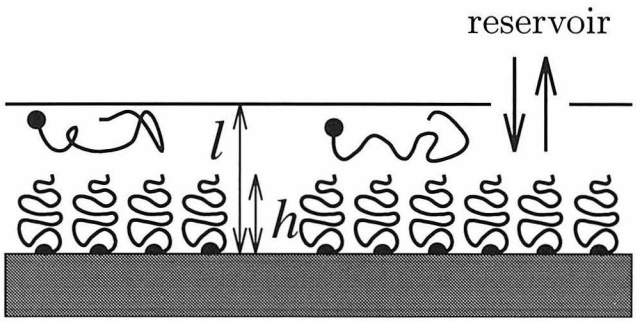

Figure 3.6: Schematic illustration of an open system film of thickness l. The film is in equilibrium with a reservoir of fixed chemical potential.

When the thickness of the film l, shown schematically in Figure 3.6, is much larger than the thickness of the self-assembled polymer brush (SAPB) in an unbounded fluid h, the system is relatively insensitive to film thickness. However, for $l \leq h$ the confinement of the SAPB becomes important. When the SAPB is confined to $l < h$, the chains begin to desorb. This is another consequence of the self-regulating configuration discussed in Section 3.3.1 above. The chains have adsorbed to the limit set by ϵ, and therefore any additional configurational entropy cost of confinement surpasses the threshold, leading to desorption rather than compression. For this reason the profiles shown in Figure 3.7 appear cropped rather than squeezed by the liquid-air interface. Away from the interface the local balance described in the scaling arguments and reflected in $\Phi_a(z)$ is relatively unaffected. This is in sharp contrast to irreversibly grafted polymer brushes, which cannot desorb and are therefore squeezed as l decreases. In the irreversibly grafted case, the local density throughout the brush will increase and the shape of the profile will change (tending toward a flat profile as excluded volume interactions begin to dominate). The confinement of the SAPB to a thin film also has thermodynamic consequences which will be described after

the appropriate quantities are defined.

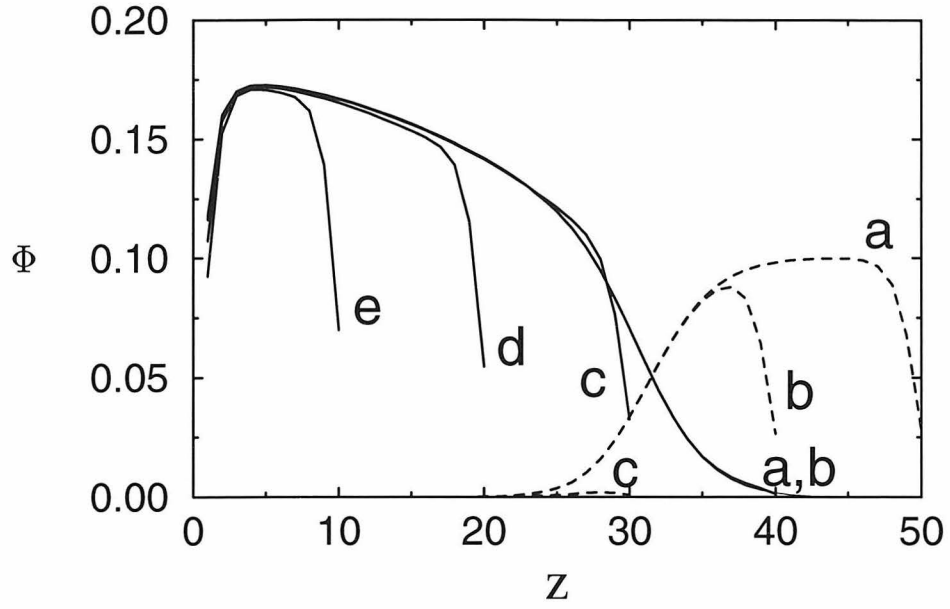

Figure 3.7: The segment density profile is shown for several l as the film is increasingly confined. $N = 200$, $\epsilon = 20$, $\Phi^{\text{res}} = 0.1$, $l = 50$ (a), 40, (b), 30 (c), 20 (d), 10 (e). The normal distance z is in units of the lattice spacing. The solid lines show the end-adsorbed chains while the dotted lines show the free chains. For films of less than 30 lattice spacings the density of free chains is so small that it is not visible at this scale. Notice that the brush profile is unaffected by variations in the film thickness so long as $l > h$, leading to the nearly complete overlap of the brush profiles a and b. For thinner films $l < h$, the profile is cropped by the liquid-air interface rather than "squeezed," leaving the profile away from the film boundary largely unaffected.

3.4.2 Open system thermodynamics

The thermodynamics of this system are the same as described in the previous section with the addition of a van der Waal potential and of l-dependence to W^{final}, $\tilde{f}^{\text{ex}}$ and $\Delta\tilde{w}$.

$$W^{\text{initial}} = A\gamma^{\circ}_{SA} \tag{3.15}$$

$$\begin{aligned} W^{\text{final}}(\mu, l) &= F[\Phi(\mu), l] - (n\mu + n_s\mu_s) \\ &\quad + A(\gamma_{LA} + \gamma_{SL}) + A\frac{H}{12\pi l^2} \end{aligned} \tag{3.16}$$

$$\Delta\tilde{w}(\mu, l) = \frac{1}{A}\Delta W(\mu, l) \tag{3.17}$$

$$= \frac{1}{A}\left[W^{\text{final}}(\mu, l) - W^{\text{initial}}\right] \tag{3.18}$$

$$= \tilde{f}^{\text{ex}}[\Phi(\mu), l] - S + \frac{H}{12\pi l^2} \tag{3.19}$$

Here H is the Hamaker constant and is assumed to be positive [26]. The cost of confining a self-assembled EAP brush to a thin film is shown in Figure 3.8. As described in the previous section, the chains in the brush are not squeezed by the confinement, but instead selectively desorb, leading to a loss in adsorption energy. The free energy cost of confinement in Figure 3.8 is nearly proportional to the decrease in σ observed in Figure 3.7. Thus, *the cost of confinement of a self-assembled brush in a thin film arises from the decrease in adsorption density and the attendant decrease in the adsorption energy ϵ, while for irreversibly grafted polymer brushes the increase in segment density is the origin of the free energy cost.* An increase in the excess free energy as the brush is being compressed corresponds to a repulsive force between the solid-liquid and liquid-air interfaces. In fact, the results presented in Figure 3.8 can be applied almost quantitatively to the related problem of the interaction between two surfaces with reversibly formed brushes separated by $2l$, after removing the S and H contributions (which, however, does not alter the repulsive nature of the force). The only correction comes from the possibility of interbrush penetration, which is minimal for long-chain brushes [10]. The behavior of the interaction forces between surfaces with weakly end-adsorbed polymers is explored more fully in Reference [27].

In addition to the prominent free energy cost of confinement, Figure 3.8 has a second feature with dramatic consequences for spreading. At a film thickness corresponding to the uncompressed brush height, there is a small minimum, shown in an expanded scale at the top of Figure 3.8, arising from the so-called depletion attraction [28]. This refers to the attractive interaction between interfaces in polymer solution, an effect first studied in the destabilization of colloidal suspensions in polymer solutions, and later shown to lead to an attraction between polymer brush coated surfaces in polymer solution [29, 24]. The driving force for the attraction is the configurational entropy cost of a polymer near a hard wall or other impenetrable interface. In the absence of other interactions, this entropy cost leads to a depletion in polymer concentration near the interfaces of length δ, which, in the semidilute regime, should be approximately the correlation length. When the two interfaces approach each other by a distance of less than 2δ, some polymer solution is moved from

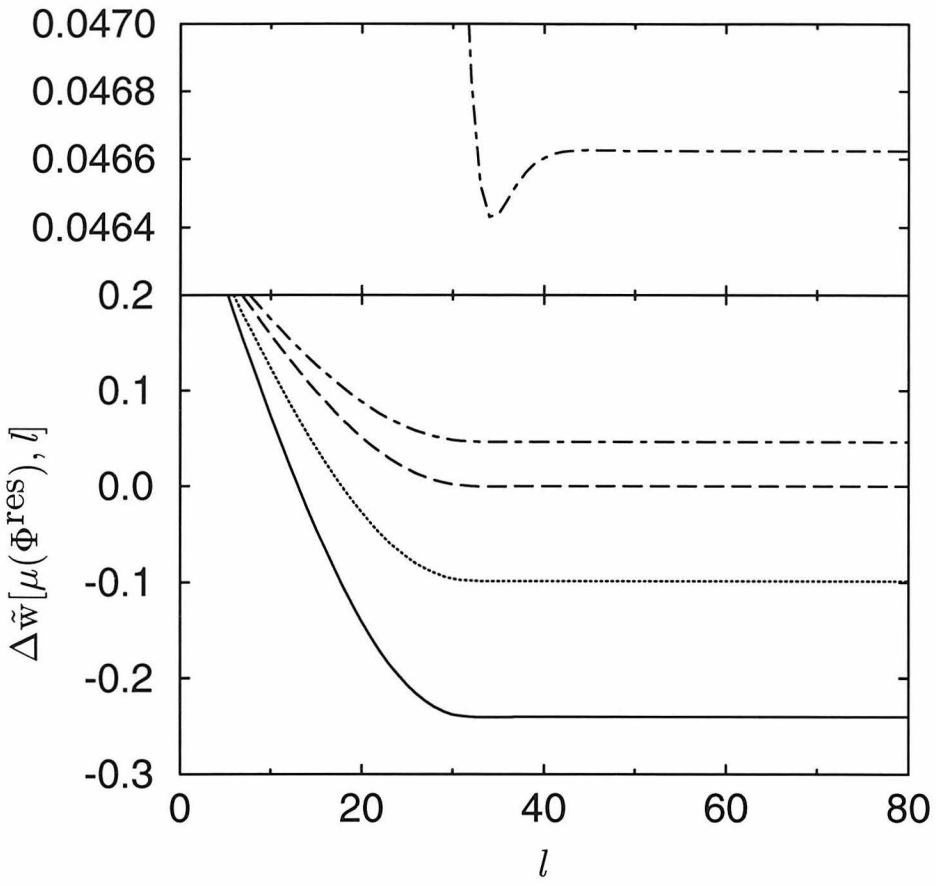

Figure 3.8: The excess grand potential per unit area of the film is shown upon confinement to a film of thickness l (in units of the lattice spacing). $N = 200$, $\epsilon = 20$, $\mu = \mu(\Phi^{\rm res} = 0.3)$ solid line, $\mu = \mu(\Phi^{\rm res} = 0.2)$ dotted line, $\mu = \mu^* = \mu(\Phi^{\rm res} = 0.1317)$ long-dashed line, $\mu = \mu(\Phi^{\rm res} = 0.1)$ dot-dashed line. All four curves show very small minima at $l \approx h$ where they appear to become flat. The minimum in the $\mu(\Phi^{\rm res} = 0.1)$ curve is shown above in an expanded scale, the minima in the other curves are quite similar. In all cases these minima are the global minima and thus $l_o^* \approx h$ independent of $\Phi^{\rm res}$.

its unfavorable position near the wall into the bulk state, and the attendant entropy gain causes the attraction. In our case the one hard wall is the air-liquid interface. The other wall is the interface of the liquid with the self-assembled polymer brush. Although not strictly a hard wall, the brush allows only very limited penetration of the free polymers and therefore results in a depletion of the free polymers near the tip of the brush, similar to a hard wall.

3.4.3 The equilibrium film thickness of an open system is nearly independent of composition

In the spreading problem the brush-liquid and liquid-air interfaces collapse into a single brush-air interface due to the depletion attraction at $l \approx h$. The minimum created by the depletion interaction in Figure 3.8 is necessarily shallow, especially compared to the large interfacial tensions and brush compression costs shown in the same figure. However, in the absence of additional effects not included in this paper, this free energy minimum determines the optimal film thickness l_o^* for the open system:

$$\left.\frac{\partial \Delta\tilde{w}(\mu, l)}{\partial l}\right|_{\mu} = 0 \qquad \text{at} \qquad l = l_o^*. \tag{3.20}$$

Furthermore, it can be shown that the film at thickness l_o^* is stable against thermal fluctuations, i.e., that the fluctuation in the film thickness around l_o^* is much smaller than both l_o^* and the width of the minimum[3]. By virtue of the origin of the depletion attraction, the equilibrium film thickness of a spreading film in equilibrium with a reservoir is very nearly h, the brush height. Since the brush height is independent of Φ (see Section 3.3), the film thickness is independent of Φ. Thus the surprisingly simple and general conclusion of this section is that *the film thickness of a spreading film in equilibrium with an infinite reservoir is independent of* Φ *and very nearly the height of the self-assembled polymer brush in an unbounded fluid.*

3.5 Spreading of a finite droplet of fixed composition

In this section we consider the spreading of a drop of fixed volume and composition (a closed system) on a surface of unlimited area. This situation is most directly related to the experimental situation. The limited availability of EAPs leads to substantially different results than what is found for an open system. The thermodynamics for the closed system is discussed is Section 3.5.1. However, the film thickness and the phase diagram for the closed system are more conveniently obtained by constructing a semi-open system in which the volume of the liquid is fixed but the composition is allowed to vary according to equilibrium

[3]For parameters used in the figures, the magnitude of thermal fluctuations is estimated as less than 2 Kuhn lengths using the expression in Reference [30].

with a reservoir of specified chemical potential. The relationship between the closed and the semi-open systems is discussed is Section 3.5.2. The two systems are shown schematically in Figures 3.9 and 3.10 respectively.

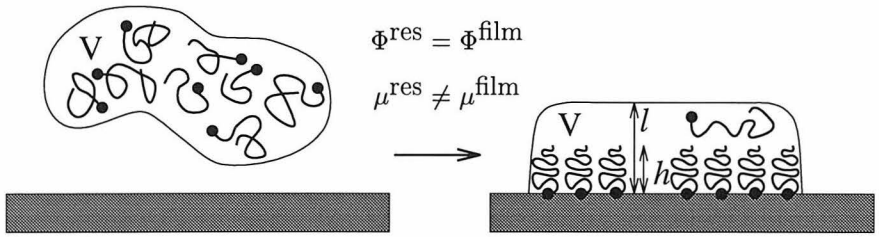

Figure 3.9: Schematic illustration of the closed system of volume V spreading on the solid surface to form a pancake of thickness l. In the closed system the composition of the liquid is fixed.

3.5.1 Closed system thermodynamics

The appropriate thermodynamic potential for a closed system is the Helmholtz free energy change per unit volume $\Delta f(\Phi, l)$ upon spreading a droplet of fixed volume V and composition Φ with initially negligible interfacial area into a pancake-like film of uniform thickness l and resulting interfacial area V/l as shown in Figure 3.9. The Helmholtz free energy of the initial state is

$$F^{\text{initial}}(\Phi) = V f^{\text{bulk}}(\Phi) + A\gamma^{\circ}_{SA}, \tag{3.21}$$

where A is the area of the initially bare surface of the solid and $f^{\text{bulk}}(\Phi)$ is the Helmholtz free energy per unit volume of a bulk liquid of composition Φ, and is therefore the limit $f^{\text{bulk}}(\Phi) = \lim_{l\to\infty} f(\Phi, l) = f^{\text{res}}(\Phi)$. The Helmholtz free energy of the final state is

$$\begin{aligned} F^{\text{final}}(\Phi, l) &= V f(\Phi, l) + \frac{V}{l}(\gamma_{LA} + \gamma_{SL}) \\ &\quad + \left(A - \frac{V}{l}\right)\gamma^{\circ}_{SA} + \frac{V}{l}\frac{H}{12\pi l^2}. \end{aligned} \tag{3.22}$$

Thus

$$\Delta f(\Phi, l) = \frac{\Delta F(\Phi, l)}{V} \tag{3.23}$$

$$= \frac{1}{V}\left[F^{\text{final}}(\Phi, l) - F^{\text{initial}}(\Phi)\right] \tag{3.24}$$

$$= f(\Phi, l) - f^{\text{res}}(\Phi)$$

$$+\frac{1}{l}(\gamma_{LA}+\gamma_{SL}-\gamma_{SA}^{\circ})+\frac{1}{l}\frac{H}{12\pi l^2} \tag{3.25}$$

$$= \frac{1}{l}\left[\tilde{f}^{\rm ex}(\Phi,l)-S+\frac{H}{12\pi l^2}\right] \tag{3.26}$$

where $\tilde{f}^{\rm ex}(\Phi,l)\equiv l\times[f(\Phi,l)-f^{\rm res}(\Phi)]$ is the same excess free energy per unit area as in the expression for $\Delta w\,[\mu(\Phi^{\rm res}),l]$ except that Φ rather than $\mu(\Phi^{\rm res})$ is specified.

As before, the equilibrium film thickness for a closed system is obtained by minimizing $\Delta f(\Phi,l)$ with respect to l, at constant Φ,

$$\left.\frac{\partial\Delta f(\Phi,l)}{\partial l}\right|_{\Phi}=0 \qquad \text{at} \qquad l=l_c^*. \tag{3.27}$$

If $\Delta f(\Phi,l)$ has a global minimum at a finite l, then the film will spread to a pancake of that thickness, while if the minimum falls at infinite l, the system forms a macroscopic droplet.

3.5.2 Thermodynamic relationship of semi-open and closed systems

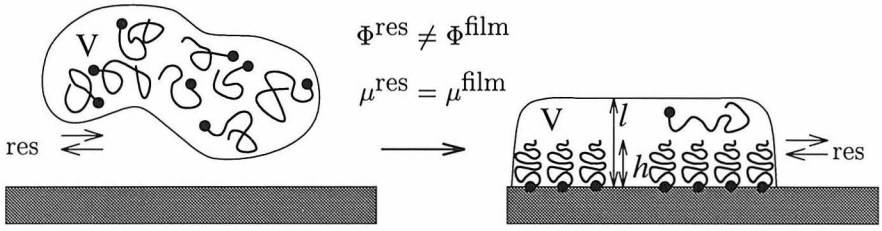

Figure 3.10: Schematic illustration of the semi-open system of volume V spreading on the solid surface to form a pancake of thickness l. In the semi-open system the chemical potential μ is fixed, allowing for exchange with a reservoir.

Although it is possible to study the closed system directly, it is more convenient and elucidating to obtain the same results by thermodynamic connection to the open system. In order to facilitate that comparison, we define a semi-open system in which the system volume is held fixed but the composition is allowed to vary to maintain a designated chemical potential. This system is illustrated in Figure 3.10. Because the volume of this system is fixed, the relevant thermodynamic potential is the grand potential per unit volume, $\Delta w(\mu,l)$, which is defined

$$\Delta w(\mu,l)=\frac{1}{V}\Delta W(\mu,l)=\frac{1}{l}\Delta\tilde{w}(\mu,l), \tag{3.28}$$

where $\Delta W(\mu, l)$ is the quantity defined in Section 3.3 Equation 3.12. The semi-open and closed potentials ($\Delta w(\mu, l)$ and $\Delta f(\Phi, l)$ respectively) are compared term by term,

$$\Delta w = \frac{1}{l}\left\{\tilde{f}^{\text{ex}}[\Phi(\mu), l] - S + \frac{H}{12\pi l^2}\right\} \tag{3.29}$$

$$\Delta f = \frac{1}{l}\left\{\tilde{f}^{\text{ex}}[\Phi, l] - S + \frac{H}{12\pi l^2}\right\}, \tag{3.30}$$

which shows only one dissimilar term. $\tilde{f}^{\text{ex}}[\Phi(\mu), l]$ and $\tilde{f}^{\text{ex}}[\Phi, l]$ differ in that μ is held constant in the semi-open system, while Φ is held constant in the closed system. *However, l^*_{so} which minimizes the semi-open system at μ also minimizes the closed system which has the same actual composition* ($\Phi = \Phi(\mu)$), i.e.,

$$\left.\frac{\partial \Delta w(\mu, l)}{\partial l}\right|_{\mu} = \left.\frac{\partial \Delta f[\Phi(\mu), l]}{\partial l}\right|_{\Phi} = 0 \quad \text{at} \quad l = l^*_{so} = l^*_c \tag{3.31}$$

This is demonstrated by applying the chain rule to the semi-open system derivative

$$\left.\frac{\partial \Delta w(\mu, l)}{\partial l}\right|_{\mu} = \left.\frac{\partial \Delta w(\mu, l)}{\partial l}\right|_{\mu,\Phi} + \left.\frac{\partial \Delta w(\mu, l)}{\partial \Phi}\right|_{\mu,l} \left.\frac{\partial \Phi}{\partial l}\right|_{\mu}. \tag{3.32}$$

However, the term

$$\left.\frac{\partial \Delta w(\mu, l)}{\partial \Phi}\right|_{\mu,l} = 0 \tag{3.33}$$

because the composition of an open system is determined by minimizing Δw. Then, since

$$\left.\frac{\partial \Delta w(\mu, l)}{\partial l}\right|_{\mu,\Phi} = \left.\frac{\partial \Delta f[\Phi(\mu), l]}{\partial l}\right|_{\Phi} \tag{3.34}$$

the two derivatives are equal when the composition is the same. Thus l^*_o for the open system is equal to l^*_c for the equivalent closed system at $\Phi(\mu)$.

3.5.3 The equilibrium film thickness of a closed system depends upon composition

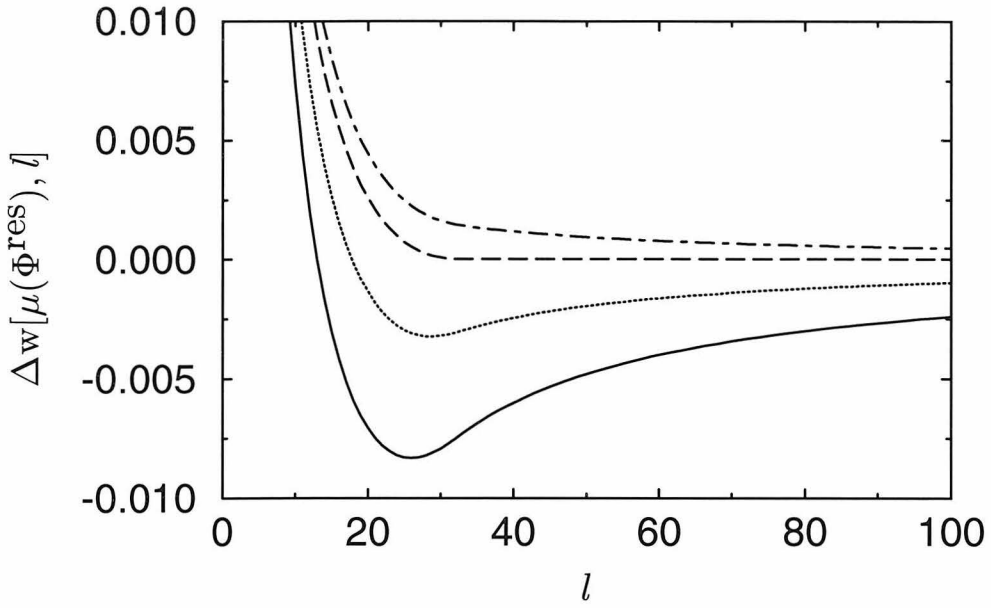

Figure 3.11: The excess grand potential per unit volume as a function of l (given in units of the lattice spacing). This figure is constructed from the data in Figure 8, and parameters of the system are the same as indicated there. Notice, however, that the location of the minimum in these figures is not independent of $\Phi^{\rm res}$, and indeed can vary from less than h, to h at coexistence, and then, for nonspreading droplets, to infinity. The long-dashed line is at the coexistence μ and has two shallow equal minima at $l \approx h$ and $l \to \infty$.

To find the equilibrium film thickness, it is first necessary to obtain $\Delta w(\mu, l)$ which results directly from the data shown in Figure 3.8 after division by l. This data is presented in Figure 3.11. Notice that in this case the minima do not fall at $l \approx h$ regardless of Φ. Instead *the minimum falls at $l \to \infty$ for nonspreading films, and at $l < h$ for spreading films.* Exactly at the threshold $\tilde{f}^{\rm ex}(\Phi, l) = S$ there are two minima of equal depth, one at $l \approx h$ (this feature is too small to be seen on the figure) and another at $l \to \infty$. At this chemical potential the droplet is in equilibrium with the spread film of thickness $l \approx h$. In Figure 3.12 l_c^* is shown as a function of Φ for $\epsilon = 20$. As additional EAP is added, the film thins. As more chains become adsorbed, they prefer to spread laterally to relieve crowding, even at the cost of some compression. This is in contrast to the open system in which l_o^* is always h, independent of Φ.

3.5.4 Phase diagram

Another important feature of Figure 3.12 is the discontinuity in l_c^*. At the spreading transition the film thickness goes from h discontinuously to ∞. This corresponds to a discontinuity

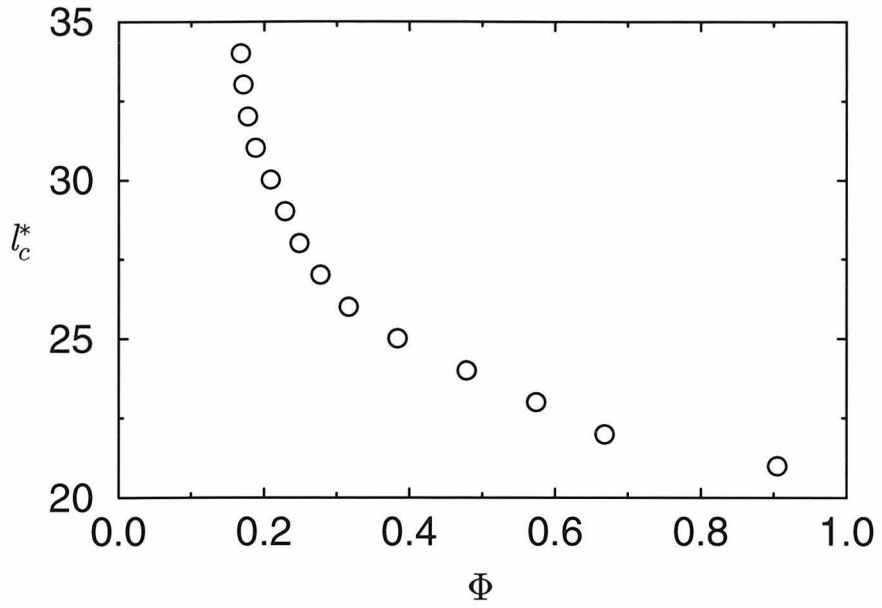

Figure 3.12: The equilibrium droplet thickness l_c^* (in units of the lattice spacing) of a finite droplet spread on an infinite area as a function of the EAP content of the system Φ for $N = 200$, $\epsilon = 20$. At the coexistence curve $l_c^* \approx h$ as in the open system, but as excess EAP is added beyond what is required to form a uniform film, the film spreads out, thinning the film at the expense of compressing the EAP brush.

also in the actual composition of the system Φ at the transition from a uniform film to a bulk droplet state (although μ varies continuously; it is related to Φ by $\Phi = \int_0^{l_c^*} \Phi(\mu, z)dz$). The state of a system with composition which falls between the allowed values for a bulk droplet or a uniform film is a bulk droplet state and a spread film state in coexistence (with the same μ) as shown in Figure 3.13. By plotting the transition from spreading to

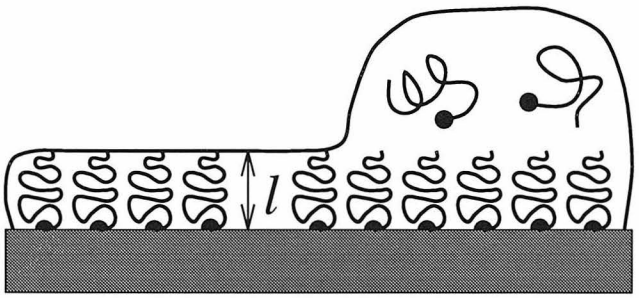

Figure 3.13: When the film is constrained to a thickness greater than the brush height, $l > h$, the excess fluid may dewet the surface of the EAP film as shown in this schematic illustration.

nonspreading as a function of Φ and ϵ, a phase diagram for the closed system is constructed, as shown in Figure 3.14. There are several features of the phase diagram worthy of special

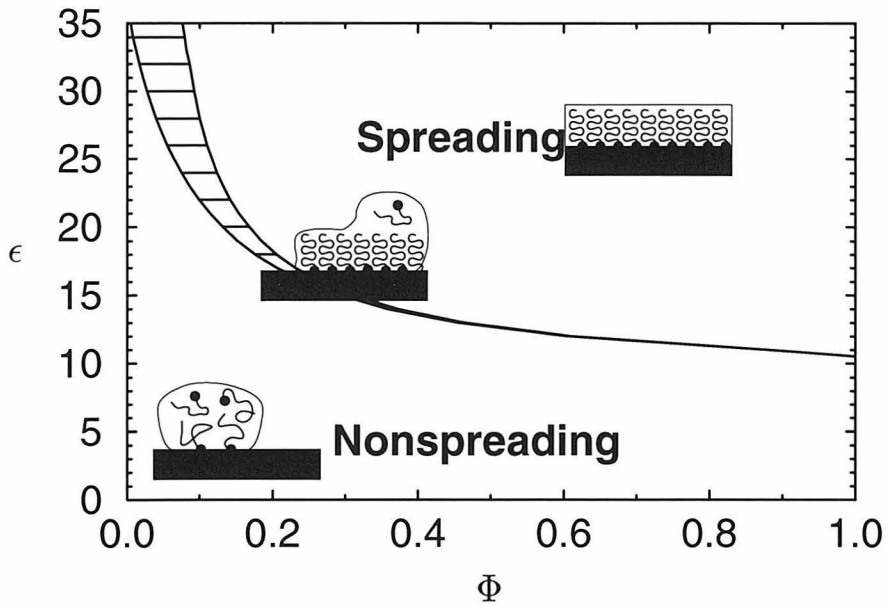

Figure 3.14: The phase diagram for spreading as a function of the system composition Φ and end attachment energy ϵ for $N = 200$. Notice that at high end attachment energy ϵ, a vanishingly small quantity of EAP additive will result in some spreading, but a significantly larger quantity is required to convert the whole volume of the droplet to a uniform wetting layer.

attention. First notice that there is a threshold ϵ (about 10.5) below which even a melt of the EAP chains will not spread on the surface (this value depends, of course, on S and weakly on H). Above this threshold the amount of EAP additive required to stabilize a surface falls rapidly, and at $\epsilon = 30$, for example, only 3% EAP will cause some spreading and 9% percent will result in a uniform film. Addition of more EAP will result in some thinning of the film, as shown in Figure 3.12 above.

3.6 Stabilization of mechanically cast films

In the previous sections we have examined the spreading of a finite droplet into a thin film. In industrial applications, however, the reverse process of stabilizing a mechanically cast film against irregularity and rupture is often more important. In lithographic processes in the semiconductor industry, for example, it is often desirable to apply a uniform thin film by spin coating. If the liquid-solid pair being used has a negative S value, the film will not be stable and will break up into droplets. The addition of an EAP additive can change this, leading under the right circumstances to a stable film. The *equilibrium* thickness of the stabilized film depends upon the amount of EAP present. However, the *mechanically*

cast film will not necessarily have a thickness of precisely l_c^*, leading to the possibility of film deformation or rupture. In this section the implications of equilibrium self-assembled polymer brush (SAPB) formation on the stability of films of arbitrary thickness and composition are described. The problem should be examined in several parts. First the formation of a stable liquid film which covers the solid surface is considered, and then the stability of such films against thickness irregularities.

3.6.1 Covering the surface

The formation of a film which will cover the solid-liquid surface depends upon the EAP content and adsorption energy ϵ of the system as summarized in the phase diagram in Figure 3.14. If a mechanically spread film of any thickness has inadequate EAP content to spread (Φ and ϵ in the nonspreading portion of the phase diagram), the film can be expected to break up into droplets, leaving essentially the whole solid surface in contact with air. If, on the other hand, the EAP content puts the system in the spreading portion of the phase diagram, the liquid can be expected to cover a surface of area up to $A^{\text{covered}} = V/l_c^*$ (V is the volume of the cast film). If the area of the initially coated surface is greater than this, the film will dewet the surface to leave the excess area uncovered at equilibrium. Finally, if the EAP content puts the system in the coexistence regime, the lever rule can be used to determine what fraction of the volume is in the film and the area covered by that portion can be obtained as above. The remainder of the liquid can be expected to form bulk droplets on top of the spread film as indicated in Figure 3.13.

3.6.2 Instability of thick films

Provided that a spincast film is stable against dewetting as evaluated above, there remains the possibility that irregularities in the film thickness could occur, even while the *bare* solid surface is never exposed. In particular, it is clear from the preceding analysis that the equilibrium film thickness of an EAP system is always less than the thickness of the self-assembled brush (for closed systems) or equal to it (for open systems). The film will remain stable against thickness irregularities for thickness less than l_c^*. However, if a mechanically cast film is thicker than l_o^*, the excess liquid will form droplets on top of the film, effectively acting as a reservoir for the film beneath them and maintaining the thickness of the film at l_o^*.

There are some features of the depletion-attraction induced dewetting of the *brush covered* surface which distinguish it from the dewetting of the *dry* surface. First, the depletion attraction provides the only driving force for brush surface dewetting, and it is thus independent of S and any enthalpic interactions. This is intuitively reasonable because the dewetting of the brush exposes the same liquid area to air, and the γ_{LA} contribution to S is the same for the brush and the liquid (to a first approximation), since the segments are chemically identical. The van der Waals contribution is likewise negligible, since the liquid is on a layer of the same chemical composition which is already relatively thick. Although the depletion attraction free energy minimum leading to this dewetting is rather shallow, it is the sufficient to maintain film thickness against thermal fluctuations [30]. Therefore, it provides an adequate driving force for the breakup of the liquid into droplets above the EAP film.

Recent experimental results of Yerushalmi-Rosen and Klein offer a possible example of the depletion attraction induced dewetting described above [2, 3]. They examined the stability of spincast oligostyrene films on silicon stabilized by self-assembled polystyrene brushes. These films form pockmark-like irregularities in the surface thickness which do not penetrate to the silicon substrate. We suggest that these are caused by the collapse of the liquid-air interface into the brush-liquid interface. They observe a subsequent stabilization of the film uniformity when additional EAP or unfunctionalized polystyrene is present which is not explained in our treatment. This may be due to the shallowness of the free energy minimum which is responsible for the equilibrium film thickness l_o^*. Interactions neglected in our model may become comparable to the attraction arising from entropic depletion. If so, a more detailed model becomes necessary. In particular, the assumption that the surface tension contribution of the polymer and the monomer are identical, which results in a concentration-independent spreading power, may break down, especially as the concentration of unadsorbed chains above the brush goes from dilute to semi-dilute.

The experiments in References [2] and [3] include consideration of an additional polymer species with no adsorbing group. We have also obtained results for this three component system, which, however, are not presented in this work for the sake of clarity. We found that, while the nonadsorbing polymer does modify the phase diagram for spreading (in particular widening the coexistence regime), it does not reduce or eliminate the depletion attraction, and therefore will not stabilize thin films or lead to films thicker than the equilibrium brush

height.

3.7 Concluding Remarks

In concluding this study we will highlight the strengths of end-adsorbing polymer (EAP) additives as spreading agents and film stabilizers, and also review the complexity added to the problem upon formation of a self-assembled brush structure.

The principal strength of an EAP additive is that it can induce spreading at liquid-solid interfaces which would otherwise not occur because of an unfavorable spreading coefficient S. Further, upon spreading, the properties of the film are largely independent of S and the Hamaker constant H, and can be tailored by the characteristics and quantity of the EAP additive. The adsorbing head group and chain length can be specifically chosen to achieve a desirable thickness of the spreading film, which can be further modified by controlling the amount of additive used.

Although S and H set the thickness of a thin film for simple liquids, their role is far less significant in films containing a self-assembled EAP brush. The van der Waals forces described by H become almost negligible (they are reduced by l^{-2}). The role of S in an EAP system is to determine the minimum EAP content and ϵ required for spreading. The resulting thickness for the EAP film is primarily set by h, the brush height, although in a closed system the excess EAP content does result in an indirect relationship of l_c^* and S.

The results for spreading films lead us to some predictions about the stability of mechanically cast films. Some strong predictions about the EAP content required to cover the surface can be drawn from the phase diagram in Figure 3.14. We also predict that films mechanically spread thicker than l_o^* will be unstable and will break up into droplets of liquid above a swollen brush surface as shown in Figure 3.13. Two caveats must accompany this prediction. First, the driving force for this phenomena is the rather weak depletion attraction, which may be overwhelmed in a real system by factors not considered in the present model (but is robust against thermal fluctuations). Secondly, we make no predictions about the kinetics of film breakup, which is likely to depend on many factors including the EAP content of the liquid film above the droplet, the interpenetration of the brush and unadsorbed polymers, and the presence of impurities.

3.8 Acknowledgement

We thank Jacob Klein and Nily Dan for stimulating discussion. We thank especially Jacob Klein for bringing our attention to References [2] and [3] which initiated this study. Financial support from the National Science Foundation under grants DMR9220733 and ASC9217368 and the Camille and Henry Dreyfus Foundation is gratefully acknowledged.

Bibliography

[1] Moreau, W. M. *Semiconductor Lithography*; Plenum: New York, 1988.

[2] Yerushalmi-Rozen, R.; Klein, J.; Fetters, L. J. *Science* **1994**, *263*, 5148.

[3] Yerushalmi-Rozen, R.; Klein, J. *Langmuir* **1995**, *11*, 2806.

[4] Shaw, D. J. *Introduction to Colloid and Surface Chemistry*; Butterworth-Heinemann Ltd.: Boston, 1992.

[5] Schick, M. In *Liquids at Interfaces:* Les Houches, session XLVIII; Charvoli J.; Joanny, J. F.; Zinn-Justin, J. Eds.; Elsevier Science Pub.: New York, 1990.

[6] de Gennes, P. G. *Rev. Mod. Phys.* **1985**, *57*, 827.

[7] Brochard-Wyart, F.; di Meglio, J.-M.; Quéré, D.; de Gennes, P. G. *Langmuir* **1991**, *7*, 335.

[8] Halperin, A.; Pincus, P.; Alexander, S. *J. Physique Lett.* **1985**, *46*, L-543.

[9] Boudoussier, M. *J. Physique* **1987**, *48*, 445.

[10] Martin, J. I.; Wang, Z. -G. *J. Phys. Chem.* **1995**, *99*, 2833.

[11] Carignano, M. A.; Szleifer, I. *J. Chem Phys* **1993**, *98*, 5006; *J. Chem Phys* **1994**, *100*, 3210.

[12] Johner, A.; Marques, C. M. *Phys. Rev. Lett.* **1992**, *69*, 1827.

[13] Leibler, L.; Adjari, A.; Mourran, A.; Coulon, G.; Chatenay, D. In *Macromolecular Systems*; Teramoto, A.; Kobayashi, M.; Norisuje T.; Springer Verlag: Berlin, 1994.

[14] Martin, J. I.; Wang, Z. -G. unpublished results.

[15] Liu, Y.; Rafailovich, M. H.; Sokolov, J.; Schwarz, S. A.; Zhong, X.; Eisenberg, A.; Kramer, E. J.; Sauer, B. B.; Satija, S. *Phys. Rev. Lett.* **1994**, *73*, 440.

[16] Schlanger, L.; Leermakers, F. A. M.; Koopal, L. K. *J. Chem. Soc., Faraday Trans.* **1996**, *92*, 579.

[17] Dan, N. *Langmuir* **1996**, *12*, 1101.

[18] de Gennes, P. G. *Macromolecules* **1980**, *13*, 1069.

[19] Alexander, S. *J. Physique* **1977**, *38*, 983.

[20] Milner, S. T.; Witten, T. A.; Cates, M. E. *Europhys. Lett.* **1988**, *5*, 413. Milner, S. T.; Witten, T. A.; Cates, M. E. *Macromolecules* **1988**, *21*, 2610.

[21] Halperin, A.; Tirrell, M.; Lodge, T. P. *Adv. Polym. Sci.* **1992**, *100*, 31.

[22] de Gennes, P. G. *Macromolecules* **1982**, *15*, 492; Eisenriegler, E.; Kremer, K.; Binder, K. *J. Chem. Phys.* **1982**, *77*, 6296; Nemirovsky, A. M.; Freed, K. F. *J. Chem. Phys.* **1985**, *83*, 4166.

[23] Carignano, M. A.; Szleifer, I. *Macromolecules* **1995**, *28*, 3197.

[24] Wijmans, C. M.; Zhulina, E. B.; Fleer, G. J. *Macromolecules* **1994**, *27*, 3238.

[25] Safran, S. A. *Statistical Thermodynamics of Surfaces Interfaces and Membranes*; Addison-Wesley: New York, 1994.

[26] Israelachvili, J. N. *Intermolecular and Surface forces*; Academic Press: San Diego, 1992.

[27] Martin, J. I.; Wang, Z.-G.; Zuckerman, D.; Bruinsma, R.; Pincus, P. in preparation.

[28] Joanny, J. F.; Leibler, L.; de Gennes, P. G. *J. Polym. Sci.: Polym. Phys. Ed.* **1979**, *17*, 1073.

[29] van Lent, B.; Israels, R.; Scheutjens, J. M. H. M.; Fleer, G. J. *J. Colloid Interface Sci.* **1990**, *137*, 380.

[30] Bar-Ziv, R.; Safran, S. A. *Langmuir* **1993**, *9*, 2786.

Chapter 4 Forces Between Surfaces with Weakly End-Adsorbed Polymers

This work, published with Z.-G. Wang, D. Zuckerman, R. Bruinsma and P. Pincus, extends the consideration of reversible adsorption to the limit of very weak adsorption. In this limit a new set of problems arise as well as a new set of analytical tools. In particular, the question of the sign, magnitude and length scale of the different forces caused by weakly adsorbing polymers are addressed by three complimentary methods; a phenomenological argument, a more thorough thermodynamic argument, and a detailed numerical analysis of the sort described in the previous chapters of this thesis. The phenomenological and numerical results are primarily the work of myself and Z.-G. Wang, while the thermodynamic analysis is primarily the work of D. Zuckerman, R. Bruinsma and P. Pincus.

Reprinted with permission from Journal de Physique II **1997**, *7*, 1111.

Abstract

We study the interaction forces between two plates in a semi-dilute solution of polymers each having one weakly adsorbing end-group. We show that this system exhibits both repulsive and attractive interactions of comparable magnitude and well-separated length scales: when the plate separation is within a range of order the end-to-end distance of the end-adsorbed polymer, repulsion arises with a magnitude of $\epsilon\frac{\Phi}{Na^3}$ where ϵ is the end-adsorption energy, N is the degree of polymerization, a is the Kuhn length and Φ is the volume fraction of the polymer. This repulsion is due to desorption of the end-adsorbed chains. At plate separations of order the correlation length of the solution, a depletion attraction sets in with a magnitude that scales with the bulk osmotic pressure.

4.1 Introduction

The importance of polymeric additives in mediating the interactions between colloidal particles has been understood longer even than has the basic nature of polymers themselves (for instance in the stabilization of ink by addition of polymers) [1]. The action of the polymers depends upon their physical properties and concentration. The contribution of a polymeric additive to interparticle interactions (and hence to colloidal stability) ranges from purely attractive (destabilizing)—for flexible non-adsorbing homopolymers—to repulsive (stabilizing)—for irreversibly adsorbed polymers. In the first case the non-adsorbing chains are depleted near a colloid surface due to configurational entropy loss. This gives rise to an attractive interaction between the particles in which the osmotic pressure of the bulk compresses the gap in order to minimize the free energy cost of the depleted volume [2]. In fact, de Gennes [3] has shown that even the restriction to nonadsorbing chains is unnecessary to establish the sign of the interactions between two surfaces: for weakly adsorbing homopolymer chains, it can be shown that the interaction is *always* attractive for systems in full equilibrium with the bulk (an exception to this is discussed later [4]).

Irreversibly end-grafted polymers on the other hand form a hairy shell or corona around the particles which repel similarly coated particles by steric interactions [5]. This is not inconsistent with de Gennes's theorem because irreversibly grafted chains are by definition not in equilibrium with the bulk. In this paper we will show that end-adsorbed chains with finite adsorption energy ϵ produce repulsive interactions *even in full equilibrium with the bulk*[1]. This repulsion can be understood as arising from the loss of adsorption energy when adsorbed chains are squeezed out of the gap. This is a subtle point, however, because uniformly adsorbing chains are likewise squeezed out of the gap, yet this leads to attraction rather than repulsion. The end-adsorbed chains are fundamentally different, however, in that they can adopt a prefered orientation with the functional group adsorbed at the wall.

By virtue of their orientation, end-adsorbed chains are distinct from the other chains in the system. The adsorbed chains are distinguished in this respect over their whole length R (the end-to-end distance), even in a semidilute solution where the chain segments are generally indistinguishable on size scales larger than the correlation length ξ (also called

[1] This paper is concerned solely with the case of *full equilibrium*. In colloidal stabilization the system may not reach equilibrium during a Brownian collision, in which case a "restricted equilibrium" treatment such as is discussed in Reference [13] may be more appropriate.

the mesh size, which is the length scale beyond which intra-chain and inter-chain correlations are no longer distinguishable and is less than R for semi-dilute solutions [6]). When two such adsorbed layers on opposing walls begin to overlap, they will interact. The appropriate length scale for the interaction is thus the end-to-end distance of the adsorbed chain. The resulting repulsive interaction is in contrast with the attraction induced by chains which adsorb uniformly along their whole contour. The sign of the interaction is thus a consequence of the orientation of the chains and is perhaps most clearly understood by analogy with more familiar orientable systems such as magnetic fluids [7]. Magnetic particles can orient their magnetization at a wall. Two such walls will repel one another because of the frustration when the two opposite magnetizations meet in the midplane region, while ordinary surface adsorption of binary liquid mixtures always produces attraction between plates. Similarly, end adsorbed polymers will exhibit an orientation towards the surface, which will induce a repulsion between two such surfaces. This orientation arises from end-adsorption and not from the asymmetry of the molecule. In fact, telechelic or randomly functionalized chains can also be oriented this way, and will induce analogous repulsive interactions under certain circumstances. We will have more to say about other chain architectures in the conclusions, but for the sake of clarity will focus primarily on singly end-functionalized chains in the rest of the paper.

The magnitude of the end-adsorption energy ϵ will determine which interactions and length scales will be important. For very large ϵ the configuration of the system will adjust itself to maximize the number of chain ends attached to the surface. In dense solutions or melts where the polymer density near the wall cannot be significantly increased, the chains are forced to stretch normal to the surface to allow more ends to attach. In more dilute systems this stretching is accompanied by a dramatic increase in the polymer density near the surface. The interactions induced by strongly adsorbing (high ϵ) chains will be described briefly at the conclusion of this paper, but our primary focus in this work is weakly end-adsorbing chains.

In the limit of weak end-adsorption (small ϵ) in a semi-dilute solution, the *overall* segment density distribution is not significantly altered by adsorbing end-groups, since these account for only a small portion ($\frac{1}{N}$) of the overall segment density. In this limit the overall segment density will still be depleted within a correlation length ξ of the wall, and this depletion will give rise to a depletion attraction between the surfaces exactly as in the limit

of zero ϵ. The range of this depletion attraction is ξ. This depletion attraction operates simultaneously with the above mentioned desorption repulsion, *but with different ranges.* If ξ is small compared to R, the short range attraction and the long range repulsion will not locally cancel. This separation assures us that there is no threshold value of ϵ for the repulsive interaction, because any end adsorption will orient some chains, and this causes repulsion at length scale R. Thus, in the semi-dilute regime, where $a \ll \xi \ll R$ (a is the Kuhn length), the interaction potential has both a long range (R) desorption repulsion and a shorter range (ξ) attraction, reminiscent of the DLVO interaction profile, where desorption and depletion are replaced by a long range electrostatic repulsion and a short range van der Waals attraction [8]. Colloids with weakly end-adsorbed polymers thus should show a rich phase behavior, including a transition from flocculation to stabilization as a function of the volume fraction of polymer Φ and ϵ. Polymers with weak end-adsorption are currently under examination in atomic force studies of polymer surfaces [9].

In this short paper we will approach this problem through three complementary methods. In the next section we construct a phenomenological picture in the small ϵ regime. By assuming that the overall segment density profile is not significantly altered upon introduction of a moderate adsorption energy at one chain end, a schematic segment density profile for adsorbed and nonadsorbed chains can be constructed. This profile leads to a scaling prediction for the different interaction regimes between two plates and for the relevant length scales for the interaction. The most important omission of the phenomenological treatment is the coupling of the overall segment density near the wall with the adsorption energy ϵ, which will cause some increase in the segment density near the wall in order to increase the number of adsorbed chain ends. This omission is corrected in Section 4.3 by a more careful thermodynamic treatment of the interaction in the regime $\xi \ll h \ll R$ for moderate ϵ. In that section we also comment upon the factors which limit the application of de Gennes theorem regarding the attractive interplate interactions in the presence of uniformly adsorbing polymers in full equilibrium with the bulk. The thermodynamic analysis confirms the scaling prediction of the phenomenological treatment for the repulsive interaction in that regime. Confirmation of the other features of the phenomenological picture are given by a detailed numerical self-consistent field treatment described in Section 4.4. We take advantage of the broad range of parameters available to this calculation technique to make a connection between the weakly adsorbed chain limit examined in this paper, and earlier

results obtained for higher adsorption energies [10]. Finally, in the discussion and conclusion section, some rules of thumb are described for determining whether attractive, repulsive, or "DLVO type" interactions are to be expected under a given set of experimental conditions.

4.2 Phenomenological Description

We consider a semi-dilute solution of polymers of degree of polymerization N, with Kuhn length a, in a good (athermal) solvent. The volume fraction of polymer is Φ. The chains have a weak end-adsorption energy ϵ, but no other segmental attraction to the surface. For simplicity, we assume that end-groups do not interact significantly with other segments or with one another, that is, we exclude the formation of micelles. For the purpose of simplicity, we address the regime in which the adsorption energy ϵ is not sufficient to cause a significant local excess of monomer density near the surface and can be treated as a small perturbation to the case of nonadsorbing homopolymers near a hard wall; thus we limit our consideration in this section to cases where ϵ is not much larger than kT.

Chains with a weakly adsorbing head group will orient themselves so that chains near the surface will have their end-group attached to the wall. This adsorption should be essentially complete near the surface provided that ϵ is more than a few kT, but will die off gradually for chains farther from the surface with a characteristic length scale of the chain size $R \sim N^{\frac{1}{2}} a \Phi^{-\frac{1}{8}}$ [6]. The upper bound to the weak adsorption regime is defined such that there is no significant anisotropic stretching nor any significant increase in segment density near the surface. For larger ϵ, a large increase in adsorption density leads to stretching normal to the surface which is characteristic of the so-called brush regime. In the brush regime the chains stretch to a length D which scales with $Na\sigma^{-\frac{1}{3}}$ where σ is the dimensionless grafting density and is found by balancing chain stretching with adsorption energy [5, 11]. However, in the present work we concern ourselves with weak adsorption for which R and D are comparable.

In the weak end-adsorption regime, the concentration of polymer segments is depleted within one correlation length $\xi \sim a\Phi^{-\frac{3}{4}}$ of the wall due to the restriction of chain configurations by the wall [6]. Scaling predictions of the profile and interfacial free energy for noninteracting or repulsive polymer chains have been worked out by de Gennes for segment-wall interaction ranging from weakly attractive to repulsive [12]. For a noninteracting wall

the free energy of the interface is simply the work done against osmotic pressure Π to remove the solute to a distance ξ from the wall.

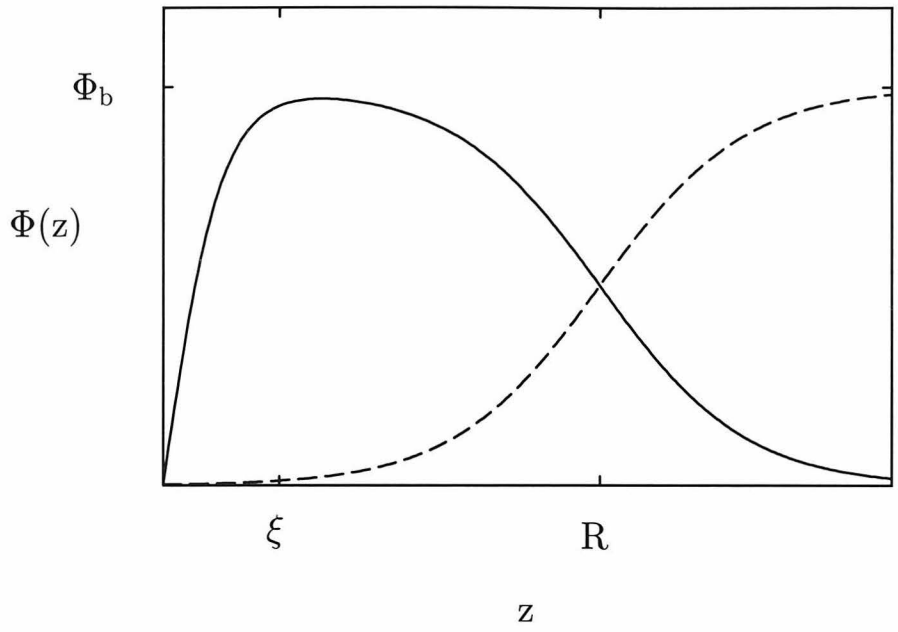

Figure 4.1: Schematic segment density profile $\Phi(z)$ for weakly end-adsorbed chains as a function of the distance z from the surface. The solid line is for chains with adsorbed end groups and the dashed line is for non-adsorbed chains.

A schematic representation of the main features of the segment density profile is shown in Figure 4.1. Numerically obtained profiles are readily obtainable from detailed self-consistent field calculations discussed in Section 4.4 below, and are consistent with the figure over a broad range of semidilute concentrations and chain lengths. The segment density of adsorbed chains is indicated with a solid line and nonadsorbed chain segment density, with a dashed line. The chain density of adsorbed chains becomes significant in the region less than one end-to-end distance R away from the wall. Also there is a depletion of the segment density within a distance ξ from the wall due to the decrease in configurational entropy.

We now consider the interaction between two surfaces of the type described above. Because the system has mirror symmetry, it is convenient to describe the plate separation by h, the distance between the hard wall and the plane of symmetry. Thus the actual plate separation is $2h$. When the plate separation is many times the chain size R, there is no interaction. For half-plate-separation $R > h > \xi$, the proximity leads to the desorption of some chains in order to prevent the chain overlap from causing an increase in chain density

(which would cause an increase in the excluded volume interactions). The adsorption energy per unit area is simply the number of adsorbed chains per unit area times ϵ, and can be expressed in terms of the segment density profile of adsorbed chains $\frac{\epsilon}{Na^3}\int \Phi_a(z)dz$. For the sample profile in Figure 4.1, we obtain a force per unit area which is repulsive and is of magnitude $\epsilon\frac{\Phi}{Na^3}$

For half-plate separation of less than the correlation length $h < \xi$, the depletion attraction becomes important. Because the chain segment density is depleted near the wall, the bulk solution exerts an osmotic pressure on the depleted region. If the concentration between the plates is depleted, the osmotic pressure leads to an attraction between them. The magnitude of the attractive interaction is given by the osmotic pressure of the bulk solution Π, although it varies with the extent of depletion.

When the free energy of a single chain between the plates—which consists of the end adsorption energy ϵ and the cost of confinement between two plates separated by $2h$—exceeds the bulk chemical potential, μ, of the semidilute solution,

$$-\epsilon + kTN\left(\frac{a}{2h}\right)^{\frac{5}{3}} > \mu \sim kT\frac{Na^3}{\xi^3\Phi}, \tag{4.1}$$

the chains will rapidly leave the gap [6]. Thus there will be some threshold spacing h_c at which the interplate chain density becomes vanishingly small (because the polymer concentration in the gap is very low, it is appropriate to use the single chain expression for the confinement cost). Upon using $\xi \sim a\Phi^{-3/4}$, the condition Equation 4.1 becomes

$$2h < \xi\left[1 + \frac{\epsilon}{kTN}\left(\frac{\xi}{a}\right)^{\frac{5}{3}}\right]^{\frac{3}{5}} \equiv 2h_c. \tag{4.2}$$

For $h < h_c$, the concentration between the plates becomes vanishingly small and the interaction is simply the bulk osmotic pressure. The length h_c is not a new length scale in the problem, but rather the half-plate separation at which the monomer concentration is completely depleted, a process that began at $h \sim \xi$. Indeed, when $\epsilon = 0$, the threshold separation for all chains leaving the gap h_c is simply $\frac{1}{2}\xi$ from Equation 4.2. The attractive contribution to the interaction begins when the depletion regimes on *both* surfaces overlap, at plate separation approximately twice the correlation length. Total chain exclusion, on the other hand, arises when the confinement of a *single* chain between the plates becomes

unfavorable; in the limit of small ϵ, this happens at plate separation approximately one correlation length. Thus, the one half prefactor is retained because it arises naturally from the phenomenological picture, as two adsorbed layers give way to one, but should not be taken to indicate that this prediction is correct to a numerical factor.

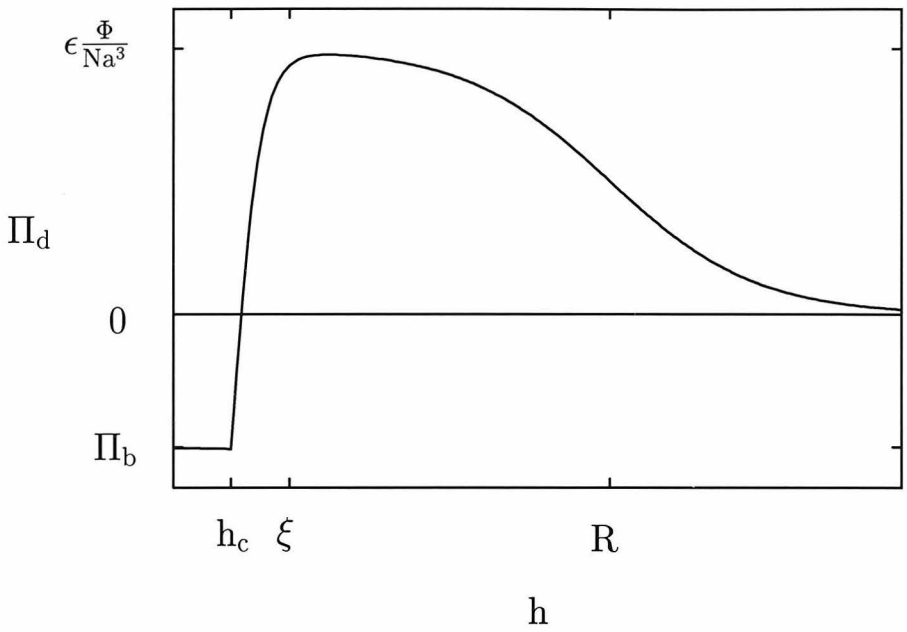

Figure 4.2: Schematic force per unit area Π_d versus h, the half gap separation.

From this phenomenological description a schematic force profile can be constructed, as is shown in Figure 4.2. The profile has three principal features. At a distance of $h \sim R$, a repulsive interaction begins with a characteristic magnitude of $\epsilon\frac{\Phi}{Na^3}$. At $h \sim \xi$ the depletion in polymer density decreases the repulsive contribution of the polymer chains and introduces an attractive osmotic term. The attraction grows as h decreases until, at $h = h_c$, all of the polymer has left the gap and the interaction is simply the osmotic pressure Π.

4.3 Thermodynamic Analysis for $\xi \ll h \ll R$

The prediction of a repulsive interaction between two plates, even in full equilibrium, is unusual and it is appropriate to give it a more careful thermodynamic treatment. We are interested in the disjoining pressure between two plates at separation $2h$ where $\xi \ll h \ll R$ and the solution is in the semidilute regime.

We assume that the segment density Φ between the plates is uniform, although not

necessarily the same as the bulk segment density Φ_b, and is in the semidilute regime $\Phi^* \ll \Phi \ll 1$, where Φ^* is the overlap volume fraction (which depends on N as $N^{-\frac{4}{5}}$) [6]. The entropic depletion in monomer density at distances less than ξ from the wall will be described as a surface term. For $\epsilon > kT$, essentially all of the adsorbing ends should be adsorbed if $h \ll R$. Under these assumptions, the excess grand potential per unit area is

$$\Delta\tilde{w} = c_1 \frac{kT}{\xi^2} + h\left[f(\Phi) - \mu_b \frac{\Phi}{a^3} + \Pi_b\right] - \frac{h}{a^3}\frac{\epsilon}{N}\Phi \tag{4.3}$$

where $f(\Phi)$ is the Helmholtz free energy per unit volume of a semi-dilute solution of volume fraction Φ given by

$$f(\Phi) \sim \frac{c_2 kT}{a^3}\Phi^{\frac{9}{4}} \tag{4.4}$$

and c_1 and c_2 are numerical constants of order unity. The first term is the cost of the depletion at the surface, the next three represent the contribution to $\Delta\tilde{w}$ from the interior of the gap, and the last term is the adsorption energy. Taking $\xi = a\Phi^{-\frac{3}{4}}$ for the correlation length inside the plates, the grand potential can be expressed entirely in terms of Φ and is minimized with respect to Φ to yield the relation

$$\frac{9}{4}c_2 kT\Phi^{\frac{5}{4}}\left(1 + \frac{2}{3}\frac{c_1}{c_2}\frac{\xi}{h}\right) = \mu_b + \frac{\epsilon}{N} \tag{4.5}$$

where

$$\mu_b \equiv a^3 \frac{\partial f}{\partial \Phi}\bigg|_{\Phi=\Phi_b} = \frac{9}{4}c_2 kT\Phi^{\frac{5}{4}} \tag{4.6}$$

is the chemical potential per monomer. Finally, the osmotic pressure Π_b of the bulk semi-dilute solution is

$$\begin{aligned} \Pi_b \equiv \Phi^2 \frac{\partial(f/\Phi)}{\partial\Phi}\bigg|_{\Phi=\Phi_b} &= \frac{5}{4}\frac{c_2 kT}{a^3}\Phi^{\frac{5}{4}}. \\ &= \frac{5}{9}\frac{\mu_b \Phi_b}{a^3} \end{aligned} \tag{4.7}$$

In the limit $h \gg \xi$ Equation 4.5 gives

$$\frac{9}{4}c_2 kT\Phi^{\frac{5}{4}} \cong \mu_b + \frac{\epsilon}{N}. \tag{4.8}$$

Substituting in the calculated expression for μ_b from Equation 4.6 leads to a monomer

density Φ between the plates which is always greater than or equal to the reservoir segment density:

$$\Phi^{\frac{5}{4}} = \Phi_b^{\frac{5}{4}} + \frac{4}{9c_2kT}\frac{\epsilon}{N} = \Phi_b^{\frac{5}{4}}\left(1 + \frac{\epsilon}{\mu_b N}\right). \tag{4.9}$$

Inserting Equation 4.8 in Equation 4.3 we obtain an expression for the disjoining pressure Π_d, which is the negative derivative of $\Delta\tilde{w}$ with respect to h,

$$\begin{aligned} \Pi_d &= -\frac{d\Delta\tilde{w}}{dh} = -\frac{\partial\Delta\tilde{w}}{\partial h} \\ &= \frac{1}{a^3}\left(-c_2kT\Phi^{\frac{9}{4}} + \mu_b\Phi - \Pi_b a^3 + \frac{\epsilon}{N}\Phi\right) \end{aligned} \tag{4.10}$$

which, using Equation 4.8, leads to

$$\begin{aligned} \Pi_d &= \frac{1}{a^3}\left(\frac{5}{9}\frac{\epsilon}{N}\Phi + \frac{5}{9}\mu_b\Phi - \Pi_b a^3\right) \\ &= \frac{1}{a^3}\left[\frac{5}{9}\frac{\epsilon}{N}\Phi + \frac{5}{9}\mu_b\left(\Phi - \Phi_b\right)\right] \end{aligned} \tag{4.11}$$

where we have used Equation 4.8.

Because $\Phi \geq \Phi_b$ it is clear that the disjoining pressure is repulsive ($\Pi_d \geq 0$). Moreover, when the bulk chemical potential (on a per segment basis) is far greater than the adsorption energy per segment

$$\mu_b \left(= \frac{9}{4}kT\Phi^{\frac{5}{4}}\right) \gg \frac{\epsilon}{N} \tag{4.12}$$

and therefore

$$\frac{\epsilon}{\mu_b N} \ll 1, \tag{4.13}$$

then the expression for Φ in Equation 4.9 can be expanded about Φ_b

$$\Phi = \Phi_b\left\{1 + \frac{4}{5}\frac{\epsilon}{\mu_b N} + \mathrm{O}\left[\left(\frac{\epsilon}{\mu_b N}\right)^2\right]\right\}. \tag{4.14}$$

Substituting this into Equation 4.11 we obtain, to leading order,

$$\Pi_d = \frac{1}{a^3}\left[\frac{5}{9}\frac{\epsilon}{N}\Phi + \frac{4}{9}\frac{\epsilon}{N}\Phi_b\right] \approx \frac{1}{a^3}\frac{\epsilon}{N}\Phi_b \tag{4.15}$$

which is the result predicted on the basis of the phenomenological model.

At first sight the prediction of a repulsive interaction between the plates appears to

contradict the theorem of de Gennes. However, this is not the case. In his treatment, de Gennes assumes that the same functional form of the free energy density $f(\Phi)$ describes both the free energy within the gap and in the bulk, and the effect of polymer-wall interaction amounts to a boundary condition [3]. This, together with the concavity of $f(\Phi)$ immediately leads to $\Delta W > 0$ and $\Pi_d < 0$. In the case of end-adsorbed polymers, however, the free energy density in the gap has a different form than the free energy density in the bulk, $f(\Phi) = -\frac{\epsilon}{Na^3}\Phi + f_b(\Phi)$ where $f_b(\Phi)$ has the same functional form as the bulk. The difference in the functional form of Helmholtz free energy density leads to the difference in interactions. In fact, a repulsive disjoining pressure can be shown to arise whenever there is a favorable energy contribution per particle in the gap.

4.4 Numerical Results

We now approach the problem with a detailed self-consistent field method, which gives us full configurational and thermodynamic information (at the mean-field level) for any adsorption energy ϵ and for polymer volume fractions Φ from the semi-dilute all the way up to the melt. In this approach [13, 14] the many-body problem is reduced to a one-body problem in a mean field which accounts for the effect of inter-chain and intra-chain interactions and polymer-solvent interactions. The one chain problem is solved exactly by enumerating all configurations on a lattice using a recursion relation. The field is obtained self-consistently by an incompressibility constraint which requires that the total chain and solvent volume fractions add up to unity. The Helmholtz free energy F is obtained from the partition function Q

$$F = -kT \ln Q(n_p, n_s) \tag{4.16}$$

where n_p and n_s are the number of polymers and solvent molecules in the system and the excess grand potential ΔW is in turn obtained from the Helmholtz free energy F, which, for an incompressible system, is given by

$$\Delta W = F - n_p\mu_p - n_s\mu_s \tag{4.17}$$

where μ_p and μ_s are the chemical potentials of the polymers and solvent molecules respectively. Because the system is incompressible, $n_s a^3 + n_p N a^3 = V$ where we have set

both the monomer volume and the solvent molecule volume equal to a^3. Substituting $n_s = V/a^3 - n_p N$ into Equation 4.17 we obtain

$$\Delta W = F - n_p N \left(\frac{\mu_p}{N} - \mu_s \right) - \frac{V}{a^3} \mu_s \tag{4.18}$$

which can be expressed in the same form as Equation 4.3 in Section 4.3:

$$\Delta W = F - n_p N \mu_b + V \Pi_b \tag{4.19}$$

where μ_b is the exchange chemical potential per monomer of the polymer in the bulk

$$\mu_b = \frac{\mu_p}{N} - \mu_s = a^3 \frac{\partial f_b}{\partial \Phi} \tag{4.20}$$

and the osmotic pressure is related to the solvent chemical potential

$$\Pi_b = -\frac{\mu_s}{a^3} = \Phi^2 \frac{\partial (f_b/\Phi)}{\partial \Phi} \tag{4.21}$$

and $V f_b \equiv F_b$ is the Helmholtz free energy in the bulk. The force is simply the negative derivative of the grand potential with respect to h.

$$\text{force} = - \left. \frac{\partial \Delta W}{\partial h} \right|_{\mu_b, \Pi_b} \tag{4.22}$$

Because of the mean-field nature of the calculation, results will scale with mean-field exponents. However, because this method enforces the incompressibility condition explicitly (as opposed to a second virial approach), it can consistently examine any value of ϵ as well as a wide range of Φ without any of the difficulties encountered in analytical treatments.

In Figure 4.3 the force profile is shown for a system of $N = 2000$, $\Phi = 0.005$ and $\epsilon = 10$. The osmotic pressure Π, polymer size R, correlation length ξ and total chain exclusion threshold h_c are shown, as is a scaling estimate of the magnitude of the repulsive force (h_c was obtained from Equation 4.2 using appropriate prefactors and mean-field exponents for consistency with the calculation). All of the features predicted by the phenomenological model are observed. Similar agreement with the schematic density and force profiles and more generally with the phenomenological description of the system is found for a large range of N and Φ in the semidilute regime. The preceding section demonstrated that $\frac{\epsilon}{Na^3}\Phi$

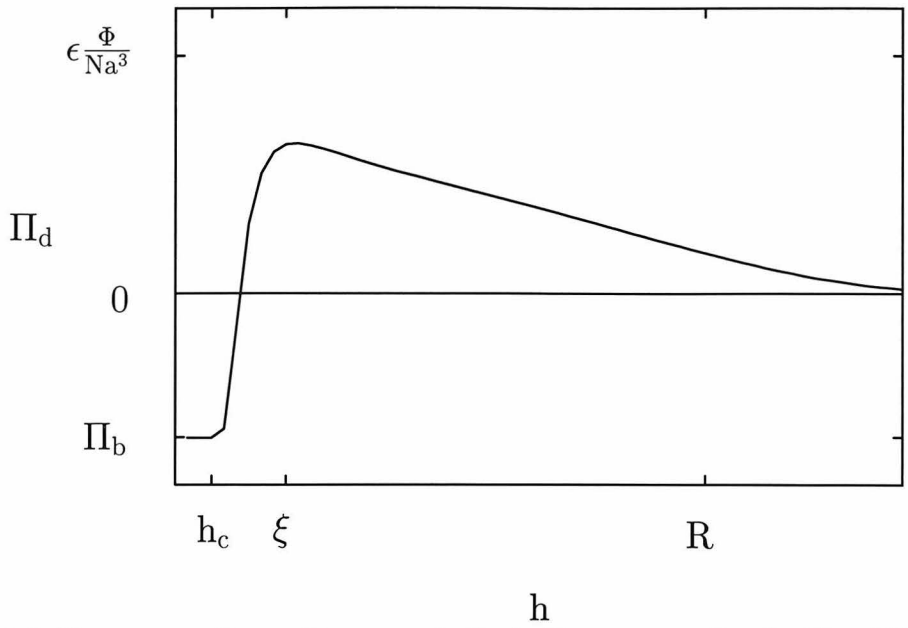

Figure 4.3: Force per unit area Π_d versus h, the half gap separation for $N = 2000$, $\Phi = 0.005$ and $\epsilon = 10$.

is the correct scaling for the repulsive interaction in the range $\xi \ll h \ll R$, while for the attractive interactions the osmotic pressure Π_b gives the appropriate scale. In all cases, the depletion induced attraction obtained numerically indeed reaches a maximum magnitude of exactly the osmotic pressure Π_b while the repulsive force reaches a maximum of magnitude $\epsilon\frac{\Phi}{Na^3}$. The numerical prefactor for the repulsive force is about 0.6 independent of Φ in the range $0.005 \leq \Phi \leq 0.2$ for $\epsilon = 10$ and $N = 2000$. For lower ϵ the assumption that all chain ends near the surface are adsorbed apparently breaks down and the numerical constant gets smaller and becomes dependent on Φ. For higher ϵ chain stretching becomes important and the polymer brush picture is more appropriate [10].

4.5 Conclusions

In this paper we have shown that weakly end-adsorbed polymers induce complex interactions between interfaces which have implications for understanding the stability of colloidal suspensions. In contrast to homogeneously adsorbing chains which, according to the theorem of de Gennes, always induce attractive interactions between surfaces when they are in complete equilibrium [3], end adsorbed chains induce repulsion at separations comparable to R and attraction at separations comparable to ξ. The end-adsorption energy ϵ plays

a crucial role in the restoration of the length scale R by orienting the polymers near the wall. In fact, even a uniformly adsorbed chain will have some orientation of nonadsorbed chain ends or "tails," and this has recently been shown by Semenov et al. to lead to a weak repulsive interaction for uniformly adsorbed polymers in full equilibrium [4]. This repulsion arises from considering the difference between the loops and tails, and is beyond the level of de Gennes theorem.

Let us review scaling estimates for the magnitude of the forces and length scales relevant to the problem. These estimates provide rules of thumb, with which the importance of the attractive and repulsive interactions can readily be gauged, and a conclusion can be reached as to whether the brush, non-adsorbing or crossover description is most appropriate in a particular system.

The interesting force profile described in this paper arises from the fact that *two* length scales are simultaneously active, $\xi \sim a\Phi^{-\nu/(3\nu-1)} \sim a\Phi^{-\frac{3}{4}}$ and $R \sim (Na^3/\Phi\xi)^{\frac{1}{2}} \sim N^{\frac{1}{2}}a\Phi^{-\frac{1}{8}}$. This occurs *only* in semi-dilute solution and for relatively weak end-adsorption (given by the criterion Equation 4.13. The magnitude of the depletion attraction in this regime is given by the bulk osmotic pressure of the system, $\Pi \sim kT\xi^{-3} \sim kT\Phi^{\frac{9}{4}}a^{-3}$ [6], and the magnitude of the repulsive interaction is $\epsilon\frac{\Phi}{Na^3}$.

Although the treatment in Sections 4.2 and 4.3 assumes weak end-adsorption in the semi-dilute regime, the prediction that the repulsive interaction scales as $\epsilon\frac{\Phi}{Na^3}$ is more robust, and is not limited by these assumptions. In dense solutions or melts, the correlation length tends toward the segment length, which causes the attractive portion of the interaction profile to disappear. However, the repulsive interaction will remain with a magnitude $\epsilon\frac{\Phi}{Na^3}$, even as Φ tends toward one. In this high concentration regime, the local segment density at the wall cannot be significantly modified by either end-adsorption or the overlap of opposing adsorbed layers on surfaces at separations of less than $2R$. Thus bringing the plates within $2R$ of one another will result in desorption and therefore repulsion of the same type described in Section 4.2. Similarly, for strong adsorption, even in dilute and semi-dilute solutions, the segment density at the wall will be quite high, characteristic of the brush regime with excluded volume interactions and stretching balancing the adsorption energy. As two brushes overlap from opposing plates, chains will desorb to avoid overcrowding. This leads to a repulsive interaction of magnitude $\epsilon\frac{\Phi}{Na^3}$, where Φ is the local segment density within the brush. Because the segment density in the brush is higher than in the bulk

solution, there is no depletion attraction on length scales much larger than the segment length. Thus in either the melt or the strongly adsorbing cases, the repulsive interaction is given by $\epsilon\frac{\Phi}{Na^3}$ where Φ is the local segment density. These conclusions have been confirmed by self-consistent field methods as described in Section 4.4, the semi-dilute in previouly published work [10] and the melt in unpublished results.

The general picture developed in this paper is also applicable to amphiphilic molecules of more complex architectures than the singly end-functionalized chains discussed in this paper. The minimum necessary condition to observe an equilibrium repulsive interaction is that all (or at least most) of the adsorbing species in a region larger than the correlation length are localized at the surface. In this case, the overlap of the adsorbed layers leads to a decrease in the adsorption density in order to maintain the local density of the rest of the chain segments. The decrease in adsorption density has an associated energy cost which leads to the repulsive interaction. This could equally well occur with telechelic chains with adsorbing groups at both ends, or even randomly functionalized chains, provided that the number of functional groups was small enough that most of them could be localized at the surface while still having the unfunctionalized portions of the chain extend into the solution a distance greater than the correlation length. However, these different chain architectures also introduce other complexities, including bridging of a single chain adsorbed on both plates [15]. This bridging can lead to an attractive interaction which is entropic in origin, and will act for the most part independently of the repulsive interaction caused by the removal of adsorbed chains. Thus more complex interaction profiles with multiple attractive and repulsive regions are possible.

4.6 Acknowledgements

Financial support from the National Science Foundation (Grant Nos. UCSB-MRL DMR-9123048, DMR-9407741, ACS-9217368), from the Department of Energy (Grant No. DOE DE-FG03-87ER45288), and from the Camille and Henry Dreyfus Foundation (TC-96-063), is gratefully acknowledged.

Bibliography

[1] Flory, P. J. *Principles of Polymer Chemistry*; Cornell University Press: Ithaca New York, 1953.

[2] Israelachvili, J. N. *Intermolecular Surface Forces*; Academic Press: San Diego, 1992.

[3] de Gennes, P.-G. *Macromolecules* **1982**, *15*, 492.

[4] Semenov, A. N.; Bonetavalos, J.; Johner, A.; Joanny, J. F. *Macromolecules* **1996**, *29*, 2179.

[5] Halperin, A.; Tirrell, M.; Lodge, T. P. *Adv. Polym. Sci.* **1992**, *100*, 31.

[6] de Gennes, P.-G. *Scaling Concepts in Polymer Physics*; Cornell University Press: New York, 1979.

[7] Bashtovoi, V. G.; Berkovsky, B. M.; Vislovich, A. N. *Introduction to Thermomechanics of Magnetic Fluids*; Smith, J., Trans; Berkovsky, B. M. Ed.; Rosensweig, R. E., Eng.-Ed. Ed.; Hemisphere Pub. Corp.: Washington, 1988.

[8] Russel, W. B.; Saville, D. A.; Schowalter, W. R. *Colloidal Dispersions*; Cambridge U. P.: New York, 1989.

[9] Joanny, J. F. private communication, 1996.

[10] Martin, J. I.; Wang, Z.-G.; Schick, M. *Langmuir* **1996**, *12*, 4950.

[11] Alexander, S. *Journal de Physique* **1977**, *38*, 983.

[12] de Gennes, P.-G. *Macromolecules* **1981**, *14*, 1637.

[13] Fleer, G. J.; Cohen Stuart, M. A.; Scheutjens, J. M. H. M.; Cosgrove, T.; Vincent, B. *Polymers at Interfaces*; Chapman and Hall: New York, 1993.

[14] Martin, J. I.; Wang, Z.-G. *J. Phys. Chem.* **1995**, *99*, 2833.

[15] Milner, S. T.; Witten, A. W. *Macromolecules* **1992**, *25*, 5495.